

Department of the Interior
U.S. Geological Survey

LANDSAT 8 (L8) DATA USERS HANDBOOK

Version 2.0

March 29, 2016

Any use of trade, firm, or product names is for descriptive purposes only and does not imply endorsement by the U.S. Government.



LANDSAT 8 (L8) DATA USERS HANDBOOK

March 29, 2016

Approved By:

K. Zanter Date
LSDS CCB Chair
USGS

EROS
Sioux Falls, South Dakota

Executive Summary

This Landsat 8 (L8) Data Users Handbook is a living document prepared by the U.S. Geological Survey (USGS) Landsat Project Science Office at the Earth Resources Observation and Science (EROS) Center in Sioux Falls, SD, and the National Aeronautics and Space Administration (NASA) Landsat Project Science Office at NASA's Goddard Space Flight Center (GSFC) in Greenbelt, Maryland.

The purpose of this handbook is to provide a basic understanding and associated reference material for the L8 Observatory and its science data products. In doing so, this document does not include a detailed description of all technical details of the L8 mission, but instead focuses on the information that the users need to gain an understanding of the science data products.

This handbook includes various sections that provide an overview of reference material and a more detailed description of applicable data user and product information. This document includes the following sections:

- Section 1 describes the background for the L8 mission as well as previous Landsat missions
- Section 2 provides a comprehensive overview of the current L8 Observatory, including the spacecraft, the Operational Land Imager (OLI) and Thermal Infrared Sensor (TIRS) instruments, and the L8 concept of operations
- Section 3 includes an overview of radiometric and geometric instrument calibration as well as a description of the Observatory component reference systems and the Calibration Parameter File (CPF)
- Section 4 includes a comprehensive description of Level 1 products and product generation
- Section 5 addresses the conversion of Digital Numbers (DNs) to physical units
- Section 6 includes an overview of data search and access using the various online tools
- Appendix A contains the applicable reference materials, along with the list of known issues associated with L8 data
- Appendix B contains an example of the Level 1 product metadata

This document is controlled by the Land Satellites Data System (LSDS) Configuration Control Board (CCB). Please submit changes to this document, as well as supportive material justifying the proposed changes, via a Change Request (CR) to the Process and Change Management Tool.

Document History

Document Number	Document Version	Publication Date	Change Number
LSDS-1574	Version 1.0	June 2015	CR 12286
LSDS-1574	Version 2.0	March 29, 2016	CR 12749

Contents

Executive Summary	iii
Document History	iv
Contents.....	v
List of Figures	vii
List of Tables	viii
Section 1 Introduction.....	1
1.1 Foreword.....	1
1.2 Background.....	2
1.2.1 Previous Missions	3
1.2.2 Operations and Management	4
1.3 Landsat 8 Mission	4
1.3.1 Overall Mission Objectives.....	4
1.3.2 System Capabilities	4
1.3.3 Global Survey Mission	5
1.3.4 Rapid Data Availability	5
1.3.5 International Ground Stations (IGSs).....	6
1.4 Document Purpose	6
1.5 Document Organization	6
Section 2 Observatory Overview.....	7
2.1 Concept of Operations	7
2.2 Operational Land Imager (OLI)	8
2.3 Thermal Infrared Sensor (TIRS).....	12
2.4 Spacecraft Overview	14
2.4.1 Spacecraft Data Flow Operations	15
Section 3 Instrument Calibration.....	17
3.1 Radiometric Characterization and Calibration Overview	17
3.1.1 Instrument Characterization and Calibration.....	19
3.1.2 Prelaunch.....	21
3.1.3 Postlaunch	23
3.1.4 Operational Radiometric Tasks.....	24
3.2 Geometric Calibration Overview	26
3.2.1 Collection Types	29
3.2.2 Prelaunch.....	29
3.2.3 OLI Geodetic Accuracy Assessment.....	30
3.2.4 Sensor Alignment Calibration	30
3.2.5 Geometric Accuracy Assessment	31
3.2.6 OLI Internal Geometric Characterization and Calibration.....	31
3.2.7 TIRS Internal Geometric Characterization and Calibration	32
3.2.8 OLI Spatial Performance Characterization.....	33
3.2.9 OLI Bridge Target MTF Estimation	34
3.2.10 Geometric Calibration Data Requirements	35
3.3 Calibration Parameters	38

3.3.1	Calibration Parameter File	38
3.3.2	Bias Parameter Files.....	41
3.3.3	Response Linearization Lookup Table (RLUT) File	41
Section 4	Level 1 Products	43
4.1	Level 1 Product Generation	43
4.1.1	Overview.....	43
4.1.2	Level 1 Processing System.....	43
4.1.3	Ancillary Data.....	45
4.1.4	Data Products	45
4.1.5	Calculation of Scene Quality.....	54
4.2	Level 1 Product Description	55
4.2.1	Science Data Content and Format.....	55
4.2.2	Metadata Content and Format	57
4.2.3	Quality Assessment Band.....	58
Section 5	Conversion of DNs to Physical Units.....	60
5.1	OLI and TIRS at Sensor Spectral Radiance.....	60
5.2	OLI Top of Atmosphere Reflectance	60
5.3	TIRS Top of Atmosphere Brightness Temperature	61
5.4	Unpacking Quality Assessment Band Bits	61
5.5	LandsatLook Quality Image (.png)	63
Section 6	Data Search and Access	65
6.1	EarthExplorer (EE).....	65
6.2	Global Visualization Viewer (GloVis).....	68
6.3	LandsatLook Viewer	70
Appendix A	Known Issues	73
A.1	TIRS Stray Light.....	73
A.2	Striping and Banding.....	76
A.3	SCA Overlaps	80
A.4	Oversaturation	81
A.5	Single Event Upsets.....	82
A.5.1	Observatory Component Reference Systems.....	83
A.6	OLI Instrument Line-of-Sight (LOS) Coordinate System	83
A.7	TIRS Instrument Coordinate System	84
A.8	Spacecraft Coordinate System	85
A.9	Navigation Reference Coordinate System	85
A.10	SIRU Coordinate System	86
A.11	Orbital Coordinate System	86
A.12	ECI J2000 Coordinate System.....	87
A.13	ECEF Coordinate System	88
A.14	Geodetic Coordinate System	89
A.15	Map Projection Coordinate System.....	90
Appendix B	Metadata File (MTL.txt)	91
References.....		96

List of Figures

Figure 1-1. Continuity of Multispectral Data Coverage Provided by Landsat Missions ...	3
Figure 2-1. Illustration of Landsat 8 Observatory	7
Figure 2-2. OLI Instrument	8
Figure 2-3. OLI Signal-To-Noise (SNR) Performance at Ltypical	10
Figure 2-4. OLI Focal Plane	11
Figure 2-5. Odd / Even SCA Band Arrangement.....	12
Figure 2-6. TIRS Instrument with Earthshield Deployed.....	12
Figure 2-7. TIRS Focal Plane	14
Figure 2-8. TIRS Optical Sensor Unit	14
Figure 3-1. Simulated OLI Image of the Lake Pontchartrain Causeway (left) and Interstate-10 Bridge (right) Targets in WRS 022/039	35
Figure 4-1. LPGS Standard Product Data Flow	44
Figure 4-2. Level 1 Product Ground Swath and Scene Size	46
Figure 4-3. A Diagram of the First Pass ACCA Algorithm	51
Figure 4-4. A Temperate Region Affected by CirrusTop image is OLI Bands 4,3,2; bottom image is OLI Band 9, the cirrus detection band.....	53
Figure 4-5. Landsat 8 Spectral Bands and Wavelengths compared to Landsat 7 ETM+	56
Figure 4-6. Quality Band (BQA.TIF) displayed for Landsat 8 Sample Data (Path 45 Row 30) Acquired April 23, 2013.....	59
Figure 5-1. Landsat Look "Quality" Image (QA.png) displayed as .jpg for reference only Landsat 8 sample data Path 45 Row 30 Acquired April 23, 2013	64
Figure 6-1. EarthExplorer Interface	66
Figure 6-2. EarthExplorer Landsat Data Sets.....	66
Figure 6-3. EarthExplorer Results - Browse Image Display	67
Figure 6-4. EarthExplorer Results Controls	68
Figure 6-5. Global Visualization Viewer (GloVis) Interface	69
Figure 6-6. The LandsatLook Viewer	70
Figure 6-7. Display of Landsat Imagery.....	71
Figure 6-8. LandsatLook Viewer Screen Display	72
Figure A-1. TIRS Image of Lake Superior Showing Apparent Time-Varying Errors	74
Figure A-2. TIRS Special Lunar Scan to Characterize the Stray Light Issue.....	75
Figure A-3. Thermal Band Errors (left group) Prior to Calibration Adjustment and (right group) After Calibration Adjustment	76
Figure A-4. Striping and Banding Observed in Band 1 (CA Band)	77
Figure A-5. Striping and Banding observed in Band 2 (Blue)	78
Figure A-6. Striping and Banding observed in TIRS Band 10	79
Figure A-7. SCA Overlap Visible in Band 9 (Cirrus Band)	80
Figure A-8. SCA Overlap Visible in TIRS Band 10.....	81
Figure A-9. Oversaturation Example in OLI SWIR Bands 6 & 7	82
Figure A-10. Example of SEU Event Measured by OLI – SEU Manifests as a Line of Single-Frame Bright Spots	83
Figure A-11. OLI Line-of-Sight (LOS) Coordinate System.....	84

Figure A-12. TIRS Line-of-Sight (LOS) Coordinates	85
Figure A-13. Orbital Coordinate System.....	87
Figure A-14. Earth-Centered Inertial (ECI) Coordinate System.....	88
Figure A-15. Earth-Centered Earth Fixed (ECEF) Coordinate Systems.....	89
Figure A-16. Geodetic Coordinate System.....	90

List of Tables

Table 1-1. Comparison of Landsat 7 and Landsat 8 Observatory Capabilities.....	5
Table 2-1. OLI and TIRS Spectral Bands Compared to ETM+ Spectral Bands	9
Table 2-2. OLI Specified and Performance Signal-to-Noise (SNR) Ratios Compared to ETM+ Performance	10
Table 2-4. TIRS Noise-Equivalent-Change-in Temperature (NE Δ T).....	13
Table 3-1. Summary of Calibration Activities, their Purpose, and How Measurements are used in Building the Calibration Parameter Files	19
Table 3-2. Summary of Geometric Characterization and Calibration Activities	29
Table 4-1. Standard: Ls8pprrrYYYYDDDGGGVV_FT.ext.....	57
Table 4-2. Compressed: Ls8pprrrYYYYDDDGGGVV.FT.ext	57
Table 5-1. Bits Populated in the Level 1 QA Band	61
Table 5-2. A Summary of Some Regularly Occurring QA Bit Settings	63
Table 5-3. Bits and Colors Associated with LandsatLook Quality Image.....	64
Table A-1. TIRS Band Variability.....	76

Section 1 Introduction

1.1 Foreword



The Landsat Program has provided over 40 years of calibrated high spatial resolution data of the Earth's surface to a broad and varied user community. This user community includes agribusiness, global change researchers, academia, state and local governments, commercial users, national security agencies, the international community, decision-makers, and the public. Landsat images provide information that meets the broad and diverse needs of business, science, education, government, and national security.

The mission of the Landsat Program is to provide repetitive acquisition of moderate-resolution multispectral data of the Earth's surface on a global basis. Landsat represents the only source of global, calibrated, moderate spatial resolution measurements of the Earth's surface that are preserved in a national archive and freely available to the

public. The data from the Landsat spacecraft constitute the longest record of the Earth's continental surfaces as seen from space. It is a record unmatched in quality, detail, coverage, and value.

The Landsat 8 (L8) Observatory offers the following features:

- **Data Continuity:** L8 is the latest in a continuous series of land remote sensing satellites that began in 1972.
- **Global Survey Mission:** L8 data systematically build and periodically refresh a global archive of Sun-lit, substantially cloud-free images of the Earth's landmass.
- **Free Standard Data Products:** L8 data products are available through the U.S. Geological Survey (USGS) Earth Resources Observation and Science (EROS) Center at no charge.
- **Radiometric and Geometric Calibration:** Data from the two sensors, the Operational Land Imager (OLI) and the Thermal Infrared Sensor (TIRS), are calibrated to better than 5 percent uncertainty in terms of Top Of Atmosphere (TOA) reflectance or absolute spectral radiance, and have an absolute geodetic accuracy better than 65 meters circular error at 90 percent confidence (CE 90).
- **Responsive Delivery:** Automated request processing systems provide products electronically within 48 hours of order (normally much faster).

The continuation of the Landsat Program is an integral component of the U.S. Global Change Research Program (USGCRP) and will address a number of science priorities, such as land cover change and land use dynamics. L8 is part of a global research

program known as National Aeronautics and Space Administration's (NASA's) Science Mission Directorate (SMD), a long-term program that studies changes in Earth's global environment. In the Landsat Program tradition, L8 continues to provide critical information to those who characterize, monitor, manage, explore, and observe the land surfaces of the Earth over time.

The USGS has a long history as a national leader in land cover and land use mapping and monitoring. Landsat data, including L8 and archive holdings, are essential for USGS efforts to document the rates and causes of land cover and land use change, and to address the linkages between land cover and use dynamics on water quality and quantity, biodiversity, energy development, and many other environmental topics. In addition, the USGS is working toward the provision of long-term environmental records that describe ecosystem disturbances and conditions.

1.2 Background

The Land Remote Sensing Policy Act of 1992 (U.S. Code Title 15, Chapter 82) directed the Federal agencies involved in the Landsat Program to study options for a successor mission to Landsat 7 (L7), ultimately launched in 1999 with a five-year design life, that maintained data continuity with the Landsat System. The Act further expressed a preference for the development of this successor System by the private sector as long as such a development met the goals of data continuity.

The L8 Project suffered several setbacks in its attempt to meet these data continuity goals. Beginning in 2002, three distinct acquisition and implementation strategies were pursued: (1) the purchase of Observatory imagery from a commercially owned and operated satellite system partner (commonly referred to as a government "data buy"), (2) flying a Landsat instrument on National Oceanic and Atmospheric Administration's (NOAA's) National Polar-orbiting Operational Environmental Satellite System (NPOESS) series of satellites, and finally (3) the selection of a "free-flying" Landsat satellite. As a result, the Project incurred considerable delays to L8 implementation. The matter was not resolved until 2007, when it was determined that NASA would procure the next mission space segment and the USGS would develop the Ground System and operate the mission after launch.

The basic L8 requirements remained consistent through this extended strategic formulation phase of mission development. The 1992 Land Remote Sensing Policy Act (U.S. Code Title 15, Chapter 82) established data continuity as a fundamental goal and defined continuity as providing data "sufficiently consistent (in terms of acquisition geometry, coverage characteristics, and spectral characteristics) with previous Landsat data to allow comparisons for global and regional change detection and characterization." This direction has provided the guiding principal for specifying L8 requirements from the beginning, with the most recently launched Landsat satellite at that time, L7, serving as a technical minimum standard for system performance and data quality.

1.2.1 Previous Missions

Landsat satellites have provided multispectral images of the Earth continuously since the early 1970s. A unique 403-year+ data record of the Earth's land surface now exists. This unique retrospective portrait of the Earth's surface has been used across disciplines to achieve an improved understanding of the Earth's land surfaces and the impact of humans on the environment. Landsat data have been used in a variety of government, public, private, and national security applications. Examples include land and water management, global change research, oil and mineral exploration, agricultural yield forecasting, pollution monitoring, land surface change detection, and cartographic mapping.

L8 is the latest satellite in this series. The first was launched in 1972 with two Earth-viewing imagers - a Return Beam Vidicon (RBV) and an 80-meter 4-band Multispectral Scanner (MSS). Landsat 2 and Landsat 3, launched in 1975 and 1978 respectively, were configured similarly. In 1984, Landsat 4 was launched with the MSS and a new instrument called the Thematic Mapper (TM). Instrument upgrades included improved ground resolution (30 meters) and 3 new channels or bands. In addition to using an updated instrument, Landsat 4 made use of the Multimission Modular Spacecraft (MMS), which replaced the Nimbus-based spacecraft design employed for Landsat 1-Landsat 3. Landsat 5, a duplicate of Landsat 4, was launched in 1984 and returned scientifically viable data for 28 years - 23 years beyond its 5-year design life. Landsat 6, equipped with an additional 15-meter panchromatic band, was lost immediately after launch in 1993.

Finally, L7 was launched in 1999 and performed nominally until its Scan Line Corrector (SLC) failed in May 2003. Since that time, L7 has continued to acquire useful image data in the "SLC-off" mode. All L7 SLC-off data are of the same high radiometric and geometric quality as data collected prior to the SLC failure.

Figure 1-1 shows the continuity of multispectral data coverage provided by Landsat missions, beginning with Landsat 1 in 1972.

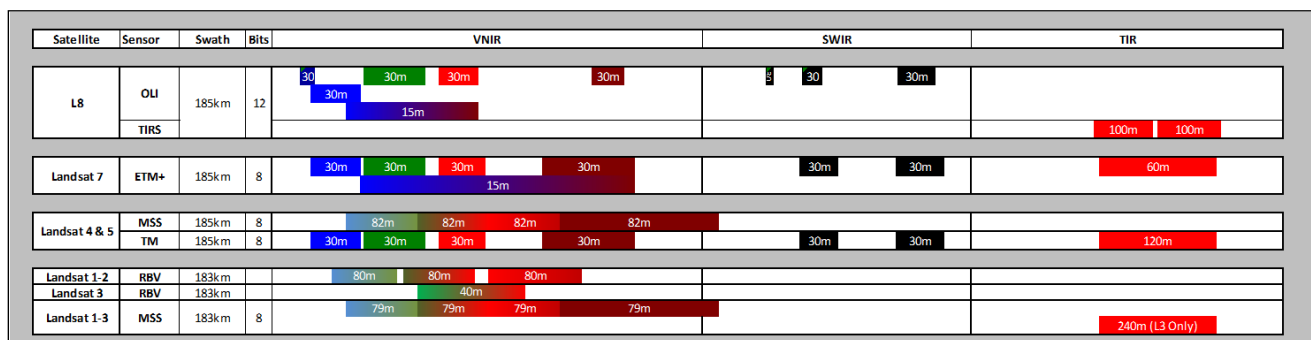


Figure 1-1. Continuity of Multispectral Data Coverage Provided by Landsat Missions

1.2.2 Operations and Management

The L8 management structure is composed of an ongoing partnership between NASA and USGS for sustainable land imaging. NASA contracted with Ball Aerospace & Technologies Corp. (BATC) to develop the OLI and with Orbital Sciences Corporation to build the spacecraft. NASA Goddard Space Flight Center (GSFC) built the TIRS. NASA was also responsible for the satellite launch and completion of a 90-day on-orbit checkout before handing operations to the USGS. The USGS was responsible for the development of the Ground System and is responsible for operation and maintenance of the Observatory and the Ground System for the life of the mission. In this role, the USGS captures, processes, and distributes L8 data and maintains the L8 data archive.

The Landsat Project at the USGS EROS Center manages the overall L8 mission operations. In this capacity, USGS EROS directs on-orbit flight operations, implements mission policies, directs acquisition strategy, and interacts with International Ground Stations (IGSs). USGS EROS captures L8 data and performs pre-processing, archiving, product generation, and distribution functions. USGS EROS also provides a public interface into the archive for data search and ordering.

1.3 Landsat 8 Mission

The L8 mission objective is to provide timely, high-quality visible and infrared images of all landmass and near-coastal areas on the Earth, continually refreshing an existing Landsat database. Data input into the system are sufficiently consistent with currently archived data in terms of acquisition geometry, calibration, coverage, and spectral characteristics to allow for comparison of global and regional change detection and characterization.

1.3.1 Overall Mission Objectives

L8 has a design life of 5 years and carries 10 years of fuel consumables. The overall objectives of the L8 mission are as follows:

- Provide data continuity with Landsat 4, 5, and 7.
- Offer 16-day repetitive Earth coverage, an 8-day repeat with an L7 offset.
- Build and periodically refresh a global archive of Sun-lit, substantially cloud-free land images.

1.3.2 System Capabilities

The L8 System is robust, high performing, and of extremely high data quality. System capabilities include the following:

- Provides for a systematic collection of global, high-resolution, multispectral data.
- Provides for a high volume of data collection. Unlike previous missions, L8 far surpasses the average collection of 400 scenes per day. L8 routinely surpasses 650 scenes per day imaged and collected in the USGS archive.
- Uses cloud cover predictions to avoid acquiring less useful data.
- Ensures all data imaged are collected by a U.S. Ground Station.

The L8 Observatory offers many improvements over its predecessor, L7. See Table 1-1 for a high-level comparison of L7 and L8 Observatory capabilities. The following subsections contain further details.

	Landsat 7	Landsat 8
Scenes/Day	~450	~650
SSR Size	378 Gbits, block-based	3.14 Terafit, file-based
Sensor Type	ETM+, Whisk-Broom	Pushbroom (both OLI and TIRS)
Compression	NO	~2.1 Variable Rice Compression
Image D/L	X-Band GXA ×3	X-Band Earth Coverage
Data Rate	150 M bits/sec × 3 Channels/Frequencies	384 M bits/sec, CCSDS Virtual Channels
Encoding	not fully CCSDS compliant	CCSDS, LDPC FEC
Ranging	S-Band 2-Way Doppler	GPS
Orbit	705 km Sun-Sync 98.2° inclination (WRS-2)	705 km Sun-Sync 98.2° inclination (WRS-2)
Crossing Time	~10:00 AM	~10:11 AM

Table 1-1. Comparison of Landsat 7 and Landsat 8 Observatory Capabilities

1.3.3 Global Survey Mission

An important operational strategy of the L8 mission is to establish and maintain a global survey data archive. L8 follows the same Worldwide Reference System (WRS) used for Landsat 4, 5, and 7, bringing the entire world within view of its sensors once every 16 days.

In addition, similar to L7, L8 operations endeavor to systematically capture Sun-lit, substantially cloud-free images of the Earth's entire land surface. Initially developed for L7, the Long Term Acquisition Plan (LTAP) for L8 defines the acquisition pattern for the mission in order to create and update the global archive to ensure global continuity.

1.3.4 Rapid Data Availability

L8 data are downlinked and processed into standard products within 24 hours of acquisition. Level 0 Reformatted (L0R), Level 1 Systematic Terrain (Corrected) (L1Gt), Level 1 Terrain (Corrected) (L1T), and LandsatLook products are available through the User Portal (UP). All users must register through EarthExplorer at <http://earthexplorer.usgs.gov>.

All products are accessible via the Internet for download via Hypertext Transfer Protocol (HTTP); there are no product media options.

As with all Landsat data, products are available at no cost to the user. The user can view available data through the following interfaces:

1. EarthExplorer: <http://earthexplorer.usgs.gov>
2. Global Visualization Viewer: <http://glovis.usgs.gov>
3. LandsatLook Viewer: <http://landsatlook.usgs.gov>

1.3.5 International Ground Stations (IGSs)

Landsat has worked cooperatively with IGSs for decades. For the first time in the history of the Landsat mission, all data downlinked to IGSs are written to the Solid State Recorder (SSR) and downlinked to USGS EROS for inclusion in the USGS Landsat archive. No unique data are held at the IGSs. For updated information and a map displaying the IGSs, please see the following:

http://landsat.usgs.gov/about_ground_stations.php.

1.4 Document Purpose

This Landsat 8 (L8) Data Users Handbook is a living document prepared by the USGS Landsat Project Science Office at the EROS Center in Sioux Falls, SD, and the NASA Landsat Project Science Office at NASA's GSFC in Greenbelt, Maryland. The purpose of this handbook is to provide a basic understanding and associated reference material for the L8 Observatory and its science data products.

1.5 Document Organization

This document contains the following sections:

- Section 1 provides a Landsat Program foreword and introduction
- Section 2 provides an overview of the L8 Observatory
- Section 3 provides an overview of instrument calibration
- Section 4 discusses Level 1 Products
- Section 5 addresses the conversion of product Digital Numbers (DNs) to physical units
- Section 6 identifies data search and access portals
- Appendix A addresses known issues associated with L8 data
- Appendix B displays the metadata file
- The References section contains a list of applicable documents

Section 2 Observatory Overview

The L8 Observatory is designed for a 705 km, Sun-synchronous orbit, with a 16-day repeat cycle, completely orbiting the Earth every 98.9 minutes. S-Band is used for commanding and housekeeping telemetry operations, while X-Band is used for instrument data downlink. A 3.14 terabit SSR brings back an unprecedented number of images to the USGS EROS Center archive.

L8 carries a two-sensor payload: the OLI, built by the BATC, and the TIRS, built by the NASA GSFC. Both the OLI and TIRS sensors simultaneously image every scene, but are capable of independent use if a problem in either sensor arises. In normal operation, the sensors view the Earth at-nadir on the Sun-synchronous Worldwide Reference System-2 (WRS-2) orbital path, but special collections may be scheduled off-nadir. Both sensors offer technical advancements over earlier Landsat instruments. The spacecraft with its two integrated sensors is referred to as the L8 Observatory.

2.1 Concept of Operations

The fundamental L8 operations concept is to collect, archive, process, and distribute science data in a manner consistent with the operation of the L7 satellite system. To that end, the L8 Observatory operates in a near-circular, near-polar, Sun-synchronous orbit with a 705 km altitude at the Equator. The Observatory has a 16-day ground track repeat cycle with an equatorial crossing at 10:11 a.m. (+/-15 min) mean local time during the descending node. In this orbit, the L8 Observatory follows a sequence of fixed ground tracks (also known as paths) defined by the WRS-2 (a path / row coordinate system used to catalog all of the science image data acquired from the Landsat 4-8 satellites). The L8 launch and initial orbit adjustments placed the Observatory in an orbit to ensure an 8-day offset between L7 and L8 coverage of each WRS-2 path.

The Mission Operation Center (MOC) sends commands to the satellite once every 24 hours via S-Band communications from the Ground System to schedule daily data collections. Long Term Acquisition Plan-8 (LTAP-8) sets priorities for collecting data along the WRS-2 ground paths covered in a particular 24-hour period. LTAP-8 is modeled on the systematic data acquisition plan developed for L7 (Arvidson et al., 2006). OLI and TIRS collect data jointly to provide coincident images of the same

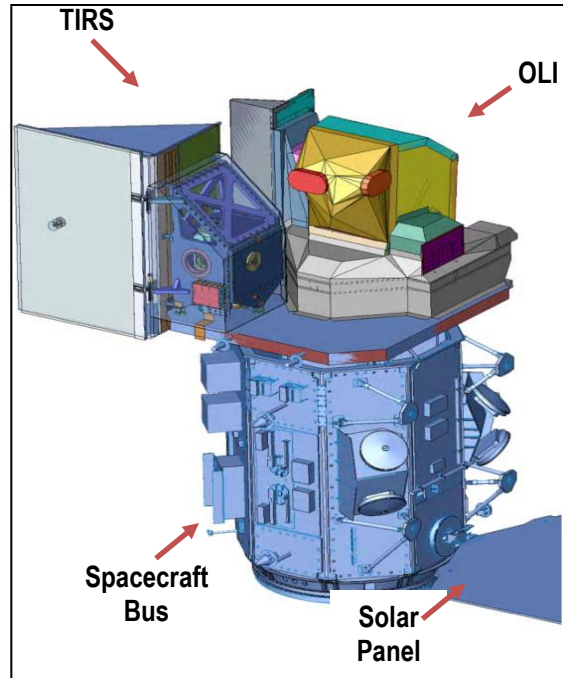


Figure 2-1. Illustration of Landsat 8 Observatory

surface areas. The MOC nominally schedules the collection of 400 OLI and TIRS scenes per day, where each scene covers a 190-by-180 km surface area. The objective of scheduling and data collection is to provide near cloud-free coverage of the global landmass for each season of the year. Since the 2014 growing season, however, the L8 mission has been routinely acquiring approximately 725 scenes per day.

The L8 Observatory initially stores OLI and TIRS data on board in an SSR. The MOC commands the Observatory to transmit the stored data to the ground via an X-Band data stream from an all-Earth omni antenna. The L8 Ground Network (GN) receives the data at several stations, and these stations forward the data to the EROS Center. The GN includes international stations (referred to as International Cooperators (ICs)) operated under the sponsorship of foreign governments. Data management and distribution by the ICs is in accordance with bilateral agreements between each IC and the U.S. Government.

The data received from the GN are stored and archived at the EROS Center, where L8 data products are also generated. The OLI and TIRS data for each WRS-2 scene are merged to create a single product containing the data from both sensors. The data from both sensors are radiometrically corrected and co-registered to a cartographic projection, with corrections for terrain displacement resulting in a standard orthorectified digital image called the Level 1T product. The interface to the L8 data archive is called the UP, and it allows anyone to search the archive, view browse images, and request data products that are distributed electronically through the Internet at no charge (see Section 6).

2.2 Operational Land Imager (OLI)

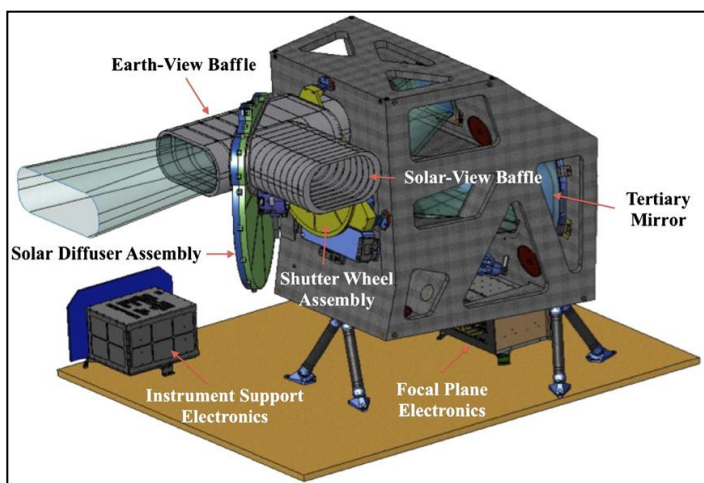


Figure 2-2. OLI Instrument

instrument focal planes collect imagery in a “push-broom” manner, resulting in a more sensitive instrument with fewer moving parts. OLI has a 4-mirror telescope, and data

The OLI sensor, which has a five-year design life, is similar in design to the Advanced Land Imager (ALI) that was included on Earth Observing 1 (EO-1), and represents a significant technological advancement over L7's Enhanced Thematic Mapper Plus (ETM+) sensor. Instruments on earlier Landsat satellites employed oscillating mirrors to sweep the detectors' Field of View (FOV) across the swath width (“whisk-broom”), but OLI instead uses long linear detector arrays with thousands of detectors per spectral band. Detectors aligned across the

generated by OLI are quantized to 12 bits, compared to the 8-bit data produced by the TM and ETM+ sensor.

The OLI sensor collects image data for 9 shortwave spectral bands over a 190 km swath, with a 30 m spatial resolution for all bands except the 15 m panchromatic band. The widths of several OLI bands are refined to avoid atmospheric absorption features within ETM+ bands. The biggest change occurs in OLI Band 5 (0.845–0.885 μm) to exclude a water vapor absorption feature at 0.825 μm in the middle of the ETM+ near-infrared band (Band 4; 0.775–0.900 μm). The OLI panchromatic band, Band 8, is also narrower relative to the ETM+ panchromatic band to create greater contrast between vegetated areas and land without vegetation cover. OLI also has two new bands in addition to the legacy Landsat bands (1-5, 7, and Pan). The Coastal / Aerosol band (Band 1; 0.435-0.451 μm), principally for ocean color observations, is similar to ALI's band 1', and the new Cirrus band (Band 9; 1.36-1.38 μm) aids in the detection of thin clouds comprised of ice crystals (cirrus clouds appear bright, while most land surfaces appear dark through an otherwise cloud-free atmosphere containing water vapor).

Landsat-7 ETM+ Bands (μm)			Landsat-8 OLI and TIRS Bands (μm)		
			30 m Coastal/Aerosol	0.435 - 0.451	Band 1
Band 1	30 m Blue	0.441 - 0.514	30 m Blue	0.452 - 0.512	Band 2
Band 2	30 m Green	0.519 - 0.601	30 m Green	0.533 - 0.590	Band 3
Band 3	30 m Red	0.631 - 0.692	30 m Red	0.636 - 0.673	Band 4
Band 4	30 m NIR	0.772 - 0.898	30 m NIR	0.851 - 0.879	Band 5
Band 5	30 m SWIR-1	1.547 - 1.749	30 m SWIR-1	1.566 - 1.651	Band 6
Band 6	60 m TIR	10.31 - 12.36	<i>100 m TIR-1</i>	<i>10.60 – 11.19</i>	Band 10
			<i>100 m TIR-2</i>	<i>11.50 – 12.51</i>	Band 11
Band 7	30 m SWIR-2	2.064 - 2.345	30 m SWIR-2	2.107 - 2.294	Band 7
Band 8	15 m Pan	0.515 - 0.896	15 m Pan	0.503 - 0.676	Band 8
			30 m Cirrus	1.363 - 1.384	Band 9

Table 2-1. OLI and TIRS Spectral Bands Compared to ETM+ Spectral Bands

OLI has stringent radiometric performance requirements and is required to produce data calibrated to an uncertainty of less than five percent in terms of absolute, at-aperture spectral radiance and to an uncertainty of less than three percent in terms of TOA spectral reflectance for each of the spectral bands in Table 2-1. These values are comparable to the uncertainties achieved by ETM+ calibration.

The OLI Signal-to-Noise ratio (SNR) specifications, however, were set higher than ETM+ performance based on results from the ALI. Table 2-2 and Figure 2-3 show the OLI specifications and performance compared to ETM+ performance for signal-to-noise ratios at specified levels of typical spectral radiance (L_{typical}) for each spectral band.

Ltypical SNR				
<u>ETM + Band</u>	<u>OLI Band</u>	<u>ETM+ Performance</u>	<u>OLI Requirement</u>	<u>OLI Performance</u>
N/A	1	N/A	130	238
1	2	40	130	364
2	3	41	100	302
3	4	28	90	227
4	5	35	90	204
5	6	36	100	265
7	7	29	100	334
78	8	16	80	149
N/A	9	N/A	50	165

Table 2-2. OLI Specified and Performance Signal-to-Noise (SNR) Ratios Compared to ETM+ Performance

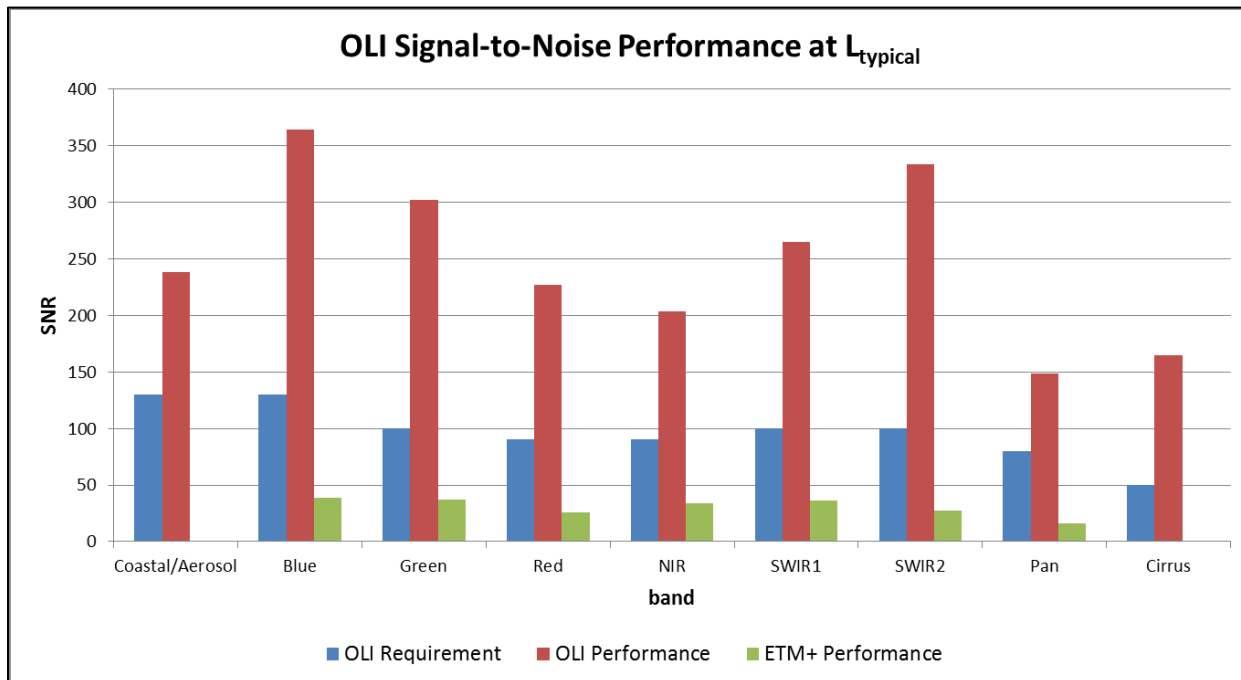


Figure 2-3. OLI Signal-To-Noise (SNR) Performance at L_{typical}

The OLI is a push-broom sensor that employs a four-mirror anastigmatic telescope that focuses incident radiation onto the focal plane while providing a 15-degree FOV covering the 190 km across-track ground swath from the nominal L8 Observatory altitude. Periodic sampling of the across-track detectors as the Observatory flies forward along a ground track forms the multispectral digital images. The detectors are divided into 14 identical Sensor Chip Assemblies (SCAs) arranged in an alternating pattern along the centerline of the focal plane (Figure 2-4).

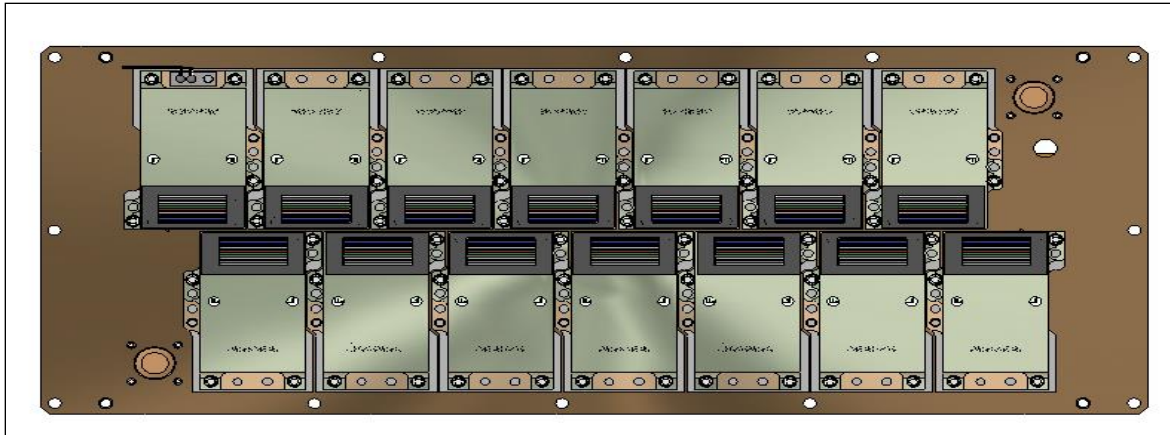


Figure 2-4. OLI Focal Plane

Each SCA consists of rows of detectors, a Read-Out Integrated Circuit (ROIC), and a nine-band filter assembly. Data are acquired from 6916 across-track detectors for each spectral band (494 detectors per SCA), with the exception of the 15 m panchromatic band, which contains 13,832 detectors. The spectral differentiation is achieved by interference filters arranged in a “butcher-block” pattern over the detector arrays in each module. Even- and odd-numbered detector columns are staggered and aligned with the satellite’s flight track. Even-numbered SCAs are the same as odd-numbered SCAs, only the order of the detector arrays is reversed top to bottom. The detectors on the odd and even SCAs are oriented such that they look slightly off-nadir in the forward and aft viewing directions. This arrangement allows for a contiguous swath of imagery as the push-broom sensor flies over the Earth, with no moving parts. One redundant detector per pixel is in each Visible and Near Infrared (VNIR) band, and two redundant detectors per pixel are in each Short Wavelength Infrared (SWIR) band. The spectral response from each unique detector corresponds to an individual column of pixels within the Level 0 product.

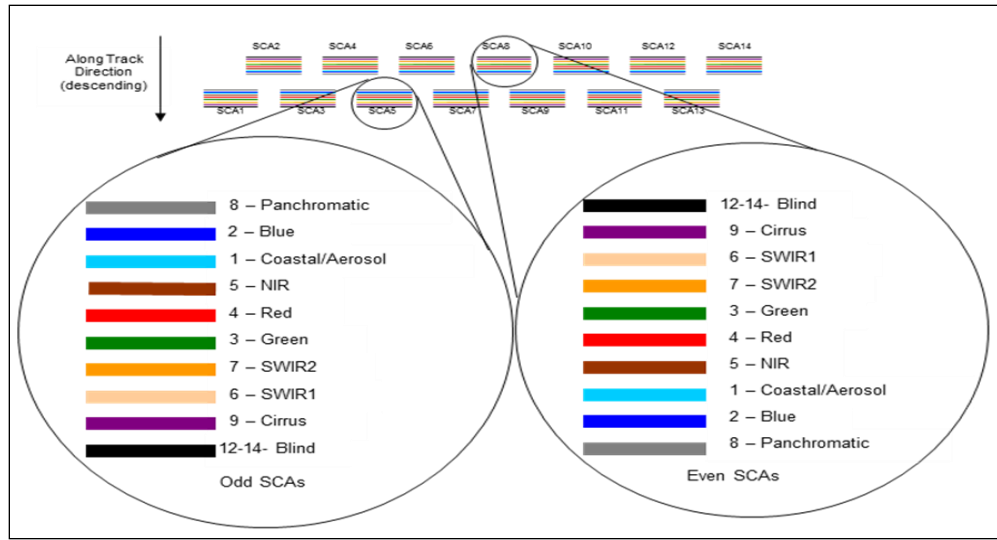


Figure 2-5. Odd / Even SCA Band Arrangement

Silicon PIN (SiPIN) detectors collect the data for the visible and near-infrared spectral bands (Bands 1 to 4 and 8). Mercury–Cadmium–Telluride (MgCdTe) detectors are used for the shortwave infrared bands (Bands 6, 7, and 9). An additional ‘blind’ band is shielded from incoming light and used to track small electronic drifts. There are 494 illuminated detectors per SCA, per band (988 for the PAN band); therefore, 70,672 operating detectors must be characterized and calibrated during nominal operations.

2.3 Thermal Infrared Sensor (TIRS)

Like OLI, TIRS is a push-broom sensor employing a focal plane with long arrays of photosensitive detectors. TIRS uses Quantum Well Infrared Photodetectors (QWIPs) to measure longwave Thermal Infrared (TIR) energy emitted by the Earth’s surface, the intensity of which is a function of surface temperature. The TIRS QWIPs are sensitive to two thermal infrared wavelength bands, enabling separation of the temperature of the Earth’s surface from that of the atmosphere. QWIPs’ design operates on the complex principles of quantum mechanics. Gallium arsenide semiconductor chips trap electrons in an energy state ‘well’ until the electrons are elevated to a higher state by thermal infrared light of a certain wavelength. The elevated electrons create an electrical signal that can be read out, recorded, translated to physical units, and used to create a digital image.

The TIRS sensor, which has a three-year design life, collects image data for two thermal bands with a 100

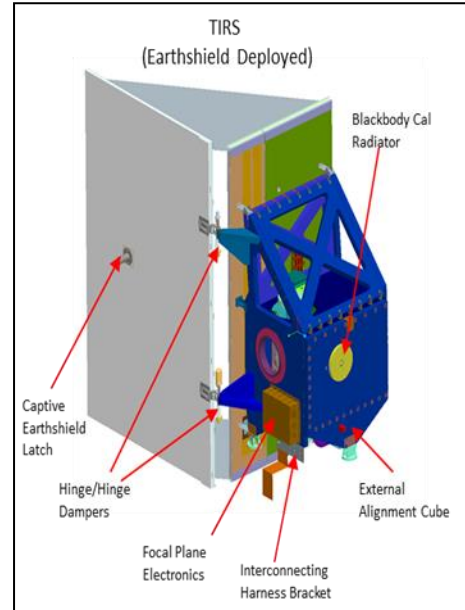


Figure 2-6. TIRS Instrument with Earthshield Deployed

m spatial resolution over a 190 km swath. The two thermal infrared bands encompass the wavelength range of the broader TM and ETM+ thermal bands (10.0–12.5 μm), and represent an advancement over the single-band thermal data. Data generated by TIRS are quantized to 12 bits. Although TIRS has a lower spatial resolution than the 60 m ETM+ Band 6, the dual thermal bands should theoretically enable retrieval of surface temperature, but stray light issues with Band 11 preclude the use of this approach.

Like OLI, the TIRS requirements also specify cross-track spectral uniformity; radiometric performance including absolute calibration uncertainty, polarization sensitivity, and stability; ground sample distance and edge response; and image geometry and geolocation, including spectral band co-registration. The TIRS noise limits (Table 2-3) are specified in terms of noise-equivalent-change-in-temperature (NE Δ T) rather than the signal-to-noise ratios used for OLI specifications. The radiometric calibration uncertainty is specified to be less than 2 percent in terms of absolute, at-aperture spectral radiance for targets between 260 K and 330 K (less than 4 percent for targets between 240 K and 260 K and for targets between 330 K and 360 K), which is much lower than ETM+ measurements between 272 K and 285 K. Currently, the performance of TIRS Band 11 is slightly out of specification because of stray light entering the optical path.

TIRS Noise-Equivalent-Change-in-Temperature (NE Δ T)				
Band	NEDT@240	NEDT@280	NEDT@320	NEDT@360
TIRS 10	0.069	0.053	0.046	0.043
TIRS 11	0.079	0.059	0.049	0.045
ETM+		0.22		

Table 2-3. TIRS Noise-Equivalent-Change-in Temperature (NE Δ T)

The TIRS focal plane contains three identical SCAs, each with rows of QWIPs (Figure 2-7). The QWIP detectors sit between a ROIC and a two-band filter assembly. An additional masked or 'dark' band is used for calibration purposes. TIRS has 640 illuminated detectors per SCA, with approximately 27-pixel overlap to ensure there are no spatial gaps. Each TIRS SCA consists of a 640-column by 512-row grid of QWIP detectors. Almost all of the detectors are obscured except for two slits that contain the spectral filters for the 12.0 μm and 10.8 μm bands. These filters provide unvignetted illumination for approximately 30 rows of detectors under each filtered region.

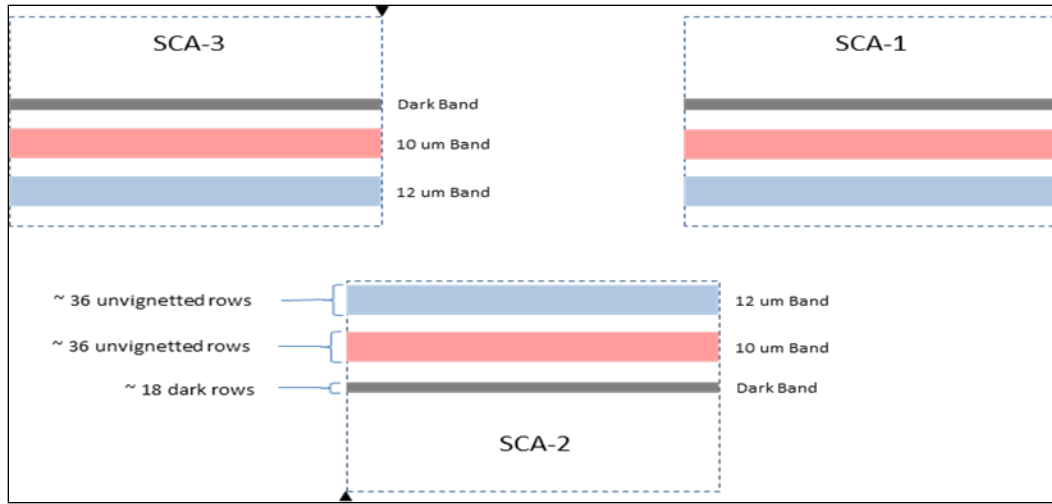


Figure 2-7. TIRS Focal Plane

Thermal energy enters the TIRS instrument through a scene select mirror and a series of four lenses before illuminating the QWIP detectors on the Focal Plane Array (FPA). Two rows of detector data from each filtered region are collected, with pixels from the second row used only as substitutes for any inoperable detectors in the primary row. The Calibration Parameter File (CPF) specifies these rows.

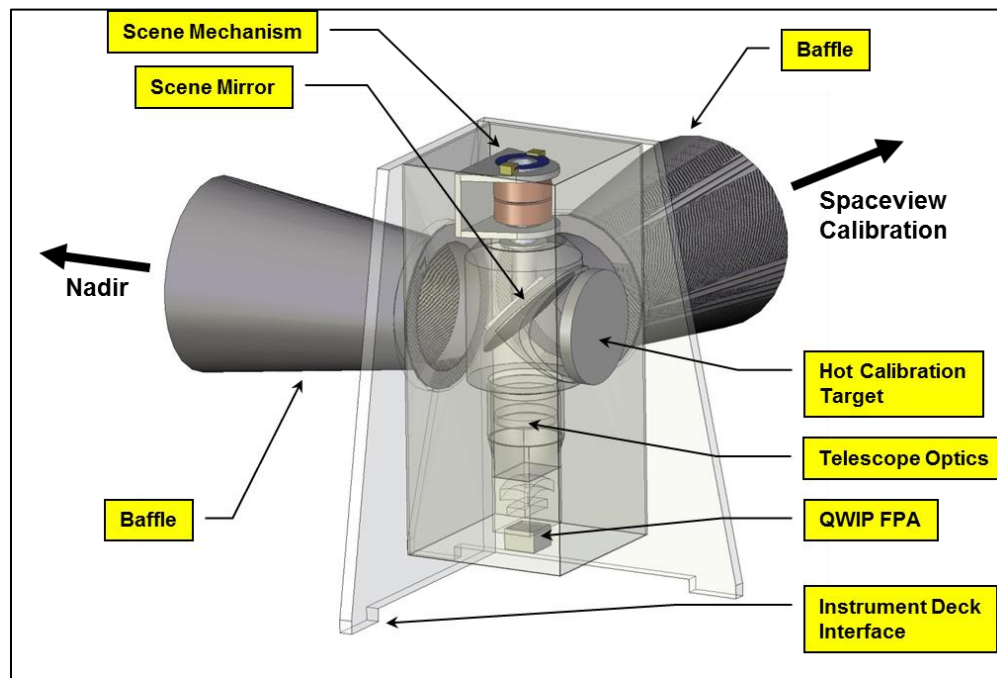


Figure 2-8. TIRS Optical Sensor Unit

2.4 Spacecraft Overview

Orbital Sciences Corporation built the L8 spacecraft at their spacecraft manufacturing facility in Gilbert, Arizona. The contract to build the spacecraft was originally awarded to

General Dynamics Advanced Information Systems (GDAIS) in April 2008, but was subsequently acquired by Orbital Sciences Corporation in 2010. Orbital assumed responsibility for the design and fabrication of the L8 spacecraft bus, integration of the two sensors onto the bus, satellite level testing, on-orbit satellite checkout, and continuing on-orbit engineering support under GSFC contract management (Irons & Dwyer, 2010). The specified design life is 5 years, with an additional requirement to carry sufficient fuel to maintain the L8 orbit for 10 years. However, the hope is that the operational lives of the sensors and spacecraft will exceed the design lives and fuel will not limit extended operations.

The spacecraft supplies power, orbit and attitude control, communications, and data storage for OLI and TIRS. The spacecraft consists of the mechanical subsystem (primary structure and deployable mechanisms), command and data handling subsystem, attitude control subsystem, electrical power subsystem, Radio Frequency (RF) communications subsystem, the hydrazine propulsion subsystem, and thermal control subsystem. All of the components, except for the propulsion module, are mounted on the exterior of the primary structure. A 9×0.4 m deployable Sun-tracking solar array generates power that charges the spacecraft's 125 amp-hour nickel-hydrogen (Ni-H₂) battery. A 3.14-terabit solid-state data recorder provides data storage aboard the spacecraft, and an Earth-coverage X-Band antenna transmits OLI and TIRS data either in real time or played back from the data recorder. The OLI and TIRS are mounted on an optical bench at the forward end of the spacecraft. Fully assembled, the spacecraft without the instruments is approximately 3 m high and 2.4×2.4 m across, with a mass of 2071 kg fully loaded with fuel.

2.4.1 Spacecraft Data Flow Operations

The L8 Observatory receives a daily load of software commands transmitted from the ground. These command loads tell the Observatory when to capture, store, and transmit image data from the OLI and TIRS. The daily command load covers the subsequent 72 hours of operations, with the commands for the overlapping 48 hours overwritten each day. This precaution is taken to ensure that sensor and spacecraft operations continue in the event of a one- or two-day failure to successfully transmit or receive commands. The Observatory's Payload Interface Electronics (PIE) ensures that image intervals are captured in accordance with the daily command loads. The OLI and TIRS are powered on continuously during nominal operations to maintain the thermal balance of the two instruments. The two sensors' detectors continuously produce signals that are digitized and sent to the PIE at an average rate of 265 megabits per second (Mbps) for the OLI and 26.2 Mbps for TIRS.

Ancillary data, such as sensor and select spacecraft housekeeping telemetry, calibration data, and other data necessary for image processing, are also sent to the PIE. The PIE receives the OLI, TIRS, and ancillary data, merges these data into a Mission Data stream, identifies the Mission Data intervals scheduled for collection, and performs a lossless compression of the OLI data (TIRS data are not compressed) using the Rice algorithm (Rice et al., 1993). The PIE then sends the compressed OLI data and the uncompressed TIRS data to the 3.14 terabit SSR. The PIE also identifies the

image intervals scheduled for real-time transmission and sends those data directly to the Observatory's X-Band transmitter. The IC receiving stations only receive real-time transmissions, and the PIE also sends a copy of these data to the onboard SSR for playback and transmission to the L8 Ground Network Element (GNE) receiving stations (USGS captures all of the data transmitted to ICs). OLI and TIRS collect data coincidently; therefore, the Mission Data streams from the PIE contain both OLI and TIRS data as well as ancillary data.

The Observatory broadcasts Mission Data files from its X-Band, Earth-coverage antenna. The transmitter sends data to the antenna on multiple virtual channels, providing for a total data rate of 384 Mbps. The Observatory transmits real-time data, SSR playback data, or both real-time data and SSR data, depending on the time of day and the Ground Stations within view of the satellite. Transmissions from the Earth coverage antenna allow a Ground Station to receive Mission Data as long as the Observatory is within view of the station antenna. OLI and TIRS collect the L8 science data. The spacecraft bus stores the OLI and TIRS data on an onboard SSR and then transmits the data to ground receiving stations.

The Ground System provides the capabilities necessary for planning and scheduling the operations of the L8 Observatory and the capabilities necessary to manage the science data following transmission from the spacecraft. The real-time command and control subsystem for Observatory operations is known as the Mission Operations Element (MOE). A primary and back-up MOC house the MOE, with the primary MOC residing at NASA GSFC. The Data Processing and Archiving System (DPAS) at the EROS Center ingests, processes, and archives all L8 science and Mission Data returned from the Observatory. The DPAS also provides a public interface to allow users to search for and receive data products over the Internet (see Section 6).

Section 3 Instrument Calibration

3.1 Radiometric Characterization and Calibration Overview

The L8 calibration activities began early in the instrument development phases and continued through On-orbit Initialization and Verification (OIV) and on through mission operations. This section describes the instrument calibration activities for the OLI and TIRS from development and preflight testing, through OIV, and into nominal mission operations, as this is how the verification of instrument performance requirements proceeded. Table 3-1 provides a summary of the various calibration measurements.

	Purpose	How this is used to develop calibration parameters
OLI Preflight Activity		
Radiance of integrating sphere measured at multiple illumination levels	Establish linearity of detectors and focal plane electronics	Known radiance levels of the integrating sphere allow for linearity coefficients to be determined
Integration time sweeps of integrating sphere	Establish linearity of detectors and focal plane electronics	Known effective radiance levels allow for linearity coefficients to be determined and compared to multiple illumination levels of the integrating sphere; these measurements can be repeated on-orbit
Heliostat illumination of the solar diffusers	Derive a measure of the transmission of the heliostat and the reflectance of the solar diffuser panels	Verify effectiveness of the solar diffuser panels on-orbit
Measurement of the spectral reflectance of the solar diffuser panels	Determine in-band spectral reflectance of the solar diffuser panels	With the known spectral reflectance of the solar diffuser panels, coefficients are determined to convert the OLI response, in DNs, to spectral reflectance
Measurement of the Bi-directional Reflectance Distribution Function (BRDF) of the solar diffuser panels	Determine the reflectance of the solar diffuser panels in on-orbit orientation	Also to determine the coefficients to convert the OLI response to spectral reflectance
Transfer radiometer measurements of the integrating sphere and solar diffuser panels at the same illumination levels as measured by the OLI	Ensure traceability of the measurements compared to those made from the solar diffuser panels	Changes to the spectral response of the instrument are determined by inflight measurements of the solar diffuser panels, and coefficients used to scale the digital numbers of the instrument response to calibrated radiances can be adjusted
SNR measured at multiple radiance levels from the integrating sphere (or solar diffuser panel)	Requirements verification and characterization of radiometric performance	

	Purpose	How this is used to develop calibration parameters
Wide-field collimator measurements of fixed geometric test patterns	To build an optical map of the detectors	Enables construction of a Line Of Sight (LOS) model from the focal plane to the Earth
Wide-field collimator measurements of fixed geometric test patterns with different reticle plates	To derive line spread functions, edge response, and modulation transfer function	
TIRS Preflight Activity		
Flood source controlled heating of louvered plate	Temperatures across the surface of the plate are analyzed to characterize the uniformity of the radiometric response across the detectors within the focal plane and across the multiple SCAs	Known radiance levels of the flood source at different temperatures allow for linearity coefficients to be determined
Integration time sweeps of flood source	Establish linearity of detectors and focal plane electronics	Known effective radiance levels allow for linearity coefficient to be determined and compared to multiple flood source temperatures; these can be repeated on-orbit
A wide-field collimator and a set of fixed geometric patterns are scanned across the focal plane	To build an optical map of the detectors	Enables construction of a LOS model from the focal plane to the Earth
A wide-field collimator and a set of fixed geometric patterns are scanned across the focal plane at multiple temperature settings	To derive line spread functions, edge response, and modulation transfer function	
OLI On-Orbit Activities		
Integration time sweeps of solar diffuser	Characterize detector linearity	Potentially update linearization coefficients
Solar diffuser collects	Noise characterization including SNR, absolute radiometric accuracy characterization, uniformity characterization, radiometric stability characterization, relative gain calibration, absolute calibration (both radiance and reflectance)	The known reflectance of the diffuser panel is used to derive updated relative and absolute calibration coefficients
Long dark collects	Radiometric stability and noise (impulse noise, white noise, coherent noise and 1/f noise) characterization	
Extended solar diffuser collects	Monitor the detector stability (within-scene)	
Stimulation lamps data collects	Monitor the detector stability over days	
Side-slither maneuver	Characterize detector relative gains, in order to improve uniformity by reducing striping	Scanning the same target with detectors in line enable updated relative gains to be calculated
Focal Plane Module (FPM) overlap statistics	Normalize the gain of all the SCAs, to improve uniformity	Relative gain characterization

	Purpose	How this is used to develop calibration parameters
Cumulative histograms	Characterize striping in imagery	Relative gain characterization
Lunar data collection	Characterize stray light and characterize the absolute radiometric accuracy	
Characterization of Pseudo-Invariant Calibration Sites	Monitoring of temporal stability of OLI and TIRS instruments	Monitoring trends in Pseudo-Invariant Calibration Side (PICS) responses indicates a need for absolute radiometric calibration updates
TIRS On-Orbit Activities		
Integration time sweeps with black body and deep space	Monitor linearity of detectors and focal plane electronics	Determine calibration need to update linearity coefficients
Varying black body temperature over multiple orbits	Characterize detector linearity	
Black body and deep space collects	Noise (Noise Equivalent Detector Radiance ((NEdL))	Relative gain characterization
Long collects (over ocean?)	Coherent noise, 1/f	Relative gain characterization
Vicarious calibration		Absolute radiometric calibration

Table 3-1. Summary of Calibration Activities, their Purpose, and How Measurements are used in Building the Calibration Parameter Files

3.1.1 Instrument Characterization and Calibration

3.1.1.1 Description of Calibration Data Collections

A distinction is made between the calibration activities that measure, characterize, and evaluate instrument and system radiometric performance, and those that are used to derive improved radiometric processing parameters contained in the L8 CPF for use by the Level 1 Product Generation System (LPGS). The measurement and evaluation activities are referred to as characterization operations, while the parameter estimation activities are referred to as calibration. Although both types of activities contribute to the “radiometric calibration” of the L8 OLI and TIRS instruments, the remainder of this document uses the term “characterization” to refer to radiometric assessment and evaluation operations and the term “calibration” to refer to those associated with estimating radiometric processing parameters.

Shutter Collects

Shutter collects provide the individual detector dark levels or biases, which are subtracted during ground processing from each detector's response in Earth images. This removes variations in detector dark current levels, reducing striping and other detector-to-detector uniformity issues in the imagery. These normal shutter collects are acquired before daylight imaging begins and after daylight imaging ends. An extended shutter collect is acquired about every three months and is about 36 minutes in duration. These longer shutter collects provide a measure of stability over typical Earth imaging intervals.

Stimulation Lamp Collects

The stimulation lamps are used to monitor the detector stability over days. While incandescent lamps tend to be poor absolute calibration sources, they excel at showing changes in detector response over relatively short periods. Three sets of stimulation lamps get used at three different frequencies: daily, bimonthly, and every six months. These different usages enable differentiation between detector changes and lamp changes.

Solar Diffuser Collects

The solar diffuser panels provide reflective references that were characterized prior to launch. Their regular use of the primary diffuser enables detector stability to be monitored and potential changes in calibration to be fed back into the ground processing system to maintain accuracy of the Earth imagery products. The second solar diffuser panel is used every six months as a check on stability of the primary (working) diffuser. Longer, 60-second collects of the working solar diffuser are used to monitor the within scene detector response stability. Diffuser collects are also used to characterize the system noise and SNR performance, absolute radiometric accuracy, uniformity, and relative detector gains.

In an additional solar diffuser data collect, the integration time sweep, a series of collects at different detector integration times, is performed at a constant signal level. These collects allow an on-orbit assessment of the OLI detector electronics' linearity. In an attempt to better characterize the OLI's full detector-electronic chain linearity, two extended (60-second) diffuser collects were performed during solar eclipses (November 3, 2013, and April 29, 2014). Here, the uniform diffuser signal was obtained at a significantly lower radiance level than normal (about 40 percent and 10 percent), to allow evaluating and updating relative non-linearities between detectors.

Lunar Collects

Imaging the moon approximately every 28 days enables an independent measure of the OLI radiometric stability, as the moon is an extremely stable source. While the lunar surface is very stable, the viewing geometry can vary dramatically, so the lunar irradiance-based model, Robotic Lunar Observatory, is used to consider the viewing geometry. The lunar collects are also used to evaluate stray light effects and to find any other artifacts that might be visible. The moon is a good source for these artifacts because it is bright compared to the surrounding space.

Side Slither Collects

During a side slither data collect, the spacecraft is yawed 90°, so that the normally cross-track direction of the focal plane is turned along track. Here, each detector in an SCA tracks over nearly identical spots on the ground. By performing these side slither maneuvers over uniform regions of the Earth, individual detector calibration coefficients can be generated to improve the pixel-to-pixel uniformity. These maneuvers are performed over desert or snow / ice regions about every three months to monitor and potentially improve the pixel-to-pixel uniformity.

Examples of characterization activities include assessments of the following:

- The detector response to the solar diffusers, to radiometric accuracy and calibrating detector response
- The 60-second radiometric stability, to evaluate the absolute radiometric uncertainty and detect changes in detector response
- The detector response to stimulation lamp, to evaluate and detect changes in gain
- Radiometric uniformity (Full FOV, banding 1, banding 2, and streaking as defined in the OLI Requirements Document) and all artifacts affecting the radiometric accuracy of the data, and SCA discontinuity differences characterized by gathering statistics information in the overlap areas between the SCAs
- Deep space data and blackbody data to evaluate the absolute radiometric uncertainty of the TIRS instrument and detect changes in gains and biases to determine radiometric stability
- Dropped frames per interval, for trending the total number detected, and excluding flagged dropped frames in all characterization algorithms

Examples of calibration activities include derivation of the following:

- Bias model parameters for each detector. The bias model for OLI is constructed using data from associated shutter images, video reference pixels, dark (masked) detectors, and associated telemetry (e.g., temperatures). The bias model for TIRS uses data from deep space images, dark (masked) detectors, and associated telemetry (e.g., temperatures). These bias model coefficients are used to derive the bias that needs to be subtracted from the detector during product generation.
- The relative gains for all active detectors, to correct the detector responses for "striping" artifacts.
- Gain determination to enable the conversion from DN to radiance and determine the accuracy of the radiometric product.
- The TIRS background response determination.

3.1.2 Prelaunch

Operational Land Imager

Preflight instrument performance and data characterization proceeded from the subsystem level (e.g. focal plane module and electronics) to fully integrated instrument and Observatory testing and analysis. Instrument testing and performance requirements verification were performed at multiple stages of development to ensure the integrity of performance at the component, subsystem, and system levels.

For radiometric calibration of the OLI, an integrating sphere was used as the National Institute of Standards (NIST) traceable radiance source. The OLI was connected to the integrating sphere in a configuration that enabled the instrument to measure the output radiances from a prescribed set of illumination levels from xenon and halogen lamps. In

addition, integration time sweeps of full illumination at successively shorter detector exposure times were used to establish the linearity of the detectors and focal plane module electronics. Measurements of the integrating sphere at various radiance levels were also used to characterize the linearity. These and the integration time sweeps are used to determine the reciprocity between the two.

BATC, the manufacturer of the OLI, used a heliostat to facilitate the Sun as a calibration source for prelaunch testing. The heliostat captured and directed sunlight from the rooftop of the BATC facility to the solar diffuser panels of the instrument placed in a thermal vacuum chamber inside the facility.

The spectral reflectance and BRDF of the panels were characterized at the University of Arizona. A transfer spectroradiometer was used to measure the radiances from the integrating sphere and the solar diffuser panels at the same illumination levels as measured by the OLI to ensure traceability of the measurements compared to those made from the solar diffuser panels. On orbit, any changes to the spectral response of the instrument are determined by inflight measurements of the solar diffuser panels, and coefficients used to scale the DNs of the instrument response to calibrated radiances can be adjusted.

The SNR for each of the OLI spectral bands is characterized at a prescribed radiance level, referred to as $L_{typical}$. The SNR is defined as the mean of the measured radiances divided by their standard deviation. A curve is fit to the SNR at the measured radiance levels and is evaluated at the prescribed $L_{typical}$. The SNR is measured at multiple stages of the instrument build, culminating the testing of the fully integrated instrument. The high SNR combined with the 12-bit quantization of the OLI radiometric response provides data that enhance our ability to measure and monitor subtle changes in the state and condition of the Earth's surface.

The prelaunch verification of instrument and spacecraft radiometric performance specifications was carried out as part of the instrument and spacecraft manufacturers' development, integration, and test programs. The radiometric characteristics of the OLI instrument were measured during instrument fabrication and testing at BATC facility. Because the TIRS instrument is a NASA in-house development, prelaunch characterization and testing was carried out at the NASA GSFC. Additional measurements and tests were performed at Orbital Sciences Corporation (OSC) as the L8 spacecraft was being fabricated and integrated with the OLI and TIRS payloads.

A Horizontal Collimator Assembly (HCA) and a set of fixed geometric patterns are scanned across the focal plane to build an optical map of the detectors that enables construction of a LOS model from the focal plane to the Earth. A similar process is used with a different reticle plate to derive line spread functions. These measurements assist with characterizing the alignment of detectors within a given SCA as well as with aligning adjacent SCAs. These are fundamental parameters required for constructing the geometric models to achieve many of the geometric requirements.

Thermal Infrared Sensor

A louvered plate with stringently controlled heating was used as a flood source and placed within the TIRS FOV so that temperatures across the surface of the plate could be analyzed to characterize the uniformity of the radiometric response across the detectors within the focal plane and across the multiple SCAs. The flood source was measured at multiple temperature levels and at multiple integration time sweeps, in order to characterize the linearity of the detector responses.

A blackbody of known temperature was used as a calibration source to provide radiance to the detectors from which output voltages were converted to DNs. TIRS also measured a space-view port with a cold plate set at 170 K mounted on it, and the DNs output from the instrument were converted to radiance. The blackbody radiances were scaled by a “view factor” that was determined by viewing through the Earth-view (nadir) port.

Earth-view measurements were made at several temperature settings in order to establish a relationship among the temperature, DN levels, and radiance. These measurements were then combined with the blackbody and space-view measurements to derive a final set of coefficients for scaling DNs to radiances. Detector linearization was performed prior to the bias removal for TIRS because temperature contributions from instrument components were also being captured.

Similar to the approach taken with OLI, a wide-field collimator and a set of fixed geometric patterns were scanned across the focal plane to build an optical map of the detectors that enabled construction of a LOS model from the focal plane to the Earth. Instead of these targets being viewed under fixed illumination settings, these targets were presented and contrasted by controlled temperature settings. These measurements assisted with characterizing the alignment of detectors within a given SCA as well as with aligning adjacent SCAs. These were fundamental parameters required for constructing the geometric models to achieve many of the geometric requirements.

3.1.3 Postlaunch

Radiometric characterization and calibration will be performed over the life of the mission using the software tools developed as part of the L8 Image Assessment System (IAS) and the Calibration Validation Toolkit (CVTK). The IAS provides the capability to perform radiometric characterization routinely, to verify and monitor system radiometric performance, and to estimate improved values for key radiometric calibration coefficients. On-orbit activities include those that occur during the OIV period characterization and calibration and post-OIV nominal operations.

Characterization activities include the following:

- Noise – characterizing the OLI response to shutter, lamp, diffuser, and lunar acquisitions, and the TIRS response to deep space views, On-Board Calibrator

(OBC) collects, and lunar acquisitions are used to assess various detector noise characteristics, including coherent, impulse, SNR, NEdL, and ghosting.

- Stability - characterizing the response of OLI to the solar diffusers, stim lamps, and lunar acquisition, and TIRS to the OBC for assessing the transfer-to-orbit response, the short-term (within-orbit) and long-term stability, diffuser and lunar acquisition reproducibility for OLI, and post-maneuver recovery reproducibility for TIRS.

Calibration activities include the following:

- Absolute Radiometric Response – characterizing the OLI solar diffuser, lunar irradiance, PICS, and underfly acquisitions with L7, and TIRS OBC, PICS, and underfly acquisitions with L7, to assess the absolute radiometric response and derive the initial on-orbit absolute gain CPF values.
- Relative Radiometric Response – characterizing the OLI diffuser, yaw, and PICS, and TIRS OBC, yaw, and PICS sites for assessing the SCA-to-SCA and pixel-to-pixel relative response / uniformity. Special OLI diffuser and TIRS OBC integration time sweep collects are characterized to assess detector linearity, and possible updates to the CPF linearity calibration coefficients.

Key radiometric CPF parameters that may need updates include absolute gains, relative gains, bias (default values), linearity Lookup Tables (LUTs), diffuser radiances (OLI), lamp radiances (OLI), OBC LUTs (TIRS), diffuser non-uniformity (OLI), OBC non-uniformity (TIRS), inoperable detectors, out-of-spec detectors, and detector select mask.

3.1.4 Operational Radiometric Tasks

The goals of these tasks are as follows:

- To demonstrate that the L8 mission meets or exceeds all radiometric requirements, particularly those that were deferred for formal verification on-orbit
- To perform an initial on-orbit radiometric calibration (relative and absolute) that makes it possible to achieve the previous goal, and that prepares the mission for routine operations
- To initialize and continue the process through nominal operations of evaluating OLI Key Performance Requirements (KPRs) by establishing an initial on-orbit performance baseline
- To trend radiometric characterization parameters throughout the mission

3.1.4.1 OLI Characterization Tasks

A number of OLI characterizations and requirements verifications relate strictly to whether the instrument performance meets specifications, and therefore are not strongly tied to the coefficients stored in the CPF that require on-orbit updates. These requirements include stability (60-second, 16-day), noise (overall, impulse, coherent, 1/f), stray light, ghosting, bright target recovery, detector operability, and detectors out-of-specification.

Three lunar calibration acquisitions were made during the commissioning period; each acquisition comprises 15 individual image scans, performed over two consecutive orbits. Each OLI and TIRS SCA is scanned across the Moon, with one scan repeated in both orbits to provide a check on continuity of the observations. Lunar acquisitions are performed when the Earth-Sun-Moon configuration provides lunar phase angles in the -9 to -5 degree or the +5 to +9 degree ranges. The Moon traverses each phase angle range once per month, with the positive and negative angle ranges occurring approximately one day apart. In routine operations, one phase angle range is selected for all lunar acquisitions; during commissioning, both cases were collected. The timing of the commissioning period led to three pairs of nominal lunar acquisition opportunities: one in late March 2013 just before the under-fly of L7, one in late April 2013 after achieving the operational orbit, and one in late May 2013.

3.1.4.2 OLI Calibration Tasks

The OLI instrument was radiometrically calibrated before launch. The OLI viewed an integrating sphere monitored by a spectrometer that had been calibrated relative to a source that is traceable to a reference in the NIST Facility for Spectroradiometric Calibrations (FASCAL) facility. The gains (DN / radiance) from this calibration were stored in the CPF. The OLI's response to the diffuser panels was measured using the Sun as the source through a heliostat. Using the OLI gains, the radiance of the diffuser was measured and was corrected for the heliostat and the atmospheric transmittance to obtain a "predicted" TOA radiance for the diffuser. Additionally, the OLI diffuser's directional reflectance factors for the on-orbit illumination and view geometries were measured in the laboratory before launch, giving the diffuser a reflectance calibration. These data were used to derive "prelaunch" TOA radiance calibration coefficients. The first on-orbit measurements of the solar diffuser panel were compared to the "predicted" and "prelaunch" values to perform the transfer to orbit analysis.

A fundamental requirement of the Landsat Program is to provide a record of consistently calibrated image data. Therefore, OLI data need to be consistent with data from the previous Landsat sensors. Although the instruments are calibrated consistently before launch and monitored before launch through on-orbit commissioning, there is still a need to check the calibration relative to previous Landsat instruments and update the calibration parameters as necessary.

Procedures were developed to characterize any shift in calibration that may occur through launch and into orbit. Two methods of validating the absolute radiometric calibration include cross-calibration with L7 ETM+ via simultaneous observations and use of the PICS.

Although one of the goals of the Ground System is to generate OLI images as free of striping and banding as is practicable, it cannot be expected that OLI images over uniform areas will be completely free of banding or striping, especially when extreme contrast stretches are applied. There are a number of contributors to banding and striping: inadequately characterized differential non-linear responses among detectors;

inadequately characterized relative gain and bias parameters; instability in gain, bias, or non-linearity; and spectral differences across or between SCAs.

3.1.4.3 TIRS Characterization Tasks

A number of TIRS characterizations and requirements verifications relate strictly to whether the instrument meets performance specifications, and therefore are not strongly tied to the coefficients stored in the CPF that require on-orbit updates. These requirements include stability (60 second, 16-day), noise (overall, impulse, coherent, 1/f), stray light, ghosting, bright target recovery, detector operability, and detectors out-of-specification.

Three lunar acquisitions were performed during the commissioning period. Each acquisition comprises 15 individual image scans, performed over two consecutive orbits. Each TIRS SCA is scanned across the Moon, with one scan repeated in both orbits to provide a check on continuity of the observations. As with OLI, the TIRS lunar acquisitions are performed when the Earth-Sun-Moon configuration provides lunar phase angles in the -9 to -5 degree or the +5 to +9 degree ranges. During the operational mission lifetime, lunar acquisitions will be performed monthly as defined for the OLI.

3.1.4.4 TIRS Calibration Tasks

TIRS data need to be consistent with data from the previous sensors, so by extension, L8 TIRS data need to be cross-calibrated with L7 ETM+ data. At least two techniques will be used for this comparison and calibration (i.e., simultaneous data acquisitions collected during the under-fly of L7 and non-simultaneous observation of well-characterized targets). TIRS was carefully characterized and calibrated before launch, and procedures were developed to be able to characterize any shift in calibration that may occur during launch and insertion into orbit.

3.1.4.5 TIRS Relative Response - Uniformity Evaluation

As with the OLI, a number of factors may contribute to banding and striping in TIRS imagery: inadequately characterized differential non-linearity among detectors; inadequately characterized relative gain and bias; instability in gain, bias, or non-linearity; and spectral differences across or between SCAs.

3.2 Geometric Calibration Overview

This subsection describes the geometric characterization and calibration activities performed over the life of the L8 mission, using the software tools developed as part of the L8 IAS. The IAS provides the capability to perform four types of geometric characterization routinely to verify and monitor system geometric performance, and four types of geometric calibration to estimate improved values for key system geometric parameters. These are the parameters contained in the CPF for use in the Level 1 product generation. The measurement and evaluation activities are referred to as characterization operations, while the parameter estimation activities are referred to as calibration.

The geometric characterizations include the following:

1. Assessment of the absolute and relative geodetic accuracy of Level 1G data (Geodetic Characterization)
2. Assessment of the geometric accuracy of Level 1T products (Geometric Characterization)
3. Assessment of the accuracy of multi-temporal OLI image-to-image registration (Image-to-Image Registration Characterization)
4. Assessment the accuracy of OLI and TIRS band-to-band registration (Band-to-Band Registration Characterization)

A fifth characterization algorithm will be used to evaluate OLI spatial performance on-orbit. This Modulation Transfer Function (MTF) bridge characterization algorithm uses images of selected ground targets (e.g., the Lake Pontchartrain Causeway) to estimate the OLI sensor edge response. The characterizations performed during the commissioning period were used to establish an OLI performance baseline to serve as a basis for comparison in evaluating the OLI KPRs throughout the life of the mission. The characterizations of primary interest as KPRs are OLI band registration accuracy and spatial performance.

The geometric calibrations include the following:

1. Determination of the alignment between the spacecraft navigation reference frame and the OLI payload LOS (Sensor Alignment Calibration)
2. Determination of corrections to the prelaunch OLI panchromatic band lines of sight, including relative alignment of the OLI sensor chip assemblies (OLI Focal Plane Calibration)
3. Determination of the alignment between the TIRS and OLI sensors, including the relative alignment of the TIRS sensor chip assemblies (TIRS Alignment Calibration)
4. Determination of corrections to the band location field angles for both OLI and TIRS (Band Alignment Calibration)

The most critical geometric calibration activities are to measure and verify the L8 spacecraft, OLI, and TIRS system performance using the geodetic, geometric, band-to-band, image-to-image, and spatial characterization capabilities; to monitor the OLI sensor to spacecraft attitude control system alignment calibration; and to monitor the TIRS-to-OLI alignment calibration. This includes verifying and, if necessary, updating the OLI and TIRS focal plane (SCA-to-SCA), and band alignment calibrations.

Monitoring and refining the OLI-to-spacecraft and TIRS-to-OLI alignment knowledge is critical to ensure that the Level 1 product accuracy specifications can be met. These calibration parameters were not expected to change greatly through launch but may require minor refinement on-orbit. The results of these calibration activities are used to verify that the system is performing within specifications and to create the CPFs used by the IAS and the LPGS to create Level 1 products that meet the L8 accuracy requirements. The calibration activities will continue throughout the life of the mission to

monitor the stability of the system's geometric and spatial performance and to identify and characterize any systematic variations in the system's geometric parameters as a function of time, temperature, and location. A longer sequence of calibration observations over a range of conditions will be needed to isolate, model, and characterize these higher-order behaviors. Table 3-2 summarizes these activities, along with the prelaunch activities.

	Purpose	How this is used to develop calibration parameters
OLI Preflight Activity		
Initial LOS directions for detectors using design locations	Establish nominal focal plane locations for individual detectors, bands, and SCAs	Gives nominal detector focal plane locations that can then be adjusted
Edge and line target analysis through thermal vacuum testing	Provide prelaunch adjustment to initial LOS of individual detectors	Allows refinement to initial LOS design model for detectors
TIRS Preflight Activity		
Initial LOS directions for detectors using design locations	Establish nominal focal plane locations for individual detectors, bands, and SCAs	Gives nominal detector focal plane locations that can then be adjusted
Edge and line target analysis through thermal vacuum testing	Provide prelaunch adjustment to initial LOS of individual detectors	Allows refinement to initial LOS design model for detectors
OLI On-Orbit Activities		
OLI Geodetic Accuracy Assessment	Ensure Level 1 Systematic imagery meet horizontal accuracy requirements and measures product accuracy prior to application of ground control	Folds into the OLI instrument to Attitude Control System alignment parameters
OLI to Attitude Control System Alignment	Improves in-flight knowledge of OLI to the Attitude Control System	OLI instrument to Attitude Control System alignment parameters
Geometric Accuracy Assessment	Evaluates the accuracy of the Level 1 Terrain-Precision corrected imagery and measures product accuracy after application of ground control	
Image-to-Image Registration Assessment	Ensures ability to co-register Level 1T imagery and measures OLI-to-OLI and OLI-to-reference ability	
OLI Focal Plane Calibration	Ensures accuracy between and within SCA geometry of the OLI Pan imagery and corrects for SCA-to-SCA misalignment	Allows for adjustment to OLI LOS parameters
Band-to-Band Registration Assessment	Measures the ability to align OLI and TIRS bands within a Level 1T image	Folds into the updating of the LOS parameters
Band Alignment Calibration	Adjusts OLI LOS parameters based on band-to-band registration assessment	Allows for adjustment of the OLI LOS parameters
OLI Spatial Characterization	Characterizes OLI system transfer function on orbit	

	Purpose	How this is used to develop calibration parameters
TIRS On-Orbit Activities		
TIRS Internal Geometric Characterization	Measures the ability to align the two TIRS bands within a Level 1T	Folds into updating of the TIRS LOS parameters
TIRS Internal Geometric Calibration	Adjusts TIRS LOS parameters based on TIRS internal geometric characterization	Allows for adjustment of the TIRS LOS parameters
TIRS Alignment Calibration	Measures the ability to align 3 SCAs of TIRS to the OLI instrument	Allows for adjustment of TIRS to OLI alignment parameters

Table 3-2. Summary of Geometric Characterization and Calibration Activities

3.2.1 Collection Types

Lunar Collects

Due to differences in the viewing geometry between lunar collects and nominal Earth collects, lunar collects are used only for measuring the alignment of the cirrus band with the other OLI bands.

Earth Collects

Geometric characterization and calibration is performed on nominal nadir-viewing Earth collects. The major difference associated with these collects and the type of characterization or calibration that is performed depends on the reference imagery for which it is characterized, and in some cases, eventually calibrated against. Three types of reference imagery are used for geometric characterization and calibration, including the Global Land Survey (GLS), Digital Orthophotoquad (DOQ) mosaics, and Satellite Pour l'Observation de la Terre (SPOT) mosaics.

3.2.2 Prelaunch

OLI Prelaunch

An initial OLI geometric model that defined the LOS for the detectors on the focal plane was calculated using the nominal design locations of the detectors and telescope optical system. This initial or nominal design was then updated using edge and line targets that were projected on to the focal plane through the optical system during prelaunch thermal vacuum testing. This model was then considered an as-built prelaunch set of LOSs for each detector for which each band for each SCA could be adjusted postlaunch using the IAS geometric characterization and calibration processes.

TIRS Prelaunch

An initial TIRS geometric model, consisting of a detector and sensor chip assembly within the focal plane along with the optics of the telescope, was determined based on its assembly through instrument and component design and final integration to the spacecraft. This included the focal plane and detector placement, the telescope and optical components, and the TIRS-to-spacecraft alignment measurements. These components were then updated during prelaunch using measurements taken during thermal vacuum testing. Targets were projected into the TIRS FOV at operator-

selectable locations, allowing for careful identification of both the target within the focal plane and the origination of the target itself. This model was then considered an as-built prelaunch set of LOSs for each detector for which each band for each SCA could be adjusted postlaunch using the IAS geometric characterization and calibration processes.

3.2.3 OLI Geodetic Accuracy Assessment

The purpose of the geodetic accuracy assessment is to ensure that the L8 Level 0R data can be successfully processed into Level 1 systematic products that meet the system requirement of 65 meters at a circular error with 90 percent confidence (CE90) horizontal accuracy.

Predefined Ground Control Points (GCPs) (consisting of image chips with known geodetic positions) are automatically correlated with data from the OLI SWIR1 (for Global Land Survey 2000-based (GLS2000) control) or panchromatic bands (for DOQ control) to measure the discrepancy between the known ground location and the position predicted by the OLI geometric model.

The results of the control point mensuration are used for analysis by the IAS geodetic characterization software. The precision-correction software also combines the estimated attitude error from the precision solution with the current best estimate of OLI-to-spacecraft alignment from the CPF, to compute the adjusted alignment that would make the resulting attitude error zero. This apparent alignment is stored in the geometric trending database for subsequent use by the sensor alignment calibration procedures.

The geodetic accuracy characterization software processes the control point residuals (deleting those identified as outliers) to generate summary statistics and a geodetic accuracy analysis report each time the precision correction solution process is successfully completed. The geodetic accuracy results are stored in the geometric characterization trending database, with a flag to indicate the control type used (GLS or DOQ).

3.2.4 Sensor Alignment Calibration

The goal of the sensor alignment calibration is to improve the in-flight knowledge of the relationship between the OLI instrument and the spacecraft attitude control system reference frame. Sensor alignment calibration uses the results of the GCP processing conducted both as part of routine L1T product generation (using GLS2000 control) and as part of calibration / validation analysis activities over geometric calibration sites (using DOQ control). The end-to-end OLI geolocation accuracy error budget assumes that the IAS is able to estimate this alignment to an accuracy of 33 microradians (3σ) over periods as short as one 16-day WRS-2 cycle.

The potential need for a sensor alignment calibration updates will be identified by monitoring the geodetic accuracy characterization results. If persistent geolocation accuracy biases are observed, then that would suggest the need for generating an

updated sensor alignment matrix for inclusion in the CPF. Automated software tools are used to detect the existence of a new alignment calibration solution and to perform automated testing of the new and old calibration solutions against a set of test scenes extracted from the list of retrieved alignment calibration scenes. A new alignment matrix will be generated whenever a new version of the CPF is scheduled for release, nominally on a quarterly basis; therefore, any slowly varying seasonal alignment variations will be accounted for.

3.2.5 Geometric Accuracy Assessment

The purpose of the geometric accuracy assessment is to evaluate the accuracy of Level 1T image products using an independent set of GCPs. Although the geodetic accuracy characterization results report both the pre- and post-GCP correction scene accuracy statistics, the post-fit statistics are not an unbiased estimate of the actual accuracy of the corrected scene. An independent geometric accuracy assessment is performed by correlating the final L1T product with a separate set of GCPs that were withheld from the original precision correction solution. Scenes for which the number of available GCPs was too small to permit withholding some from the precision correction process do not have validation points. The geometric accuracy assessment procedure runs as a part of the standard L1T product generation flow.

3.2.6 OLI Internal Geometric Characterization and Calibration

OLI internal geometric accuracy refers to internal geometric distortions within the OLI images due to errors in the relative alignment of the 14 SCAs, also known as FPMs, on the OLI focal plane. If the OLI LOS model knowledge of the pointing for each SCA is slightly inaccurate, this will result in internal geometric distortions in the L1T products and, potentially, visible image discontinuities at SCA boundaries. Although the OLI LOS model is carefully characterized prelaunch, tools are available to detect and, if necessary, correct any SCA-to-SCA misalignment that may be observed by updating the OLI LOS model calibration. These tools are implemented in the IAS as the image-to-image registration accuracy characterization and the OLI focal plane calibration algorithms.

The OLI panchromatic band is used as the geometric reference for the entire instrument.

The image-to-image registration accuracy and the pattern of registration errors may indicate the presence of unwanted internal distortions in the OLI image that could be addressed by refining the OLI focal plane calibration. The following subsections describe the details of the image-to-image registration assessment and OLI focal plane calibration procedures individually.

3.2.6.1 Image-to-Image Registration Assessment

The goal of the image-to-image registration assessment is to verify the L8 requirement that multi-temporal images of the same WRS scene can be successfully co-registered to an accuracy of 0.4 (LE90) multispectral pixels (i.e., 12 meters). The image-to-image assessment procedure uses GCPs that have been extracted from a previously

generated L1T image, or that match the points used to correct the pre-existing L1T product, to perform precision and terrain correction of a new acquisition to Level 1T. It then performs a point-by-point comparison of the two images using automated image correlation.

Image-to-image registration assessment using the panchromatic band demonstrates the accuracy of the overall precision correction solution as well as the internal geometric fidelity of the images.

3.2.6.2 OLI Focal Plane Calibration

The OLI focal plane calibration is intended to detect and measure systematic deviations of the OLI lines-of-sight for each SCA from the model measured during prelaunch characterization. Any significant deviations detected will be folded back into the CPF as updates to the LOS model Legendre polynomial coefficients.

3.2.6.3 Band-to-Band Registration Assessment

The band-to-band registration assessment measures the relative alignment of the nine OLI and two TIRS spectral bands after processing to L1T to verify that the 4.5-meter (LE90) OLI, 18-meter (LE90) TIRS, and 30-meter (LE90) OLI-to-TIRS band-to-band registration requirements are met.

3.2.6.4 Band Alignment Calibration

The purpose of band placement calibration is to estimate improved values for the locations of the spectral bands on the OLI and TIRS focal planes for inclusion in the CPF. The band locations are embodied in the LOS model Legendre coefficients for each OLI and TIRS band / SCA. OLI and TIRS band alignment would use essentially the same algorithm but would process separately.

The panchromatic band is used as the reference for the OLI solution because it is the band used to perform the sensor alignment and focal plane calibrations. TIRS Band 10 is used as the reference for TIRS band alignment since it is also used in TIRS alignment calibration. The OLI cirrus band is only used for lunar and high-altitude terrestrial targets.

3.2.7 TIRS Internal Geometric Characterization and Calibration

The TIRS geometric alignment calibration procedure accomplishes both internal and external geometric alignment calibration for the TIRS instrument. TIRS internal geometric accuracy can be degraded by internal geometric distortions within the TIRS images due to errors in the relative alignment of the three SCAs on the TIRS focal plane. If the TIRS LOS model knowledge of the pointing for each SCA is slightly inaccurate, this will result in internal geometric distortions in the L1T product images and, potentially, visible image discontinuities at SCA boundaries.

TIRS external geometric accuracy refers to the accuracy with which TIRS data can be registered to corresponding OLI data and to an absolute ground coordinate system.

This accuracy is dependent primarily on accurate knowledge of the alignment between the OLI and TIRS instruments.

The alignments of both the OLI and TIRS instruments relative to the spacecraft Attitude Control System (ACS) frame were measured during Observatory integration, but due to the accuracy limitations of these measurements and the likelihood of launch shift and zero-G release altering these alignments, on-orbit TIRS alignment estimation was updated to achieve the TIRS geometric accuracy requirements. Although the TIRS LOS model was also carefully characterized prelaunch, TIRS alignment calibration provides the tools needed to detect and, if necessary, correct any SCA-to-SCA misalignment that may be observed while updating the TIRS LOS model calibration.

The TIRS 10.8 micron band (Band 10) is used as the geometric reference for aligning the TIRS instrument to the OLI. Band 10 is also used as the reference band in TIRS band alignment calibration. As the TIRS geometric reference, internal SCA-to-SCA focal plane alignment is also performed using Band 10.

The following subsection describes the details of the TIRS alignment calibration procedure.

3.2.7.1 TIRS Alignment Calibration

The TIRS alignment calibration measures systematic deviations of the TIRS lines-of-sight for each SCA from the model measured during prelaunch characterization while simultaneously measuring the global misalignment of all three TIRS SCAs relative to the OLI. These measurements are used to compute updates to the TIRS-to-OLI and, indirectly, TIRS-to-ACS alignment matrices as well as updates to the TIRS LOS model Legendre polynomial coefficients, with the results being folded back into the CPF.

A control reference image of coincident OLI SWIR bands with good emissive-to-reflective band correlation is used for calibration. The TIRS alignment calibration procedure compares a precision- and terrain-corrected TIRS Band 10 SCA-separated image with a coincident OLI SWIR1 band SCA-combined reference image processed with the same spacecraft geometric model and scene-framing parameters. This enables measurement of the overall TIRS-to-OLI alignment, as well as the relative alignment of the individual TIRS SCAs.

3.2.8 OLI Spatial Performance Characterization

OLI spatial performance, expressed as the slope and width of the instrument's response to a unit edge / step function, was carefully characterized during prelaunch testing. The experience of the L7 ETM+, which suffered from gradually degrading spatial fidelity over the first several years of on-orbit operations, led to the development of an algorithm to measure and track on-orbit spatial performance. This was done by using long bridge targets to characterize the ETM+ MTF, which is the frequency domain representation of the instrument's spatial response. This algorithm was subsequently adapted for use with push-broom sensors using ALI data, and a variant of this adapted algorithm will be used for OLI spatial characterization. A method for using lunar scans to characterize ALI

spatial performance was also developed, but the results were not sufficiently reliable for use in operational performance characterization.

No calibration activities are associated with spatial performance, although the OLI does have ground-commandable focus mechanisms, and TIRS focus can be adjusted by changing telescope temperatures. To support on-orbit focus verification, additional focus test sites have been identified to provide qualitative information about the state of OLI and TIRS focus during the commissioning period. These sites, listed in Appendix A, were selected to contain distinct targets that could be used for visual assessment as well as additional sites for quantitative analysis using the enhanced version of the spatial performance characterization algorithm. Combined with the quantitative results of the spatial performance characterization algorithm, visual inspection of the focus sites adds confidence that the OLI and TIRS are in proper focus. The derivation of any adjustments to the focus mechanism positions or TIRS telescope temperatures that may be required to improve on-orbit spatial performance would require additional analysis that is beyond the scope of this algorithm.

Spatial edge slope performance in all OLI bands (other than the cirrus band) is a KPR for OLI on-orbit performance. The derived spatial performance parameters can then be compared to the thresholds specified in the corresponding KPR to evaluate on-orbit performance. The precision of the on-orbit spatial performance estimates is such that repeated measurements are required to establish the validity that the standard performance level of any requirement is not met.

3.2.9 OLI Bridge Target MTF Estimation

The purpose of the OLI bridge target MTF estimation procedure is to use OLI acquisitions of prescribed bridge targets to derive on-orbit estimates of the OLI System Transfer Function (STF) for each OLI spectral band other than the cirrus band. The STF estimates are then used to compute the corresponding point spread function and edge response slope performance for each spectral band. The OLI bridge target MTF estimation procedure applies a model of the OLI spatial response (in the form of the system transfer function) to pre-defined models of two bridges, shown in Figure 3-1, in the Lake Pontchartrain, Louisiana area, to simulate the OLI's response to each bridge in the direction transverse to the bridge. By comparing these models to oversampled bridge profiles constructed from actual OLI image data by interleaving samples from different points along the bridge, adjusted OLI STF parameters can be estimated.

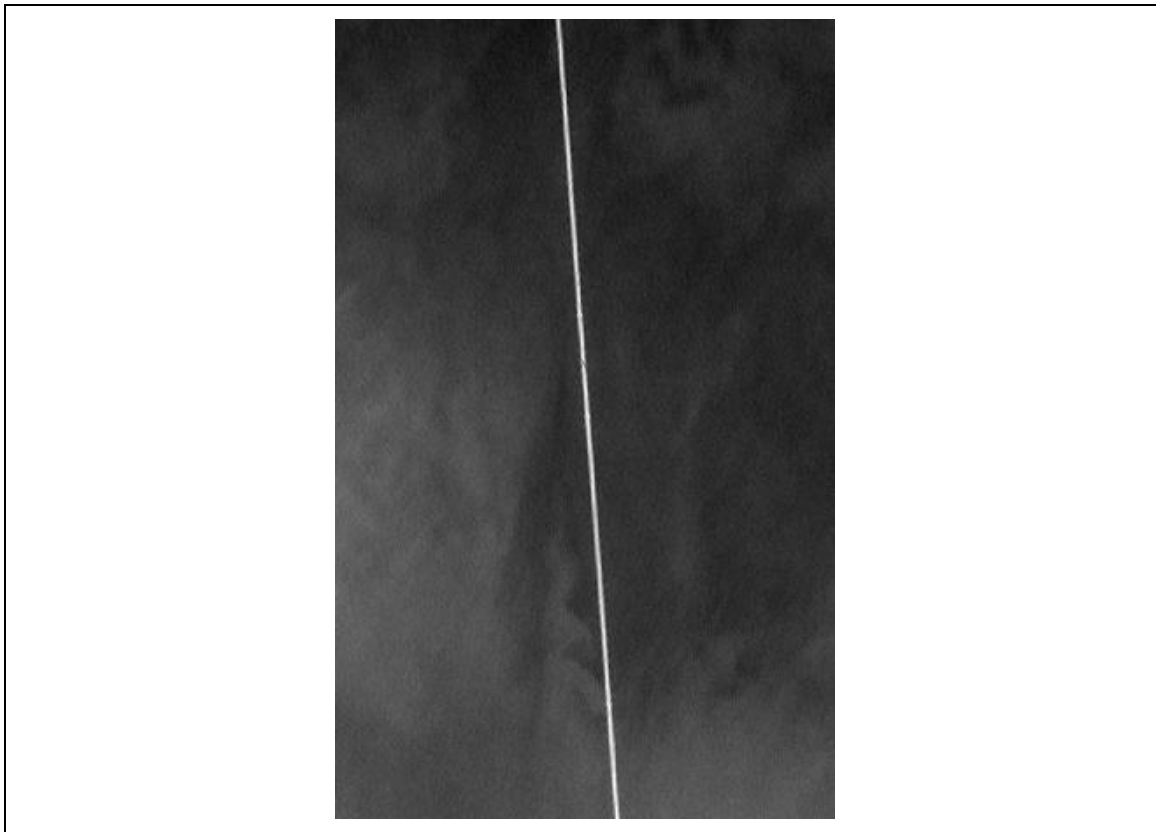


Figure 3-1. Simulated OLI Image of the Lake Pontchartrain Causeway (left) and Interstate-10 Bridge (right) Targets in WRS 022/039

3.2.10 Geometric Calibration Data Requirements

The geometric characterization and calibration operations require three primary types of supporting information: GCPs, reference images, and digital terrain data. The following subsections describe the required characteristics, potential sources, and preprocessing requirements for each of these support data types.

3.2.10.1 Ground Control Points (GCPs)

The IAS uses GCPs for all of its geometric characterization and calibration activities. In all cases, the GCPs are used to perform a precision correction solution that will ensure accurate registration of the image data to a cartographic projection and use digital elevation data to correct for relief displacement in the process. The IAS and LPGS both access a database of GCPs. These points, adopted from the L7 mission, include both the global GCP set extracted from the GLS data and the higher precision control points extracted from geometric calibration reference data (e.g., DOQ mosaics, SPOT data). GCPs from either or both control sets can be extracted by control type: GLS or DOQ (DOQ is used as a generic type indicator for all GCPs extracted from geometric calibration sources).

The GLS control database covers essentially every land scene observed from the WRS-2 orbit. The control derived from the GLS is accurate to approximately 20 meters Root

Mean Square Error (RMSE_r) absolute, but since the goal is to make L8 products that are consistent with the other products generated from the archive of historical data, GLS GCPs include image chips extracted from the ETM+ Band 5 at 30-meter GSD. These have been automatically subdivided into separate CONTROL and VALIDATION subsets in scenes where a sufficient number of points were available.

The DOQ control database only covers scenes designated as geometric calibration sites. There are two main clusters of these sites. The first set is in the United States, and was selected to provide at least one acquisition opportunity on every WRS-2 cycle day, including a group in the southwestern U.S. that is at approximately the same latitude to provide consistent acquisition conditions (position in orbit, ETM+ time-on). These contain control extracted from reduced-resolution DOQ data (panchromatic, 15-meter GSD). A second group of control scenes is in the eastern half of Australia. This control set is based on mosaics of SPOT panchromatic data provided by GeoScience Australia's National Earth Observation Group (NEOG). Being in the southern hemisphere, this set provides somewhat different orbital geometry and thermal conditions than the U.S. set. One of the primary purposes of the DOQ control set is to ensure accurate registration between L8 L1T products and the DOQ- and SPOT-derived reference imagery used for focal plane calibration.

The GLS control points were extracted from the GLS 2000 ETM+ images using an automated interest operator technique that selected points based on a local spatial operator that identified "interesting" points, and a spatial distribution test that decided which points provided the best distribution of control across the scene. A subsequent test was added to weed out points that contained only water. The GLS control has been in routine operational use for generating Landsat 5 and L7 standard L1T data products. An important note is that the GLS images themselves were generated based on a global block triangulation of L7 scenes with a sparse set of ground control provided by the National Geospatial-Intelligence Agency (NGA). The scenes that contained NGA control are more accurate than those that were positioned solely through triangulation. The NGA-controlled scene subset will therefore be given special attention when mining the geodetic accuracy and sensor alignment data for systematic within-orbit effects.

The DOQ control points were extracted from the DOQ mosaic reference images (U.S. set) and the SPOT mosaic reference image (Australia) and therefore inherit the accuracy of those products. Because the primary purpose of these points is to ensure good OLI-to-reference image registration, the absolute accuracy of these points, though believed to be better than the GLS control, is of less interest. Appendix A includes the list of geodetic characterization sites where DOQ control points are available.

3.2.10.2 Reference Images

Two types of reference images are used by the geometric super-site calibration operations described above. The first type includes previously generated L8 L1T products used in the image-to-image registration assessment process. These reference images were generated by processing L0R data through the IAS Level 1 processing software after launch, and are not discussed further here. The second type of reference

images were constructed prelaunch using a high-resolution image source. These images are used to provide the reference for OLI focal plane calibration as described above. These reference images are the subject of the remainder of this section.

The key characteristics of the focal plane calibration reference images are as follows: 1) high absolute geodetic accuracy (including removal of any terrain displacement effects); 2) internal geometric integrity (no systematic internal distortions that could be confounded with OLI focal plane alignment effects); 3) spectral similarity to the OLI panchromatic band; 4) resolution as good as or better than the OLI panchromatic band; and 5) availability in areas of minimal seasonal change and low average cloud cover. Geodetic accuracy of one-half of a panchromatic pixel (7.5 meters) should be sufficient, although higher accuracy is desirable. The internal geometric accuracy requirement disqualifies ETM+ data as a source of reference imagery, although in an emergency, ETM+ reference data (e.g., GLS) would be better than no data.

High-resolution panchromatic imagery from aerial photographs that meet the geodetic accuracy requirement have been available for years. Panchromatic satellite imagery is available from SPOT and a number of high resolution commercial missions, but the cost associated with acquiring the volume of data required to cover a Landsat scene has limited the application of these sources to a set of sites in Australia where GeoScience Australia's NEOG have provided full WRS-2 scene SPOT data coverage.

The preferred source of high-resolution reference imagery based on availability and cost are the DOQ produced under contract to the USGS. The DOQs are created by digitizing and orthorectifying panchromatic aerial photography. The DOQ products are distributed as 3.75 arc-minute quarter quads at 1-meter resolution. The DOQ geodetic accuracy is specified to meet National Map Accuracy Standards (NMAS) for 1:24,000-scale maps. This standard calls for a Circular Error (CE) of 40 feet at the 90 percent confidence level, which converts to approximately 6 meters CE one sigma, and meets the one-half OLI pixel requirement. DOQ data coverage has improved since the launch of L7, to the point where it is now possible to generate a DOQ reference image nearly everywhere in the conterminous U.S. Though still time-consuming to construct, this has made it possible to assemble sufficient DOQ reference sites to provide at least one acquisition opportunity on every WRS-2 cycle day.

SPOT data, though not quite as accurate as the DOQ data, are available globally. The primary drawback of using SPOT data is the cost. Fortunately, our colleagues at GeoScience Australia were good enough to provide several Landsat scene-sized mosaics of SPOT data in Australia for use in Landsat 5 and 7 bumper-mode calibration. These reference images will continue to be used for OLI focal plane calibration, though they can be expected to become less useful over time as the imagery become outdated.

3.2.10.3 Terrain Data

Digital terrain data are needed to provide the elevation information used by the IAS (and LPGS) Level 1 terrain-correction process. Terrain-corrected images are used in all of the geometric calibration operations described in the previous subsections. The

elevation information must completely cover the geometric calibration sites to support the terrain-correction process. The height values must be referenced to the WGS84 ellipsoid rather than mean sea level to be consistent with the ground control height values. Vertical accuracy better than 15 meters (one sigma) is desirable. This keeps terrain-induced errors below 0.1 panchromatic pixels at the edges of the OLI FOV. An accuracy of 30 meters (one sigma) is acceptable. For product generation purposes, it is also desirable that the elevation data used be consistent with the GLS 2000 reference data set. The Digital Elevation Model (DEM) data used to generate the GLS data sets meet these requirements.

Assembling a global elevation data set suitable for generating a global Landsat image base was a primary objective of the GeoCover (which evolved into the Global Land Survey) project. This resulted in a global DEM constructed from the best available source data, including the USGS National Elevation Dataset (NED) DEM data, the Canadian Digital Elevation Dataset (CDED), the NASA / NGA Shuttle Radar Topography Mission (SRTM) data, and NGA Digital Terrain Elevation Data (DTED) products. The GLS DEM provides a globally (mostly) consistent elevation data set that corresponds to the GLS imagery that defines the L8 geometric reference. Tools were developed to retrieve any specified land area from the global DEM, so the elevation data sets required to process any given scene (nadir-viewing or off-nadir) are extracted and assembled on demand from the GLS archive. The digital terrain data for the desired output product area are extracted from the GLS DEM archive, as noted above, and then preprocessed into the output space used for the calibration test scene. This DEM resampling step is part of the normal Level 1 processing sequence.

3.3 Calibration Parameters

The Calibration and Validation Team (CVT) is responsible for the sustained radiometric and geometric calibration of the L8 satellite and the TIRS and OLI sensors. To achieve this, the team assesses new imagery on a daily basis, performs both radiometric and geometric calibration when needed, and develops new processing parameters for creating Level 1 (L1) products. Processing parameters are stored in the CPF, the Response Linearity Look-Up Table (RLUT), and the Bias Parameter File (BPF), which are stamped with effectivity dates and bundled with L0R products.

3.3.1 Calibration Parameter File

The CVT updates the CPF at least every three months. Updates will likely be more frequent during early orbit checkout and will occur between the regular three-month cycles whenever necessary. Irregular updates will not affect the regular schedule. The timed release of a new CPF must be maintained because of the Universal Time Code (UTC) Corrected (UT1) time corrections and pole wander predictions included in the file. These parameters span 180 days and include approximately 45 days before and 45 days after the effective start date of each CPF. The IAS maintains an archive of CPFs, which can be accessed at http://landsat.usgs.gov/calibration_notices.php.

The CPF is time-stamped with an effective date range. The parameters in the file—Effective_Date_Begin and Effective_Date_End—designate the range of valid acquisition

dates and are in YYYY-MM-DDThh:mm:ss format (ISO 8601). The parameter file used in processing an image requires an effective date range that includes the acquisition date of the ordered image.

Through the course of the mission, a serial collection of CPFs is generated and made available for download. CPFs are replaced when improved calibration parameters for a given period are developed. The need for unique file sequence numbers becomes necessary as file contents change. Version numbers for all effective date ranges after the launch begin with 01.

The following is an example of the file-naming procedure:

L8CPFyyyy ¹ mm ¹ dd ¹ _yyyy ² mm ² dd ² .nn	
L	Constant for Landsat
8	Satellite numerical representation
CPF	Three-letter CPF designator
yyyy ¹	Four-digit effective starting year
mm ¹	Two-digit effective starting month
dd ¹	Two-digit effective starting day
-	Effective starting / ending date separator
yyyy ²	Four-digit effective ending year
mm ²	Two-digit effective ending month
dd ²	Two-digit effective ending day
.	Ending day / version number separator
nn	Version number for this file

As an example, suppose four calibration files were created on 90-day intervals, the first file updated twice, and the second and third files updated once since 2012; the assigned file names would be as follows:

File 1 L8CPF20120101_20120331.01
L8CPF20120101_20120331.02
L8CPF20120101_20120331.03
File 2 L8CPF20120401_20120630.01
L8CPF20120401_20120630.02
File 3 L8CPF20120701_20120930.01
L8CPF20120701_20120930.02
File 4 L8CPF20121001_20121231.01

The reserved sequence number 00 uniquely identifies the prelaunch CPF. Sequence numbers for subsequent time periods all begin with 01. New versions or updates increment by one. This example assumes the effectiveness dates do not change. The effectiveness date range for a file can change if an instrument change event is discovered within the nominal three-month effectiveness range. Assuming this scenario, two CPFs with new names and effective dates are spawned for the time under consideration. The effective_date_end for a new pre-event CPF would change to the day before the problem occurred. The effective_date_begin remains unchanged. A post-event CPF with a new file name would be created with an effective_date_begin corresponding to

the imaging date the problem occurred. The effective_date_end would be set to the original effective_date_end for the time under consideration. New versions of all other CPFs affected by the parameter change also would be created. The version numbers continue to increment from the original unsplit CPF.

Using this example, suppose a dead detector is discovered to have occurred on July 25, 2012. Two new CPFs are created that supersede the time period represented by file number three, version 2, and a new version of file number four is created. The new file names and sequence numbers become the following:

File 3 L8CPF20120701_20120930.01
L8CPF20120701_20120930.02
L8CPF20120701_20120724.03
L8CPF20120725_20120930.03
File 4 L8CPF20121001_20121231.01
L8CPF20121001_20121231.02

3.3.1.1 File Structure

All calibration parameters are stored as American Standard Code for Information Interchange (ASCII) text using the Object Definition Language (ODL) syntax developed by the NASA JPL. ODL is a tagged keyword language developed to provide a human-readable data structure to encode data for simplified interchange. The body of the file is composed of the following statement types:

1. Attribute assignment statement used to assign values to parameters.
2. Group statements used to aid in file organization and enhance parsing granularity of parameter sets.

To illustrate, consider the first nine parameters in the file. These nine parameters form their own group, which is called FILE_ATTRIBUTES. The syntax employed for this collection of parameters in the CPF appears as follows:

```
GROUP = FILE_ATTRIBUTES
Spacecraft_Name = "Landsat_8"
Sensor_Name = "Operational Land Imager"
Effective_Date_Begin = "2013-01-01T00:00:00"
Effective_Date_End = "2013-03-31T23:59:59"
Baseline_Date = "2013-02-13T00:01:00"
File_Name = "L8CPF20130101_20130331.05"
File_Source = "L8CPF20130101_20130331.00"
Description = "Updates to the TIRS Focal Plane, Attitude
parameters, TIRS detector offsets, and UT1 time parameters"
Version = 5
END_GROUP = FILE_ATTRIBUTES
```

3.3.2 Bias Parameter Files

The bias model calibration algorithms operate on each OLI shutter collect and each TIRS deep space collect to generate bias model parameters for each imaging band, SCA, and detector for a given time interval. The BPFs are time-stamped the same way the CPFs are time-stamped. The BPFs are generated automatically about every half orbit, or 50 minutes. Level 1 processing must wait for these BPFs to be generated prior to processing to ensure radiometric quality of the products.

The file name contains the file identifier, sensor, effective date range, and version number.

LS8BPF ^{yyyy¹} mm ¹ dd ¹ HH ¹ MM ¹ SS ¹ _ ^{yyyy²} mm ² dd ² HH ² MM ² SS ² .nn	
L	Constant representing Landsat
S	Sensor (O for OLI or T for TIRS)
8	Satellite numerical representation
BPF	Bias Parameter File
yyyy ¹	Four-digit effective starting year
mm ¹	Two-digit effective starting month
dd ¹	Two-digit effective starting day
HH ¹	Two-digit effective starting hours
MM ¹	Two-digit effective starting minutes
SS ¹	Two-digit effective starting seconds
-	Effective starting/ending date separator
yyyy ²	Four-digit effective ending year
mm ²	Two-digit effective ending month
dd ²	Two-digit effective ending day
HH ²	Two-digit effective ending hours
MM ²	Two-digit effective ending minutes
SS ²	Two-digit effective ending seconds
.	File name / extension separator
Nn	Version Number for this file (starts with 01)

3.3.3 Response Linearization Lookup Table (RLUT) File

The RLUT file contains parameters used to linearize the response of each detector to ensure the radiometric uniformity of L1 products at all brightness levels, and is a listing of floating-point numbers derived from bias-corrected DN values for every active detector. The file is defined down to the SCA / Band / Detector level with an array of up to 4096 floating-point values for each detector. The file is large and is stored in Hierarchical Data Format (HDF).

Throughout the mission, the file change history is maintained by means of effective begin and end dates plus the assignment of a version number to deal with changes that occur during the effective date period.

The file name contains the file identifier, effective date range, and version number.

LO8RLUTyyyy ¹ mm ¹ dd ¹ _yyyy ² mm ² dd ² Vnn.h5	
L	Constant representing Landsat
O	Constant representing OLI Sensor
8	Satellite numerical representation
RLUT	Response Linearization Look Up Table
yyyy ¹	Four-digit effective starting year
mm ¹	Two-digit effective starting month
dd ¹	Two-digit effective starting day
-	Effective starting / ending date separator
yyyy ²	Four-digit effective ending year
mm ²	Two-digit effective ending month
dd ²	Two-digit effective ending day
V	Date / version number separator
nn	Version number for this file (starts with 01)
.	File name / extension separator
h5	HDF file extension

Section 4 Level 1 Products

4.1 Level 1 Product Generation

4.1.1 Overview

The geometric algorithms used by LPGS at EROS were originally developed for the L8 IAS. The overall purpose of the IAS geometric algorithms is to use Earth ellipsoid and terrain surface information in conjunction with spacecraft ephemeris and attitude data, and knowledge of the OLI and TIRS instruments and L8 satellite geometry, to relate locations in image space (band, detector, sample) to geodetic object space (latitude, longitude, and elevation).

These algorithms are used to create accurate L1 output products, characterize the OLI and TIRS absolute and relative geometric accuracy, and derive improved estimates of geometric calibration parameters such as the sensor to spacecraft alignment.

4.1.2 Level 1 Processing System

The Level 1 processing algorithms include the following:

- Ancillary data processing
- L8 sensor / platform geometric model creation
- Sensor LOS generation and projection
- Output space / input space correction grid generation
- Systematic, terrain-corrected image resampling
- Geometric model precision correction using ground control
- Precision, terrain-corrected image resampling

Figure 4-1 shows the LPGS Standard Product Data Flow, which includes radiometric and geometric processing.

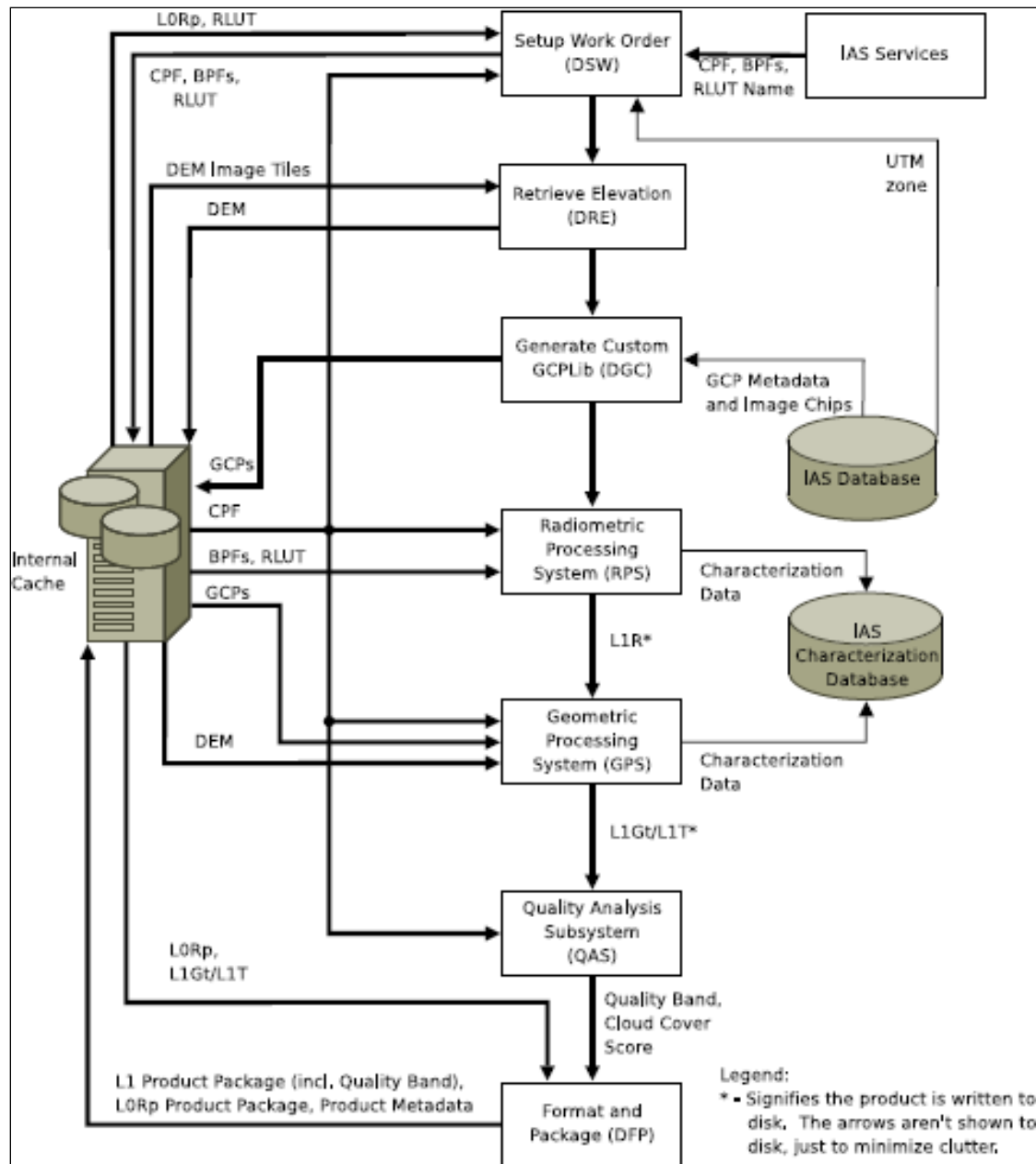


Figure 4-1. LPGS Standard Product Data Flow

The following paragraphs describe the purpose and function of each of the major LPGS Subsystems. Complete detailed designs for each Subsystem are presented in subsequent sections.

- Process Control Subsystem (PCS) – The PCS controls work order scheduling and processing. The PCS manages and monitors LPGS resources and provides processing status in response to Operator requests.
- Data Management Subsystem (DMS) – The DMS provides data management services for the LPGS and handles the external interfaces for the System. It

- provides tools for formatting and packaging products. The DMS also maintains LPGS disk space and populates temporary storage with data from ingested files.
- Radiometric Processing Subsystem (RPS) – The RPS converts the brightness of the L0R image pixels to absolute radiance in preparation for geometric correction. The RPS performs radiometric characterization of L0R images by locating radiometric artifacts in images. The RPS provides the results of characterizations performed to the IAS characterization database. The RPS corrects radiometric artifacts and converts the image to radiance.
 - Geometric Processing Subsystem (GPS) – The GPS creates L1 geometrically corrected imagery (L1G) from L1R products. The geometrically corrected products can be systematic terrain-corrected (L1Gt) or precision terrain-corrected products (L1T). The GPS provides the results of characterizations performed to the IAS characterization database. The GPS generates a satellite model, prepares a resampling grid, and resamples the data to create an L1Gt or L1T product. The GPS performs sophisticated satellite geometric correction to create the image according to the map projection and orientation specified for the L1 standard product.
 - Quality Assessment Subsystem (QAS) – The QAS performs cloud cover assessment and generates the product quality band. The QAS provides tools for visual inspection of images where a problem has been encountered while creating the product.
 - User Interface (UI) – The UI provides the Graphical User Interface (GUI) for the LPGS Operator and the Anomaly Analysis Subsystem (AAS). It allows the Operator to monitor the status of work orders and track processing anomalies.

4.1.3 Ancillary Data

The L8 OLI and TIRS geometric correction algorithms are applied to the wideband (data contained in Level 0R (raw) or 1R (radiometrically corrected)) products. Some of these algorithms also require additional ancillary input data sets. These include the following:

- Ancillary data from the spacecraft and Space Inertial Reference Unit (SIRU) provides attitude information for the spacecraft.
- Ground control / reference images for geometric test sites - used in precision correction, geodetic accuracy assessment, and geometric calibration algorithms.
- Digital elevation data for geometric test sites - used in terrain correction and geometric calibration.
- Prelaunch ground calibration results, including band /detector placement and timing, and attitude sensor characteristics.
- Earth parameters, including static Earth model parameters (e.g., ellipsoid axes, gravity constants) and dynamic Earth model parameters (e.g., polar wander offsets, UT1-UTC time corrections) - used in systematic model creation and incorporated into the CPF.

4.1.4 Data Products

One of the goals of L8 is the provision of high-quality, standard data products. About 400 scenes per day are imaged globally and returned to the United States archive. All of

these scenes are processed to a Level 1 standard product and made available for downloading over the Internet at no cost to users.

The L1T available to users is a radiometrically and geometrically corrected image. Inputs from both the sensors and the spacecraft are used, as well as GCPs and DEMs. The result is a geometrically rectified product free from distortions related to the sensor (e.g., view angle effects), satellite (e.g., attitude deviations from nominal), and Earth (e.g., rotation, curvature, relief). The image is also radiometrically corrected to remove relative detector differences, dark current bias, and some artifacts. The Level 1 image is presented in units of DNs, which can be easily rescaled to spectral radiance or TOA reflectance.

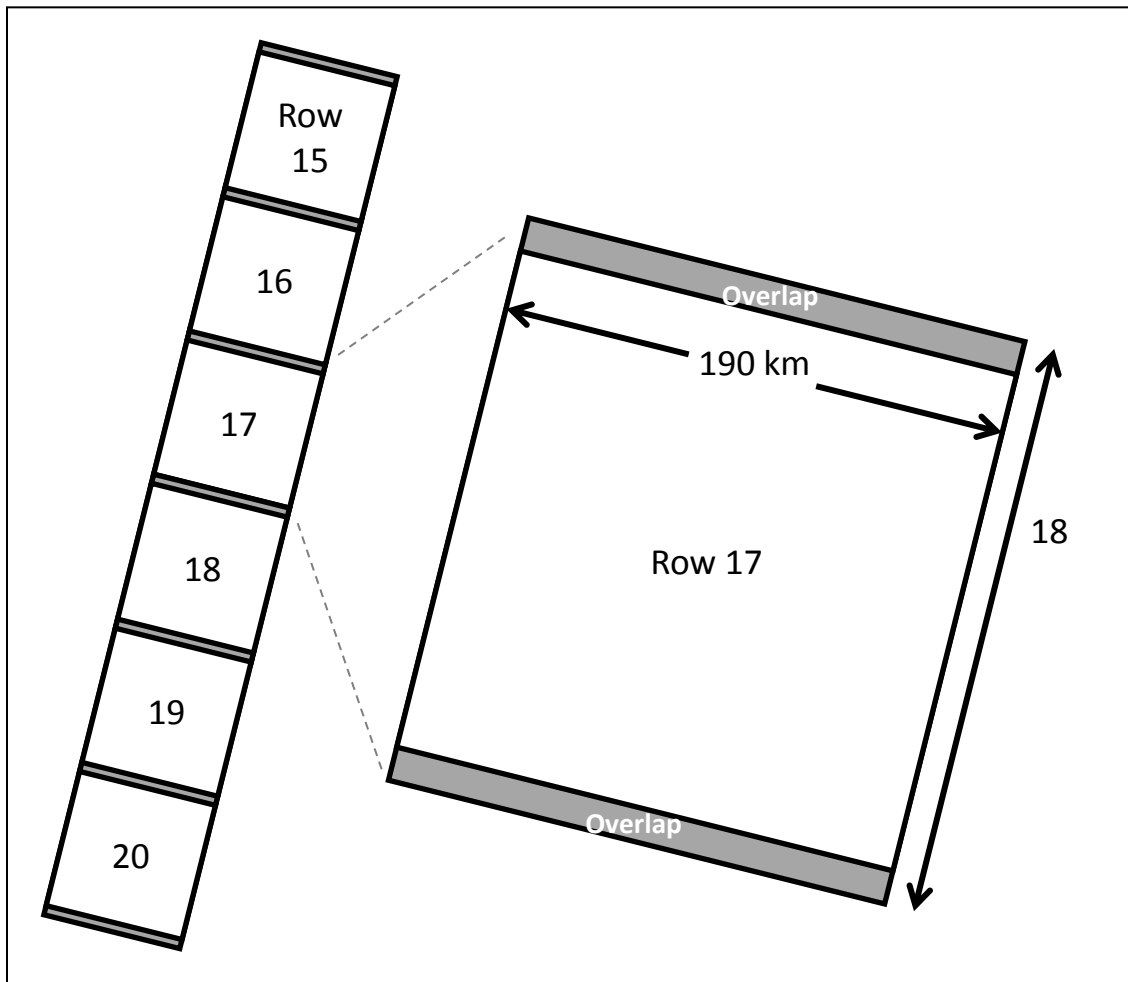


Figure 4-2. Level 1 Product Ground Swath and Scene Size

4.1.4.1 Product Components

A complete L1 product consists of 13 files, including the 11 band images, a product-specific metadata file, and a Quality Assessment (QA) image. The image files are all 16-

bit GeoTIFF images. The OLI bands are Bands 1-9. The TIRS bands are designated as Bands 10 and 11.

The QA image is a 16-bit mask, which marks clouds, fill data, and some land cover types. Subsection 5.4 gives a full description of the L8 QA mask.

The metadata (MTL) file contains identifying parameters for the scene, along with the spatial extent of the scene and the processing parameters used to generate the Level 1 product. This file is a human-readable text file in ODL format.

4.1.4.2 Product Format

The product delivered to L8 data users is packaged as Geographic tagged image file format (GeoTIFF) (a standard, public-domain image format based on Adobe's TIFF) and is a self-describing format developed to exchange raster images. The GeoTIFF format includes geographic or cartographic information embedded within the imagery that can be used to position the image in a geographic information display. Each L8 band is presented as a 16-bit grayscale image. Specifically, GeoTIFF defines a set of TIFF tags, which describes cartographic and geodetic information associated with geographic TIFF imagery. GeoTIFF is a means for tying a raster image to a known model space or map projection and for describing those projections. A metadata format provides geographic information to associate with the image data. However, the TIFF file structure allows both the metadata and the image data to be encoded into the same file.

For details on GeoTIFF format, please download the GeoTIFF Format Specification (PDF) or visit <http://trac.osgeo.org/geotiff/>.

4.1.4.3 Cloud Cover Assessment (CCA)

The L8 CCA system uses multiple algorithms to detect clouds in scene data. Each CCA algorithm creates its own pixel mask that labels clouds, cirrus, and other classification types. The separate pixel masks are then merged together into the final L1 quality band.

The separate masks are merged together via a weighted voting mechanism. Each algorithm is assigned weights for every class (cloud, cirrus, water, and snow / ice), which indicates how accurate that algorithm is expected to be when classifying that type of target. These weights are defined in the CPF. Then, for each pixel, the confidence value in each mask is used to sum the algorithm weights together:

$$high_k = \sum_{j=1}^N W_{j,k} \quad \text{if } C_{j,k} > 0.65 \\ 0 \quad \text{otherwise}$$

$$mid_k = \sum_{j=1}^N W_{j,k} \quad \text{if } 0.35 \leq C_{j,k} \geq 0.65 \\ 0 \quad \text{otherwise}$$

$$low_k = \sum_{j=1}^N W_{j,k} \quad \begin{array}{l} \text{if } C_{j,k} < 0.35 \\ \text{otherwise} \end{array}$$

Where:

j = Algorithm j of N .

At launch $N = 3$ for clouds, although two of the cloud algorithms are mutually exclusive (Automated Cloud Cover (ACCA) and AT-ACCA). For Cirrus, $N=1$.

k = Class (cloud, cirrus, water, or snow / ice).

$W_{j,k}$ = Fractional weights assigned to each algorithm (j) and class (k). Note that the sum of W over all algorithms is 1.

$C_{j,k}$ = The pixel's class k confidence value from algorithm j .

With these sums, the final score of the class (S_k) is found by simple comparison:

$$S_k = \begin{cases} \text{High if } high_k > low_k \text{ and } high_k > mid_k \\ \text{Mid if } mid_k \geq low_k \text{ and } mid_k \geq high_k, \text{ or if } high_k = low_k \\ \text{Low if } low_k > high_k \text{ and } low_k > mid_k \end{cases}$$

This final score is assigned to the pixel in the quality band. Note that the mid-confidence score – which is equivalent to 'ambiguous' – wins all ties among the CCA algorithms.

The L8 CCA system was designed to be modular, providing the ability to quickly add or remove CCA algorithms as desired. It is expected that more CCA algorithms will be added to the L8 CCA system in the near future. At launch, there were four CCA algorithms, including ACCA, See-5, Cirrus, and AT-ACCA.

4.1.4.3.1 Automated Cloud Cover (ACCA)

ACCA is an algorithm used to generate scene-wide cloud scores for previous Landsat instruments. The L8 implementation of ACCA is similar, but it uses only Pass 1, the spectral cloud identification component of the algorithm, which generates a per-pixel cloud mask. Later ACCA passes are used to bias the pass 1 results to create a single cloud score for the entire scene, so they are not useful for creating per-pixel masks.

ACCA works on Bands 3-6 of Level 1 imagery that is converted to TOA reflectance using a scene-center solar elevation angle. It also uses TIRS Band 10 imagery that have been converted to at-satellite brightness temperature. The formula for these conversions is in subsection 5.3 of this document.

Once the TOA reflectance for Bands 3-6 and the brightness temperature of Band 10 is available, ACCA uses eight different filters to classify the pixels in the scene:

1. Filter 1 – Red Brightness Threshold
 - i. *possible cloud if $Q_4 > 0.8$*
 - ii. Each Band 4 (Red) pixel in the scene is first compared to a brightness threshold. Pixel values that exceed the Band 4 threshold, which is set at .08,

- are passed to filter 3. Pixels that fall below this threshold are identified and are passed to filter 2.
2. Filter 2 – Red Non-cloud / Ambiguous Discriminator
 - i. *ambiguous if* $Q_4 \leq 0.7$
 - ii. *possible water if* $Q_4 < 0.7$
 - iii. Comparing each pixel entering this filter to a Band 4 threshold set at .07 identifies potential low-reflectance clouds. Pixels that exceed this threshold are labeled as ambiguous. Those falling below .07 are identified as non-clouds and are flagged as such in the cloud mask. Because this filter is a weak discriminator for non-cloudy water, pixels marked as non-cloudy change to 0.7 by this filter also set the Water bit in the quality band.
 3. Filter 3 – Normalized Difference Snow Index
 - i. *possible cloud if* $-0.25 < \text{NDSI} < 0.7$
 - ii. where
$$\text{NDSI} = \frac{\rho_3 - \rho_6}{\rho_3 + \rho_6}$$
 - iii. The Normalized Difference Snow Index (NDSI) is used to detect snow (Hall et al., 1995). The reflectances of clouds and snow are similar in the green band, OLI Band 3. However, in OLI Band 6, clouds have high reflectivity, while snow reflectivity is low. Pixels that fall between an NDSI range of -.25 and .7 qualify as potential clouds and are passed to filter 5. Pixels outside this NDSI range are labeled as non-cloud and passed to Filter 4.
 4. Filter 4 – Snow / Ice Threshold
 - i. *possible snow / ice if* $\text{NDSI} > 0.8$
 - ii. NDSI values above 0.8 are likely to be snow or ice. The snow / ice bit is set in the quality band for these pixels. All pixels that are passed to filter 4 are marked as non-cloud, whether or not they meet the threshold of possible snow / ice.
 5. Filter 5 – Temperature Threshold
 - i. *possible cloud if* $\text{BT} > 300 \text{ K}$
 - ii. The Brightness Temperature (BT) values are used to identify potential clouds. If a pixel value exceeds 300 K – a realistic maximum for cloud temperature – it is labeled as non-cloud. Pixels with a temperature a value less than 300 K are passed to filter 6.
 6. Filter 6 – SWIR / Thermal Composite
 - i. *possible cloud if* $(1 - Q_6)\text{BT} < 225$
 - ii. This filter is sensitive to clouds because clouds have cold temperatures ($< 300 \text{ K}$) and are highly reflective in the OLI SWIR Band 6 and therefore have low values of $(1 - \rho_6)\text{BT}$. It is particularly useful for eliminating cold land surface features that have low Band 6 reflectance such as snow and tundra. Sensitivity analysis demonstrated that a threshold setting of 225 works optimally. Pixels below this threshold are passed to filter 8 as possible clouds. Pixel values above this threshold are examined using filter 7.
 7. Filter 7 – SWIR Non-cloud / Ambiguous Discriminator
 - i. *ambiguous if* $Q_6 \geq 0.8$
 - ii. *non-cloud if* $Q_6 < 0.8$

- iii. This test admits the possibility of low-reflectance clouds. Pixels below this threshold are labeled as non-cloud, while those that exceed the threshold are labeled as ambiguous.
- 8. Filter 8 – NIR / Red Ratio for Growing Vegetation
 - i. *ambiguous if* $\frac{\rho_5}{\rho_4} \geq 2.35 \frac{\rho_5}{\rho_4} \geq 2.35$
 - ii. This filter eliminates highly reflective vegetation and is simply OLI Band 5 (NIR) reflectance divided by OLI Band 4 (Red) reflectance. In the near-infrared, reflectance for green leaves is high because very little energy is absorbed. In red wavelengths, the chlorophyll in green leaves absorbs energy so reflectance is low. This ratio results in higher values for vegetation than for other scene features, including clouds. A threshold setting of 2.35 is used. Pixels that exceed this threshold are labeled ambiguous, while pixels with ratios below this threshold are passed to filter 9.
- 9. Filter 9 – NIR/Green Ratio for Senescent Vegetation
 - i. *ambiguous if* $\frac{\rho_5}{\rho_3} \geq 2.16248$
 - ii. In the near-infrared, senescent vegetation often is higher. The NIR / Green Ratio is sensitive to chlorophyll changes and vegetation health, and the ratio tends to be higher for vegetation than many other scene features, including clouds, and thus it can be used to discriminate vegetation from these other features. A threshold setting of 2.16248 works effectively. Pixels that exceed this number are ambiguous, while pixels with ratios below this threshold are passed to filter 10.
- 10. Filter 10 – NIR / SWIR Ratio for Soil
 - i. *ambiguous if* $\frac{\rho_5}{\rho_6} \leq 1.0$
 - ii. *cloudy if* $\frac{\rho_5}{\rho_6} > 1.0$
 - iii. This filter eliminates highly reflective rocks and sands in desert landscapes and is formed by dividing the NIR (OLI Band 5) reflectance by the SWIR (OLI Band 6) reflectance. Rocks and sand tend to exhibit higher reflectance in SWIR bands than in the chlorophyll-sensing NIR band, whereas the reverse is true for clouds. A threshold setting of 1.0 works effectively. Pixels that fall below this threshold are labeled, while pixels with ratios that exceed this threshold are marked as cloudy. (No distinction is made between warm and cold clouds in the L8 implementation of ACCA.)

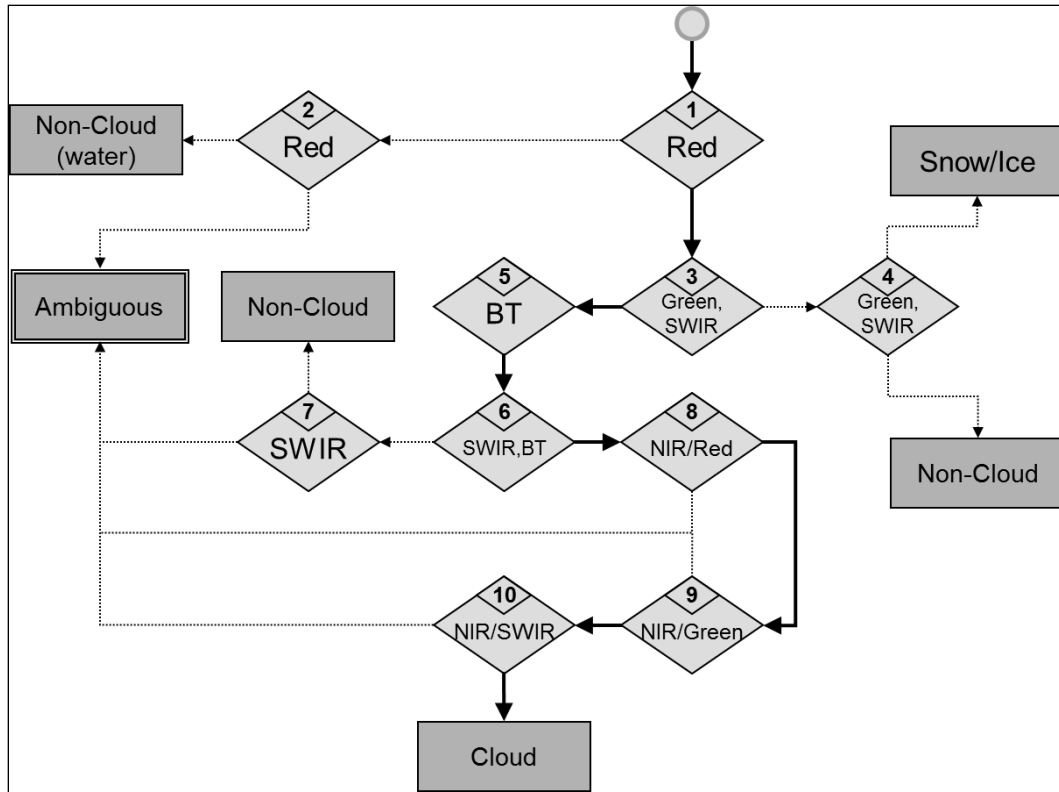


Figure 4-3. A Diagram of the First Pass ACCA Algorithm

The ACCA algorithm labels each pixel in the Level 1 scene as non-cloud, ambiguous, or cloudy. These labels are analogous to the low, medium, and high confidence cloud designations in the L1 quality band. The CCA control system takes the output from the ACCA algorithm and other CCA algorithms to generate the final Level 1 quality band.

4.1.4.3.2 See-5 CCA

See-5 CCA is a cloud algorithm developed using the concept of information entropy to split training data into thresholds that provide the maximum information. Its name comes from the software used to train the algorithm, the C5.0 software package from Rulequest Research.

The See-5 algorithm is a very large decision tree of 244 threshold tests, whose input is OLI Bands 2-7. For every pixel in an L1 scene, See-5 CCA generates a confidence score that is used to label the pixel as low, medium, or high confidence cloud. Masks created by See-5 are very accurate – this algorithm outperforms ACCA in most situations – but the algorithm itself is too convoluted to present in detail. For more information about the See-5 CCA algorithm, see Scaramuzza et al., 2012.

4.1.4.3.3 Cirrus CCA

High, thin clouds are detected using OLI Band 9, which is centered on shortwave infrared light at $1.38 \mu\text{m}$ wavelength. Light at this wavelength is strongly absorbed by water vapor in the Earth's atmosphere, so that sunlight that travels too deep into the

atmosphere cannot reflect back to the satellite. Cirrus clouds are high in the atmosphere and thus above most of the water vapor, so they are strong reflectors of this 1.38 μm radiation.

The L8 Cirrus CCA algorithm is a simple threshold test for reflectance in OLI Band 9. The threshold is set in the CPF; the at-launch threshold is 2 percent reflectance. Any object with greater reflectance in Band 9 is marked as possible cirrus.

$$\text{Cirrus if: } \rho_9 > T_{\text{cirrus}}$$

where:

ρ_9 = TOA reflectance in OLI Band 9.
(Note that this is calculated from the L1G product using a scene-center solar elevation angle.)
 T_{cirrus} = Cirrus threshold from the CPF. (0.02 at launch)

This test is very permissive, and it detects false positives over high-altitude arid regions and over the poles, where the air is very cold and dry. The cirrus test is very accurate over low-to-moderate elevation areas in non-polar regions.

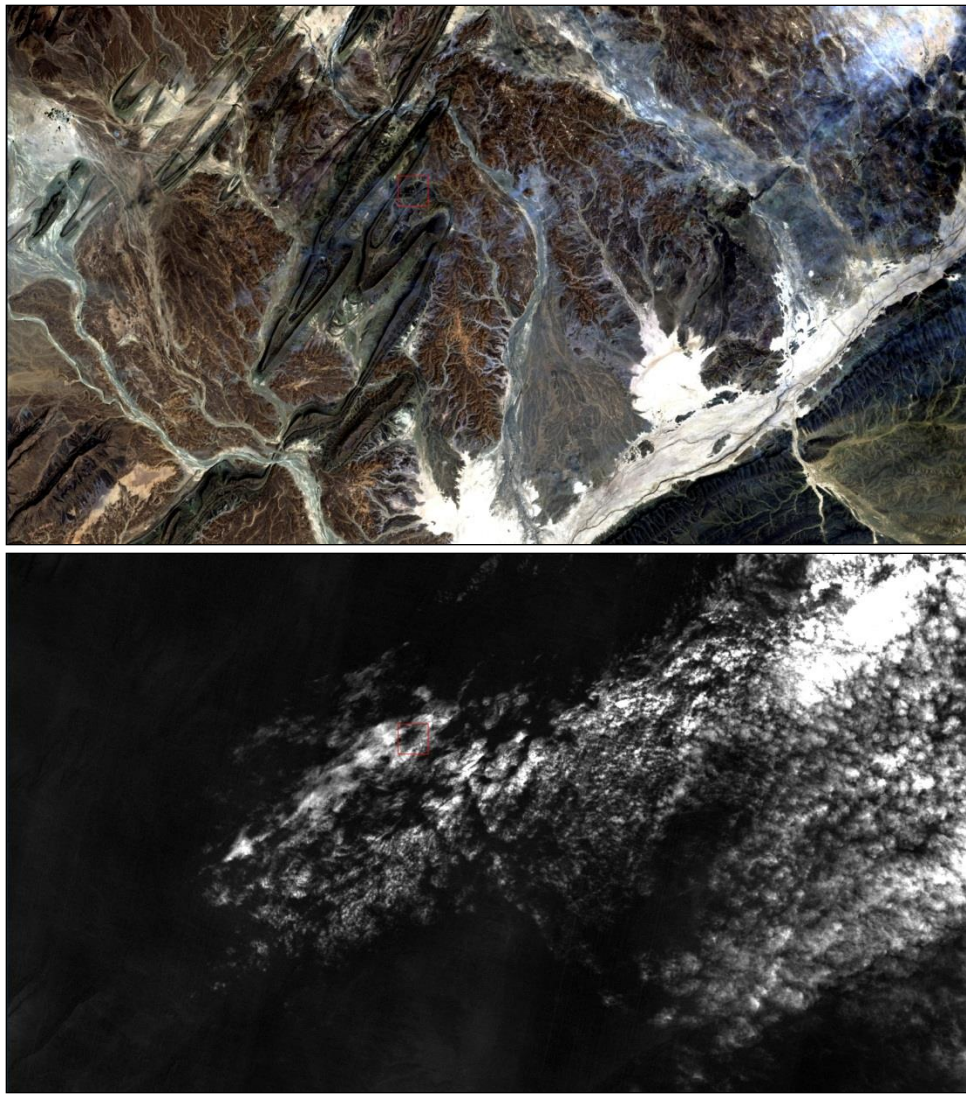


Figure 4-4. A Temperate Region Affected by Cirrus Top image is OLI Bands 4,3,2; bottom image is OLI Band 9, the cirrus detection band.

The quality band in Level 1 products contains a cirrus flag that reports high, medium, or low probability of cirrus for each pixel in the scene. This is intended as an aid to users, to indicate how each pixel may be affected by thin, high-altitude clouds that may or may not be visible in other bands of the imagery.

4.1.4.3.4 AT-ACCA

The 'Artificial Thermal' (AT) variant of the ACCA algorithm is intended for use only when thermal data from the TIRS instrument are not available. It uses the reflectance of Bands 2-7, calculated from L1 data using a scene-center solar elevation angle, to approximate the brightness temperature of the missing thermal band. This AT band is intended only for use in the AT-ACCA algorithm, and is not available to the public. Once the AT band is created, the AT-ACCA algorithm uses it as a replacement for BT in the same threshold filters as the normal ACCA algorithm. Note that ACCA and AT-ACCA

are never run together. If a thermal band exists, ACCA is run; if no thermal band exists, then AT-ACCA is used.

A large number of pixels are labeled ambiguous by the filters in the AT-ACCA algorithm. To reduce the number of ambiguous pixels, a second pass is made using an additional suite of disambiguation threshold tests. These disambiguation tests are only applied to pixels labeled ambiguous by the AT-ACCA. The tests are simple thresholds that are statistically unlikely to indicate clouds among data normally marked as ambiguous by ACCA. If a pixel passes any two of these tests, it is labeled as non-cloud. Pixels that pass only one or zero tests remain ambiguous. Similar to the ACCA algorithm, the AT-ACCA's labels of non-cloud, ambiguous, and cloud pixels are analogous to the low, medium, and high confidence cloud designations in the L1 quality band.

For full details on the AT band, the AT-ACCA algorithm, and the AT-ACCA disambiguation tests, see Scaramuzza et al., 2012.

4.1.5 Calculation of Scene Quality

The quality algorithm is calculated by the following two formulas:

$$\begin{aligned} \text{SIQS} &= 9 - [\text{SNF}/\text{ANF} * (\text{NDF} / \text{DFBP} + \text{NCF} / \text{CFBP})] \\ \text{IIQS} &= 9 - [(\text{NDF}/\text{DFBP} + \text{NCF}/\text{CFBP})] \end{aligned}$$

Where:

SIQS = Scene Image Quality Score

IIQS = Interval Image Quality Score

SNF = Standard number of video frames in a scene [7001 for OLI, 2621 for TIRS]

ANF = Actual number of frames in the scene / interval

NDF = Number of dropped frames in the scene / interval

DFBP = Dropped Frame Break Point: dropped frame count at which the quality score drops by one point. [2]

NCF = Number of video frame CRC failures in the scene / interval

CFBP = CRC Failures Break Point: Video frame CRC failure count at which the quality score drops by one point. [100]

Numbers in brackets are configurable. If changed, the quality algorithm version is updated and the new values documented

Image_Quality_OLI

Values: 0–9, where

9 = Best

0 = Worst

-1 = quality not calculated or assessed

Image_Quality_TIRS

Values: 0–9, where
9 = Best
0 = Worst
-1 = quality not calculated or assessed

4.2 Level 1 Product Description

4.2.1 Science Data Content and Format

The L8 instruments, OLI and TIRS, represent an evolutionary advance in technology. OLI builds upon Landsat heritage and technologies demonstrated by the ALI. As such, OLI is a push-broom sensor with a four-mirror telescope and uses 12-bit quantization. The OLI collects 30-meter data for visible, near infrared, and short wave infrared spectral bands as well as provides for a 15-meter panchromatic band. New with OLI is the addition of a 30-meter deep blue Coastal Aerosol band (Band 1) for coastal water and aerosol studies and a 30-meter Cirrus band (Band 9) for cirrus cloud detection. Additionally, the bandwidth has been refined (narrowed) for six of the heritage bands.

The TIRS instrument collects data for two narrow spectral bands in the thermal region, formerly covered on previous Landsat instruments by one wide spectral band. Although TIRS is a separate instrument, the 100-meter TIRS data are registered to the OLI data in order to create radiometrically, geometrically, and terrain-corrected 12-bit data products.

These sensors both provide improved SNR radiometric performance quantized over a 12-bit dynamic range. This translates into 4096 potential grey levels in an image compared with only 256 grey levels in previous 8-bit instruments. Additionally, improved signal-to-noise performance enables better characterization of land cover state and condition.

4.2.1.1 Science Data Content

In addition to Table 2-1 in Section 2, Figure 4-5 compares L8 spectral bands and wavelength to that of L7 ETM+.

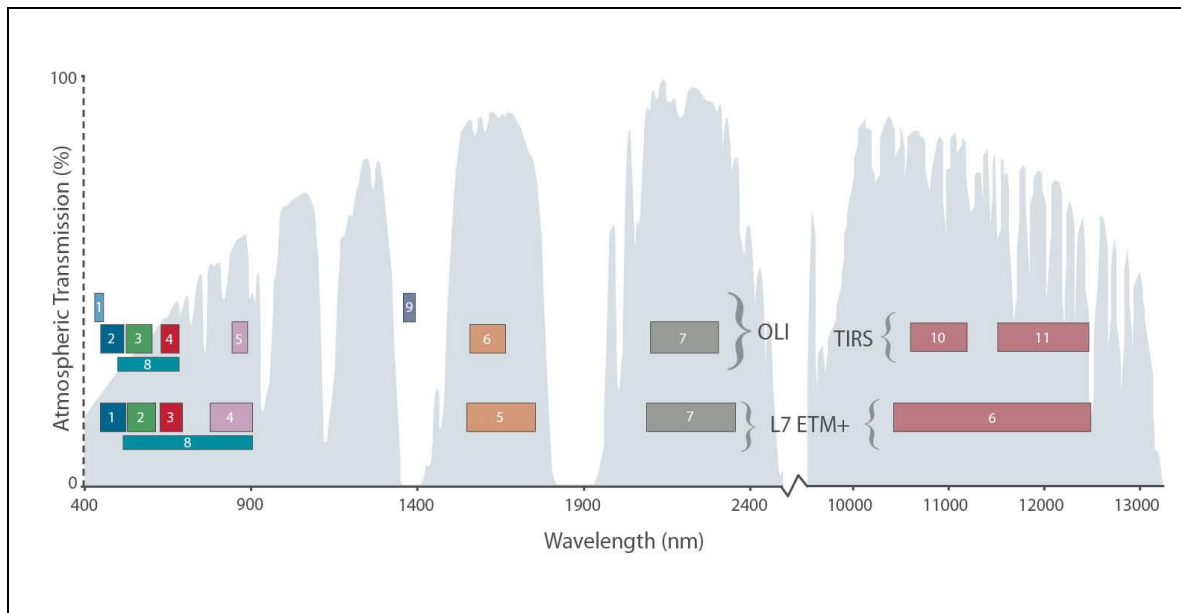


Figure 4-5. Landsat 8 Spectral Bands and Wavelengths compared to Landsat 7 ETM+

4.2.1.2 Science Data Format

L8 acquires high-quality, well-calibrated multispectral data over the Earth's land surfaces. On average, over 500 unique scenes are acquired per day across the globe and sent to the USGS EROS Center for storage, archive, and processing. All of these scenes are either processed to an L1Gt product or to a standard L1T product. The highest available product derivative is made available for download over the Internet at no cost to users. A complete standard Level 1 product consists of 13 files, including OLI Bands 1-9 (one file per band), TIR Bands 10 & 11 (one file per band), a product-specific metadata file, and a QA file.

[LSDS-809 Landsat 8 \(L8\) Level 1 \(L1\) Data Format Control Book \(DFCB\)](#) is an excellent reference for L8 product format and information. The following paragraphs summarize the Level 1 data format.

For details on GeoTIFF format, please refer to the [GeoTIFF Format Specification \(PDF\)](#) or visit <http://trac.osgeo.org/geotiff/>.

In addition to GeoTIFF, the data incorporate cubic convolution resampling, North Up (Map) image orientation, and Universal Transverse Mercator (UTM) map projection (Polar Stereographic projection for scenes with a center latitude greater than or equal to -63.0 degrees) using the WGS84 datum.

The format of the final output product is a tar.gz file. Specifically, the files are written to a tar file format and then compressed with the gzip application. Of note, the tar file does not contain any subdirectory information. Therefore, uncompressing the file places all of the files directly into the current directory location.

Table 4-1 and Table 4-2 address the standard and compressed file-naming conventions for L8 L1 products.

File Naming Convention	
Identifier	Description
L	Landsat
s	Sensor of: O = OLI, T = TIRS, C = Combined TIRS and OLI Indicates which sensor collected data for this product
8	Landsat mission number
ppp	Satellite orbit location in reference to the Worldwide Reference System-2 (WRS-2) path of the product
rrr	Satellite orbit location in reference to the WRS-2 row of the product
YYYY	Acquisition year of the image
DDD	Acquisition day of year
GGG	Ground station ID
VV	Version
_FT	File type, where FT equals one of the following: image band file number (B1–B11), MTL (metadata file), BQA (quality band file), MD5 (checksum file)
.ext	File extension, where .TIF equals GeoTIFF file extension, and .txt equals text extension

Table 4-1. Standard: *Ls8ppprrrYYYYDDDGGSVV_FT.ext*

Compressed File Naming Convention	
Identifier	Description
L	Landsat
s	Sensor of: O = OLI, T = TIRS, C = Combined TIRS and OLI Indicates which sensor collected data for this product
8	Landsat mission number
ppp	Satellite orbit location in reference to the Worldwide Reference System-2 (WRS-2) path of the product
rrr	Satellite orbit location in reference to the WRS-2 row of the product
YYYY	Acquisition year of the image
DDD	Acquisition day of year
GGG	Ground station ID
VV	Version
_FT	File type, where FT equals tar (tarred file)
.ext	File extension, where .gz equals zipped (compressed) extension

Table 4-2. Compressed: *Ls8ppprrrYYYYDDDGGSVV.FT.ext*

4.2.2 Metadata Content and Format

The MTL file is created during product generation and contains information specific to the L1 product ordered. The MTL file contains identifying parameters for the scene,

along with the spatial extent of the scene and the processing parameters used to generate the Level 1 product. This file is a human-readable text file in ODL format. [LSDS-809 Landsat 8 \(L8\) Level 1 \(L1\) Data Format Control Book \(DFCB\)](#) provides a complete description of the metadata file. In general, the MTL file includes the following parameters:

- Unique Landsat scene identifier
- WRS path and row information
- Scene Center Time of the date the image was acquired
- Corner longitude and latitude in degrees and map projection values in meters
- Reflective, thermal, and panchromatic band lines and samples
- File names included
- Image attributes including cloud cover, sun azimuth and elevation, and number of GCPs used
- Band minimum and maximum reflectance and radiance rescaling

4.2.3 Quality Assessment Band

The QA Band contains quality statistics gathered from the image data and cloud mask information for the scene. The QA file is a 16-bit image with the same dimensions as the standard L1T scene. Bits are allocated for some artifacts that are distinguishable after the systematic correction (Level 1G) stage of processing. The first bit (bit 0) is the least significant. Subsection 5.4 provides a full description of the L8 QA band.

Used effectively, QA bits improve the integrity of science investigations by indicating which pixels might be affected by instrument artifacts or be subject to cloud contamination. For example, Normalized Difference Vegetation Index (NDVI) calculated over pixels containing clouds will show anomalous values. If such pixels were included in a phenology study, the results might not show the true characteristics of seasonal vegetation growth. Cloud-contaminated pixels will lower NDVI values, and measures such as the timing of ‘green up’ or peak maturity would appear later than they actually occurred. A worse consequence would be that the reported reduction of vegetation growth would be taken as an indicator of environmental change, potentially prompting unnecessary land management policies or practices.

Rigorous science applications seeking to optimize the value of pixels used in a study will find QA bits useful as a first-level indicator of certain conditions. Otherwise, users are advised that this file contains information that can be easily misinterpreted and it is not recommended for general use. Robust image processing software capable of handling 16-bit data is necessary to compute statistics of the number of pixels containing each of the designated bits.

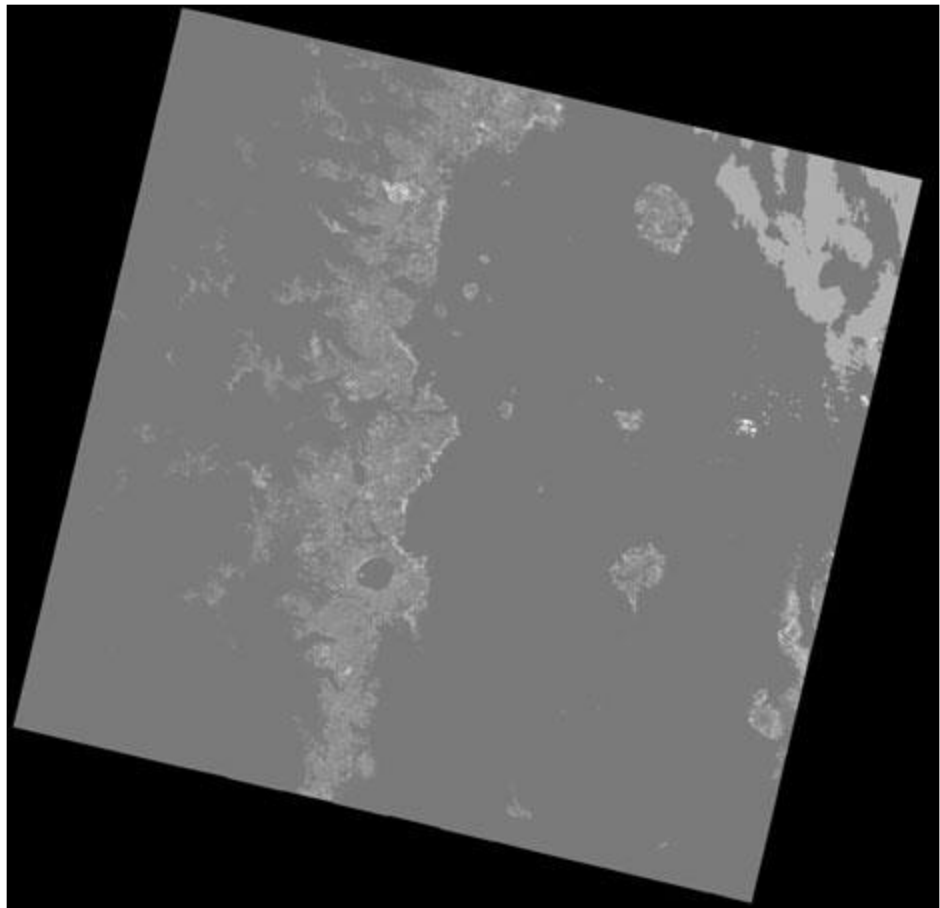


Figure 4-6. Quality Band (BQA.TIF) displayed for Landsat 8 Sample Data (Path 45 Row 30) Acquired April 23, 2013

The QA image can be stretched to emphasize the light ("1"s) and dark ("0") pixels for a quick view of general quality conditions. In the Crater Lake, Oregon, image above, the lighter pixels are likely to be affected by snow or clouds.

Section 5 Conversion of DNs to Physical Units

5.1 OLI and TIRS at Sensor Spectral Radiance

Images are processed in units of absolute radiance using 32-bit floating-point calculations. These values are then converted to 16-bit integer values in the finished Level 1 product. These values can then be converted to spectral radiance using the radiance scaling factors provided in the metadata file:

$$L_\lambda = M_L * Q_{\text{cal}} + A_L$$

where:

L_λ = Spectral radiance ($\text{W}/(\text{m}^2 * \text{sr} * \mu\text{m})$)

M_L = Radiance multiplicative scaling factor for the band
(RADIANCE_MULT_BAND_n from the metadata)

A_L = Radiance additive scaling factor for the band (RADIANCE_ADD_BAND_n from the metadata).

Q_{cal} = L1 pixel value in DN

5.2 OLI Top of Atmosphere Reflectance

Similar to the conversion to radiance, the 16-bit integer values in the L1 product can also be converted to TOA reflectance. The following equation is used to convert Level 1 DN values to TOA reflectance:

$$\rho_{\lambda'} = M_p * Q_{\text{cal}} + A_p$$

where:

$\rho_{\lambda'}$ = TOA Planetary Spectral Reflectance, without correction for solar angle.
(Unitless)

M_p = Reflectance multiplicative scaling factor for the band
(REFLECTANCEW_MULT_BAND_n from the metadata).

A_p = Reflectance additive scaling factor for the band
(REFLECTANCE_ADD_BAND_N from the metadata).

Q_{cal} = L1 pixel value in DN

Note that $\rho_{\lambda'}$ is not true TOA Reflectance, because it does not contain a correction for the solar elevation angle. This correction factor is left out of the L1 scaling at the users' request; some users are content with the scene-center solar elevation angle in the metadata, while others prefer to calculate their own per-pixel solar elevation angle across the entire scene. Once a solar elevation angle is chosen, the conversion to true TOA Reflectance is as follows:

$$\rho_{\lambda} = \frac{\rho_{\lambda'}}{\sin(\theta)}$$

$$\rho_\lambda' = \frac{\rho_\lambda}{\sin(\theta)}$$

where:

ρ_λ = TOA Planetary Reflectance (Unitless)
 θ = Solar Elevation Angle (from the metadata, or calculated)

5.3 TIRS Top of Atmosphere Brightness Temperature

TIRS data can also be converted from spectral radiance (as described above) to brightness temperature, which is the effective temperature viewed by the satellite under an assumption of unity emissivity. The conversion formula is as follows:

$$T = \frac{K2}{\ln(\frac{K1}{L_\lambda} + 1)}$$

where:

T = TOA Brightness Temperature, in Kelvin.
 L_λ = Spectral radiance (Watts/(m² * sr * μm))
 $K1$ = Thermal conversion constant for the band (K1_CONSTANT_BAND_n from the metadata)
 $K2$ = Thermal conversion constant for the band (K2_CONSTANT_BAND_n from the metadata)

5.4 Unpacking Quality Assessment Band Bits

The pixel values in the QA band file must be translated to 16-bit binary form to be used effectively. The gray shaded areas in Table 5-1 show the bits that are currently being populated in the L1 QA Band, and the conditions each describe. None of the currently populated bits is expected to exceed 88 percent accuracy in their reported assessment at this time.

16-bit Landsat 8 QA Band - Read bits from RIGHT to LEFT ← starting with Bit 0																
BIT	15	14	13	12	11	10	9	8	7	6	5	4	3	2	1	0
DESCRIPTION	Cloud Confidence		Cirrus Confidence		Snow/Ice Confidence		Reserved for Vegetation Confidence		Cloud Shadow Confidence		Water Confidence		Reserved	Terrain Occlusion	Dropped Frame	Designated Fill

Table 5-1. Bits Populated in the Level 1 QA Band

For the single bits (0, 1, 2, and 3):

- 0 = No, this condition does not exist

- 1 = Yes, this condition exists

The double bits (4-5, 6-7, 8-9, 10-11, 12-13, and 14-15), read from left to right, represent levels of confidence that a condition exists:

- 00 = "Not Determined" = For Cloud or Cirrus, the algorithm did not run. For the other confidence classifications this is a "No," as the Algorithm has no confidence that this condition exists
- 01 = "No" = Algorithm has low-to-no confidence that this condition exists (0-33 percent confidence)
- 10 = "Maybe" = Algorithm has medium confidence that this condition exists (34-66 percent confidence)
- 11 = "Yes" = Algorithm has high confidence that this condition exists (67-100 percent confidence)

For example, a pixel with a value "58384" translates to the 16-bit binary string "1110 0100 0001 0000." Reading the binary string from right to left and using Table 5-1 as an interpretation legend, this pixel is as follows:

- Bit 0 = 0 = not fill
- Bit 1 = 0 = not a dropped frame
- Bit 2 = 0 = not terrain occluded
- Bit 3 = 0 = not determined
- Bit 4-5 = 01 = not water
- Bit 6-7 = 00 = not determined
- Bit 8-9 = 00 = not determined
- Bit 10-11 = 01 = not snow / ice
- Bit 12-13 = 10 = could be cirrus cloud
- Bit 14-15 = 11 = cloudy

Certain values occur regularly and can be interpreted without unpacking them into 16-bit strings and using Table 5-1 as a reference. Table 5-2 includes some common pixel values and their meanings. A no-cost tool is available for user download that will extract the bit-packed information in the OLI QA band for easy interpretation. Details are provided at http://landsat.usgs.gov/L-LDOPE_Toolbelt.php.

Pixel Value	Cloud	Cirrus	Snow/Ice	Veg	Water	Terrain Occlusion	Dropped Frame	Fill
61440	Yes	Yes	No	No	No	No	No	No
56320	Yes	No	Yes	No	No	No	No	No
53248	Yes	No	No	No	No	No	No	No
48128	No	Yes	Yes	No	No	No	No	No
45056	No	Yes	No	No	No	No	No	No
39936	Maybe	No	Yes	No	No	No	No	No
36896	Maybe	No	No	No	Maybe	No	No	No
36864	Maybe	No	No	No	No	No	No	No
31744	No	Yes	Yes	No	No	No	No	No
28672	No	Yes	No	No	No	No	No	No
23552	No	No	Yes	No	No	No	No	No
20516	No	No	No	No	Maybe	Yes	No	No
20512	No	No	No	No	Maybe	No	No	No
20482	No	No	No	No	No	No	Yes	No
20480	No	No	No	No	No	No	No	No
1	Not Determined	No	No	Yes				

Table 5-2. A Summary of Some Regularly Occurring QA Bit Settings

5.5 LandsatLook Quality Image (.png)

The 8-bit LandsatLook Quality Image (.png) is available to download when downloading L8 data products. This file provides a quick view of the quality of the pixels to determine which scene would work best for each user's application. Only the highest confidence conditions are used to create the LandsatLook Quality image. Similar as stated above, this image may not be useful to all users. (Information on LandsatLook Images = <http://landsat.usgs.gov/LandsatLookImages.php>)

Table 5-3 gives the bits and colors associated with the LandsatLook Quality Image:

8-Bit LandsatLook QA Band - Read bits from RIGHT to LEFT ← starting with Bit 0								
Bit	7	6	5	4	3	2	1	0
Description	Cloud*	Cirrus*	Snow/Ice*	Vegetation*	Water*	Terrain Occlusion	Dropped Frame	Designated Fill

*Set for highest confidence value (11)

Table 5-3. Bits and Colors Associated with LandsatLook Quality Image

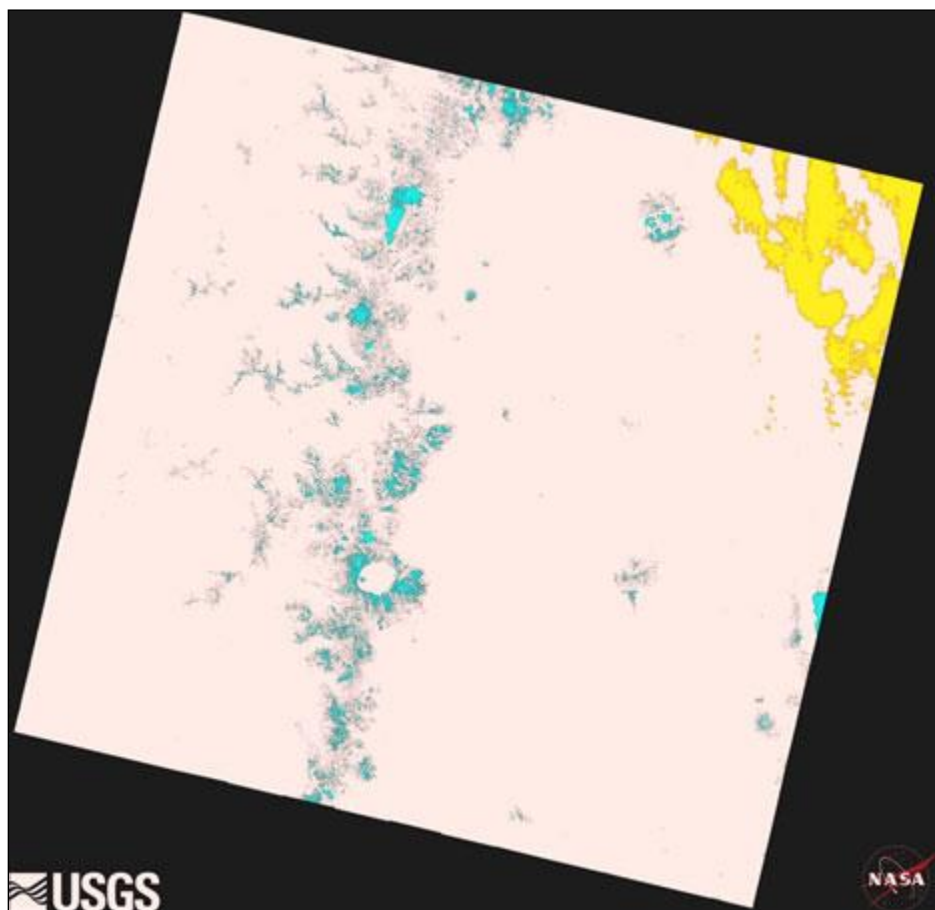


Figure 5-1. Landsat Look "Quality" Image (QA.png) displayed as .jpg for reference only Landsat 8 sample data Path 45 Row 30 Acquired April 23, 2013

Section 6 Data Search and Access

The USGS archive holds data collected by the Landsat [suite of satellites](#), beginning with Landsat 1 in 1972. Over 500 L8 scenes are added to the USGS archives each day, and become available to all users for download at no charge using the sites described in this section. All Landsat data products are distributed via Hypertext Transfer Protocol Secure (HTTPS) access. Current L8 products available include the following:

- LandsatLook “Natural Color” Image - a full-resolution, 3-band .jpg image (approximate size: 4.5 MB)
- LandsatLook “Thermal” Image - a full-a resolution, thermal band 10 .jpg image (approximate size: 2.5 MB)
- LandsatLook “Quality” Image - a full-resolution Quality Assessment band .png image (Approximate size: 2.5 MB)
- LandsatLook Images with Geographic Reference - a bundle including the “Natural,” “Thermal,” and “Quality” full-resolution images, along with .wld and .xml files with geographic reference information (Approximate size: 9.0 MB)
- Level 1 Data Product - a compressed file including all individual multispectral and/or thermal band and metadata files (Approximate size: 950 MB)

The Landsat 8 page at <http://landsat.usgs.gov/landsat8.php> contains details about L8 data products.

The interfaces outlined in the following subsections allow users to search and download L8 data held in the USGS Archives. The functionality of each differs; however, the data products are all delivered from the same location. Each interface includes a Help section to provide more details about step-by-step processes.

6.1 EarthExplorer (EE)

EE is the primary search interface accessing aerial, mapping, elevation, and satellite data held in the USGS archives, including Landsat data products. Before downloading data products, users must complete the user registration at <https://ers.cr.usgs.gov/register/>. Some functions of the Web site will work only after a successful login.

<http://earthexplorer.usgs.gov>

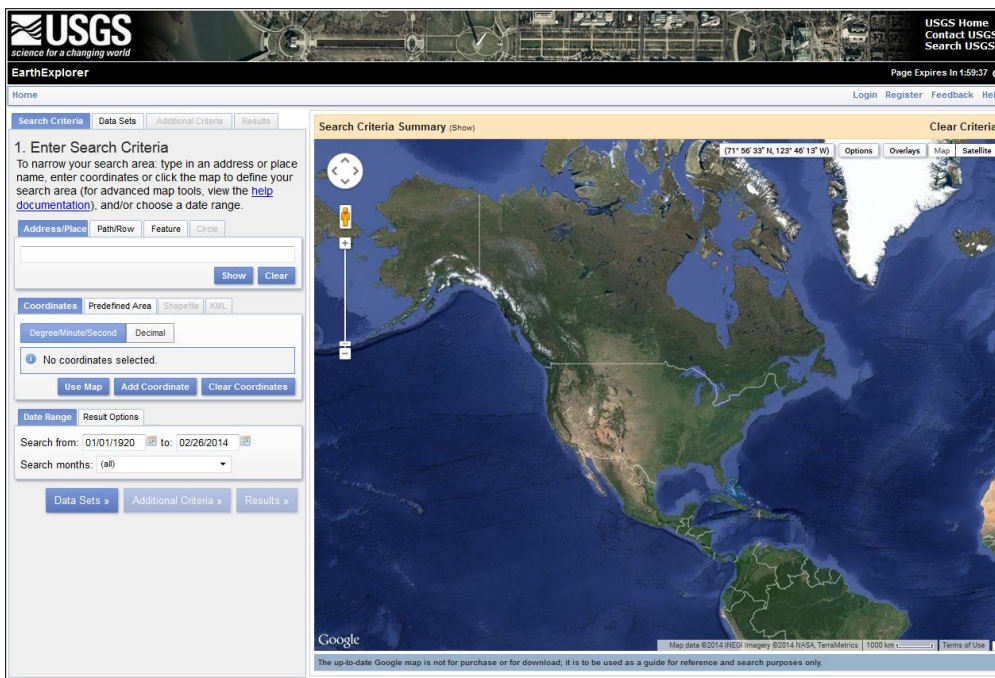


Figure 6-1. EarthExplorer Interface

The Search Criteria tab options allow users to select the geographic area of interest by typing a place name, latitude / longitude coordinates, path / row, a shape file, or .kml file. The user can also specify the date range and number of results.

The Data Sets tab lists all categories of data held in the USGS Archives. The Landsat Archive section of this tab lists all Landsat data sets from which Level 1 data products can be found:



Figure 6-2. EarthExplorer Landsat Data Sets

Each data set displays an Information button preceding the name that users can click to view more details about the data set.

After selecting the data set(s), the Additional Search Criteria button is active. The user can click this button to view the Additional Criteria (Optional) tab. This tab allows users to search by specific scene ID or Path / Row, and set cloud cover limits. Users

interested in searching nighttime imagery can select that option on this tab as well. After making their selection(s), users click the Results button, located on the bottom right side of the Additional Criteria (Optional) tab.

After a successful search, results are presented in a manner that allows users to view a browse image of the scene, a subset of the metadata file, or the footprint of a scene on the map. To view the available data products, the user clicks the Download Options icon (a green arrow) near each scene. A gold icon indicates scenes can be added to a bulk download order.

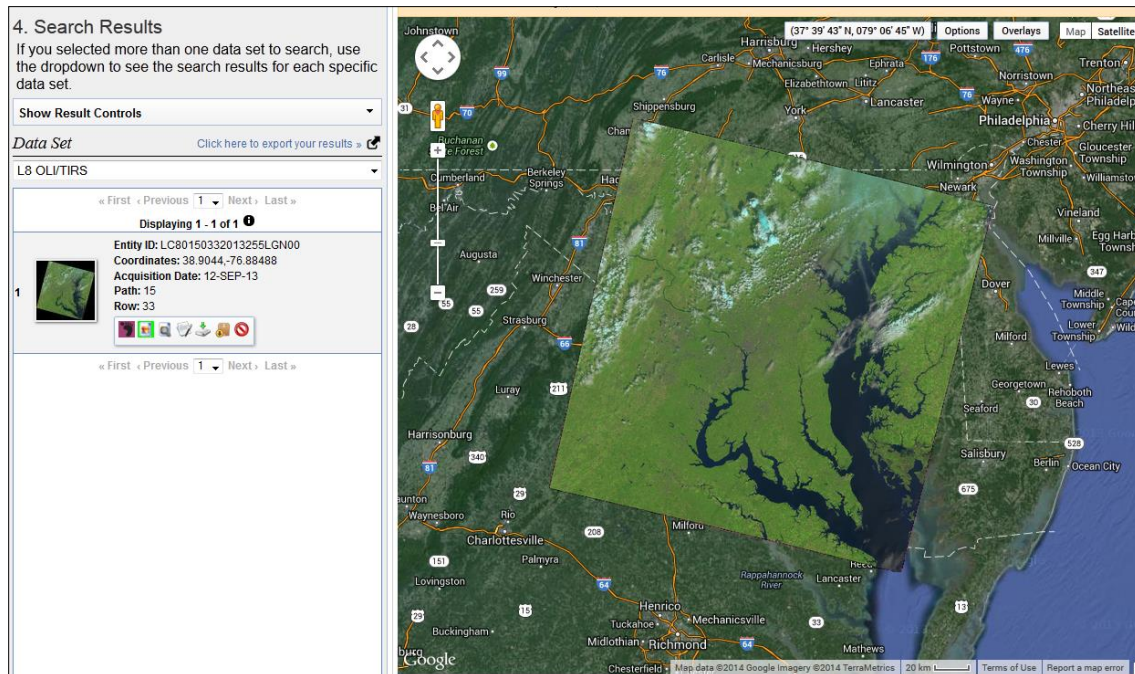


Figure 6-3. EarthExplorer Results - Browse Image Display

The Show Result Controls section (located above the results listing) allows users to view the footprints or browse of all results, or add them all to a bulk download order (see Figure 6-4).

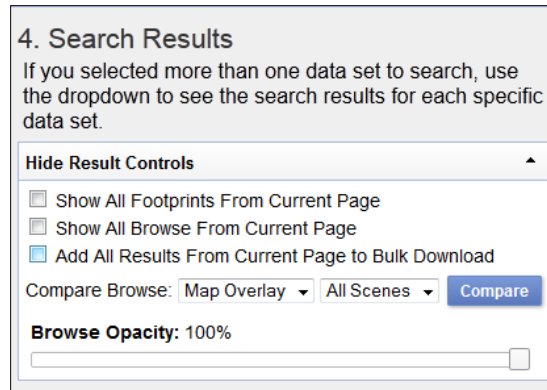


Figure 6-4. EarthExplorer Results Controls

6.2 Global Visualization Viewer (GloVis)

The GloVis Viewer is an easy-to-navigate browse-based tool that displays all available Landsat scenes held in the USGS archives.

<http://glovis.usgs.gov>

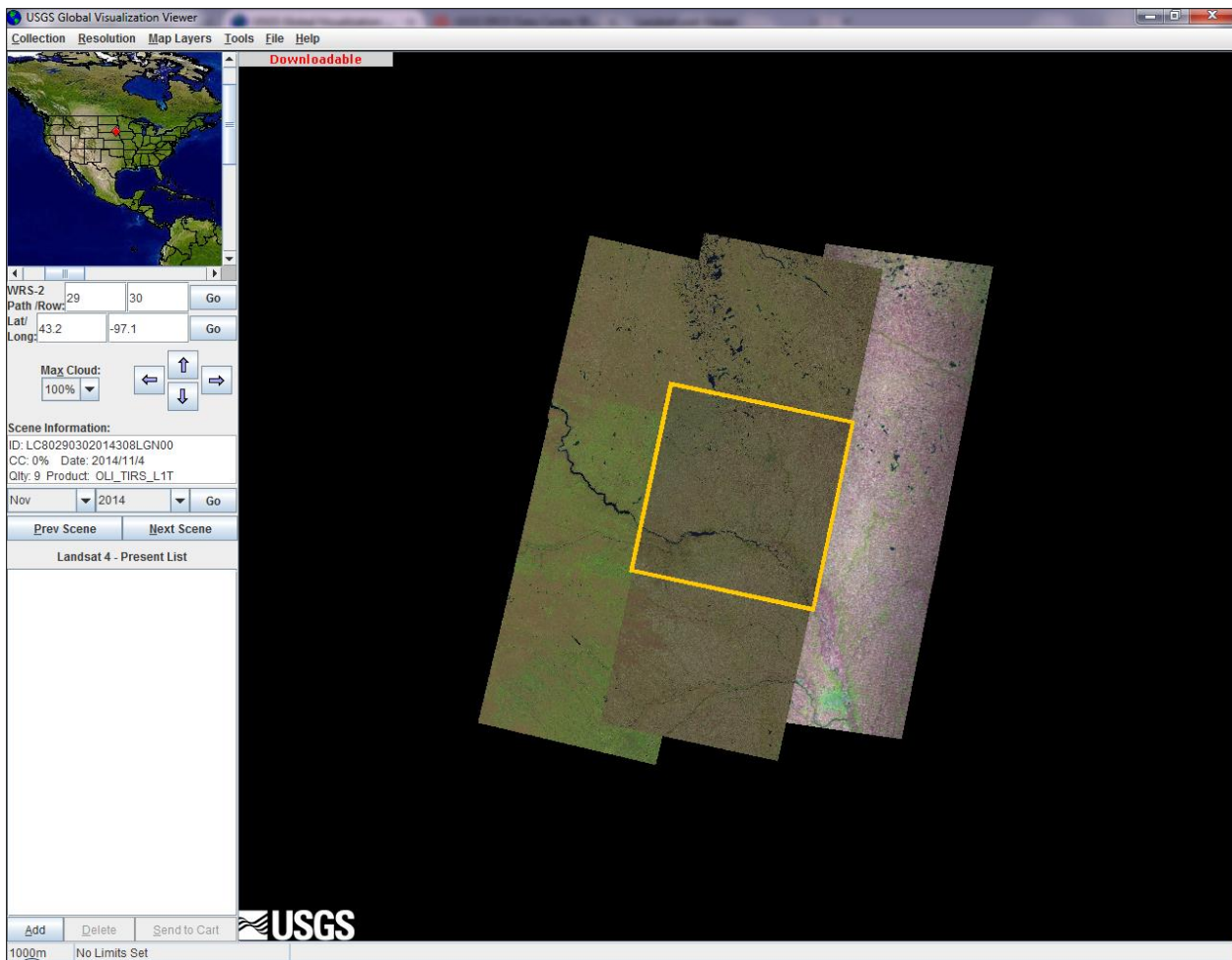


Figure 6-5. Global Visualization Viewer (GloVis) Interface

Upon opening, the viewer displays the most recent, least cloudy image of Path 29 Row 30 (southeast South Dakota). To navigate to a specific area, users type Path / Row, Lat / Long decimal coordinates, or move the map using the mouse. Regardless of where the user moves the map, GloVis displays the most recent, least cloudy image. Users can then use the arrows or the Prev Scene / Next Scene buttons on the left side of the screen to 'page' through all of the scenes covering the same Path / Row area. The user can also change the cloud cover limits (on the left side of the viewing window).

The GloVis menu options are as follows:

- The Collection menu lists the searchable data sets, including L8.
- The Resolution menu allows the user to change the display from 1000 meters (9 scenes in the view) to 250 meters (only the selected scene).
- The Map layers menu allows the user to add cities, country / admin boundaries, roads, and/or railroads to aid in the search.

- The Tools menu allows users to set search limits or search for specific scene IDs. Users can also compile and save scene lists from the tool, or upload already created scene lists.

Scenes added to the Scene List are sent to the Cart, which forwards the request to EarthExplorer and prompts users to login. The data can then be downloaded individually, or added to a bulk download order.

6.3 LandsatLook Viewer

Unlike EarthExplorer and GloVis, the LandsatLook Viewer searches only Landsat data held in the USGS archives. The easy-to-use interface allows users to type a place name or move around the globe and zoom into the area of interest.

<http://landsatlook.usgs.gov>

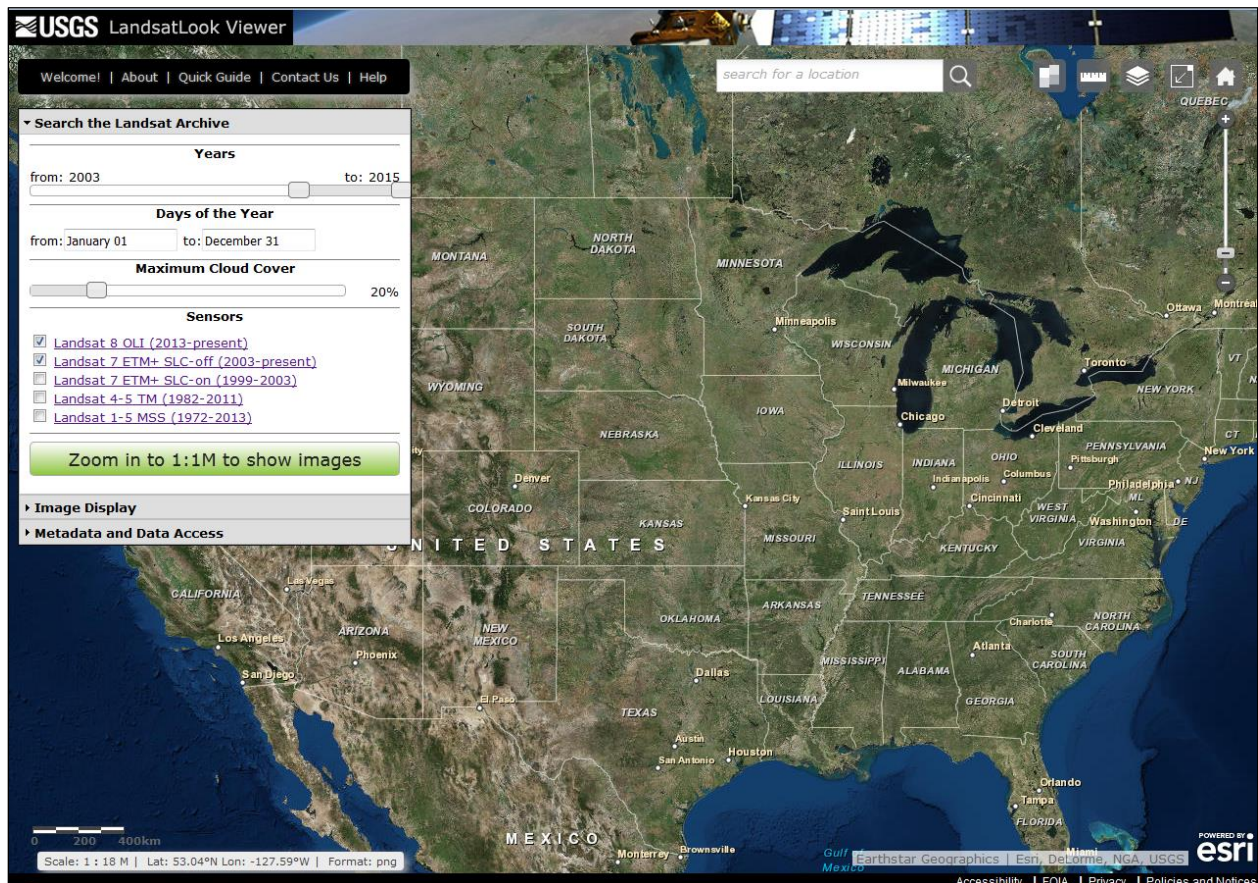


Figure 6-6. The LandsatLook Viewer

To begin a search, users can type a location in the search box and then click the magnifying glass, or zoom in to the desired geographic location. The user can then select criteria such as years, days of year, cloud cover, and Landsat sensors. The

interface displays adjacent scenes more realistically mosaicked, giving a more seamless appearance to the view.

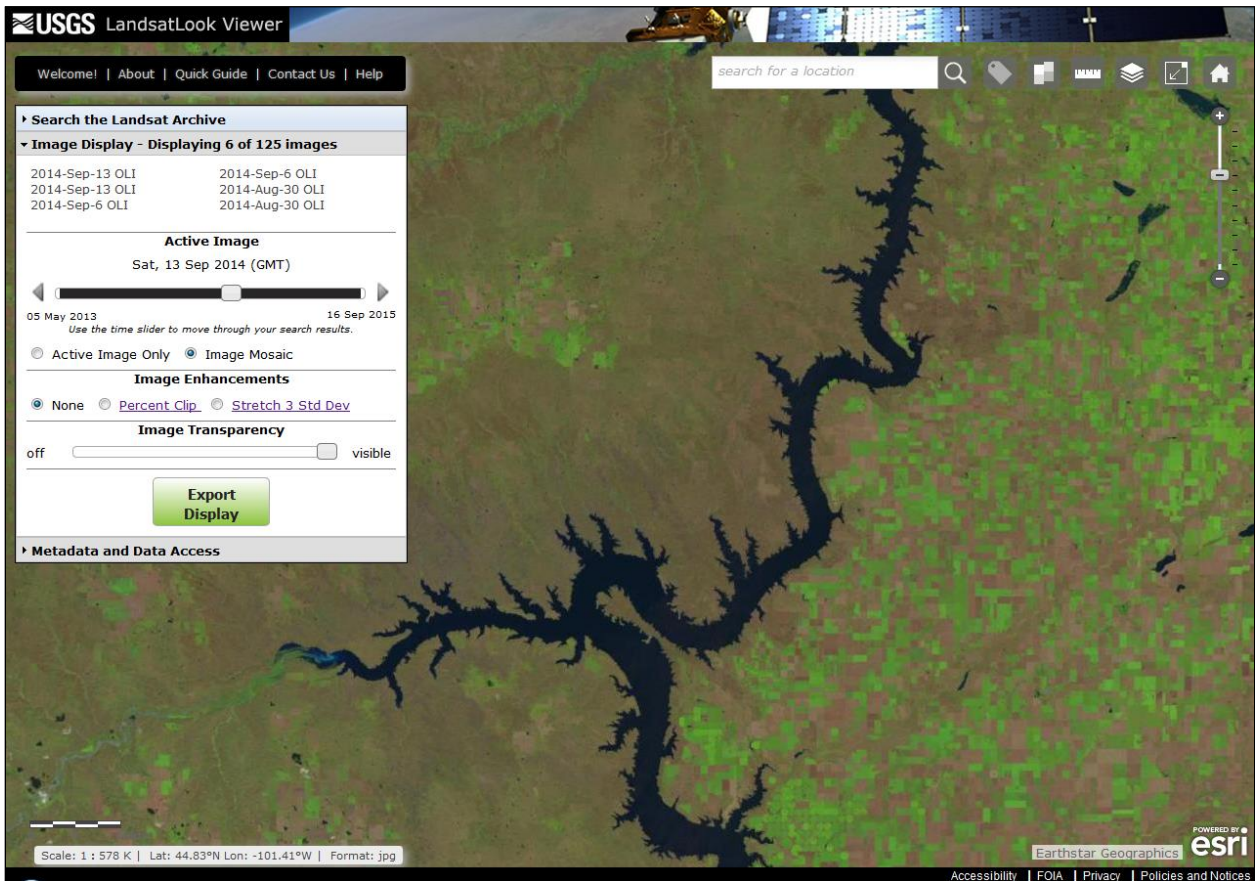


Figure 6-7. Display of Landsat Imagery

The user can easily export a file of the screen display. The user can view the Metadata and Data Access section to select and download full-resolution browse files (LandsatLook images) or Level 1 data products. The EarthExplorer login is displayed when the user selects Level 1 data products.

The screenshot shows a web-based application interface for the LandsatLook Viewer. At the top, there are three buttons: "Remove from Cart", "Get LandsatLook Image", and "Get Landsat Data". Below these buttons is a search bar with the placeholder "Search:" and a dropdown menu labeled "Show 10 entries". A table follows, with columns: Scene ID, Sensor, Acquisition Date, Path, Row, and Cloud Cover. The first row in the table is selected, indicated by a blue background. The data for the selected row is: Scene ID LC80270292014198LGN00, Sensor OLI, Acquisition Date 2014-07-17, Path 27, Row 29, and Cloud Cover 5. At the bottom of the table, there is a message "Showing 1 to 1 of 1 entries" and navigation buttons for "Previous" and "Next".

	Scene ID	Sensor	Acquisition Date	Path	Row	Cloud Cover
<input checked="" type="checkbox"/>	LC80270292014198LGN00	OLI	2014-07-17	27	29	5

Figure 6-8. LandsatLook Viewer Screen Display

Appendix A Known Issues

Certain artifacts are expected in all satellite-borne sensors, and Landsat is no exception. However, moving to a push-broom sensor configuration with few moving parts, along with thorough testing, has dramatically reduced the number of issues and artifacts that have been observed on L8. Of note, several artifacts that existed on previous Landsat instruments, including cross-track banding, scan correlated shift, and dropped scan lines, are not possible on the OLI and TIRS instruments. Other artifacts such as coherent noise and memory effect exist only at very low levels and are virtually undetectable.

USGS maintains a list of L8 OLI and TIRS calibration notices that describe new or temporary artifacts and how they are addressed and corrected. Please refer to http://landsat.usgs.gov/calibration_notices.php for up-to-date information and details regarding known issues and current artifacts. In general, the known OLI and TIRS instrument image artifacts consist of stray light (TIRS only), striping, oversaturation (OLI only), and Single Event Upsets (SEUs).

A.1 TIRS Stray Light

The TIRS instrument is well within requirements for noise and stability, as determined using its onboard calibration systems. Comparisons of L8 calibrated data to surface buoy-based predictions, however, indicated a significant overestimation of radiance (TIRS results are too hot) and high variability in these comparison results. Differences between the ground-based results and TIRS results ranged up 5 K in the TIRS Band 10 and up to 10 K in TIRS Band 11. Some of this variation is related to the time of year (i.e., the temperature differences were larger during the summer, when the land surrounding the calibration sites was warmer). Additionally, some TIRS data are affected by significant banding, a low frequency variation in signal across the FOV, particularly over the three focal plane sensor chip assembly boundaries, even when viewing uniform regions. In addition, the banding may vary within a given scene in the along-track direction.

The banding that occurs in some measurements, but not in others, was hypothesized to be caused by stray light entering the optical path from outside the direct FOV. In these cases, the out-of-field light introduced additional incident energy on the detectors that was not uniform across the detector arrays. For example, during on-orbit check out, the image in Figure A-1 was acquired over Lake Superior. The image shows that the uniformity appeared to change as the TIRS instrument scanned along track from northeast to southwest across the lake. This banding change is indicated in Figure A-1 by red arrows.

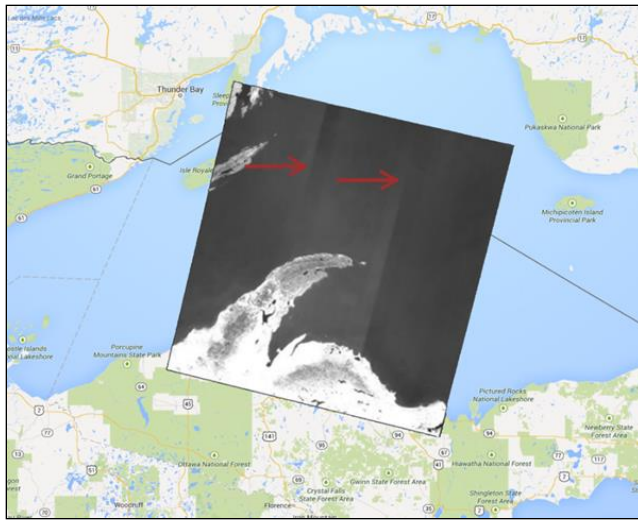


Figure A-1. TIRS Image of Lake Superior Showing Apparent Time-Varying Errors

Several scans from the Earth to the Moon were acquired in order to investigate the potential stray light in the optical system. The analysis of these lunar scans, along with subsequent optical modeling efforts, confirmed that radiance from outside the instrument's FOV was adding a non-uniform signal across the detectors and caused the observed banding. Additional scans of the Moon were acquired in order to better quantify the amount and location of stray light affecting TIRS imagery. Figure A-2 shows the results of this lunar scanning. The gray lines indicate the angle between the TIRS boresight and the Moon where there was no ghost visible in any of the TIRS detectors. The blue lines indicate where a lunar ghost was observed by at least one detector within the TIRS focal plane.

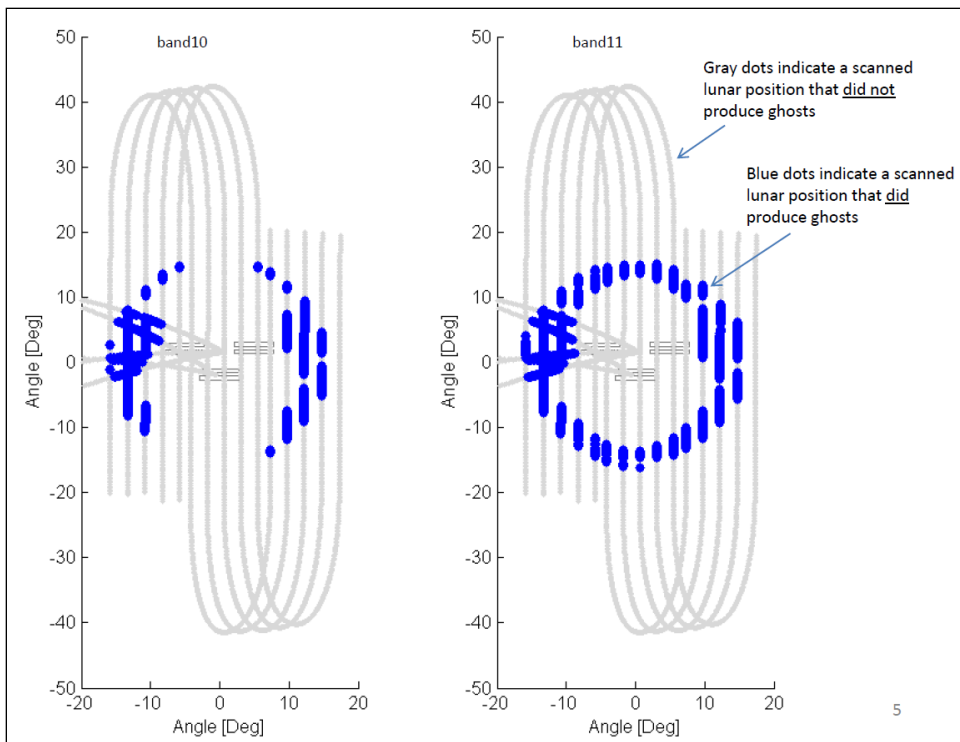


Figure A-2. TIRS Special Lunar Scan to Characterize the Stray Light Issue

The larger amount of stray light observed in Band 11 is consistent with previous observations of variation in the accuracy of the imagery based on ground measurements and the larger amount of banding. Therefore, there is little doubt that the errors observed in the current thermal band data are caused by stray light.

At this time, efforts to understand the stray light paths fully are continuing and correction methods are being developed. In the meantime, the Landsat CVT adjusted the TIRS band's radiometric bias in order to improve (but not fully eliminate) the absolute radiometric error for typical Earth scenes during the growing season. The bias corrections were implemented when the L8 data were reprocessed in February 2014. These corrections minimized the bias in temperatures derived from TIRS instrument data for typical Earth scenes. An uncertainty of ± 1 K (1 sigma) remains in temperatures derived from Band 10 data and an uncertainty of ± 2 K (1 sigma) remains in temperatures derived from Band 11 data for the test data set.

Specifically, this stray light error was estimated to be $0.29 \text{ W/m}^2/\text{sr}/\mu\text{m}$ for Band 10 and $0.51 \text{ W/m}^2/\text{sr}/\mu\text{m}$ for Band 11. Investigations showed the TIRS instrument reported a higher radiance than the water buoy measurements, as shown in the left graph of Figure A-3. The graph on the right of Figure A-3 shows the results after accounting for this average radiance error, which is the calibration adjustment that was implemented for reprocessing in February 2014. As described above, this adjustment minimizes the apparent bias, but does not change the variance in the data resulting from stray light. Additionally, colder scenes tend to be overcorrected due to this bias adjustment. The

variability in the offset, as shown in Table A-1, is about twice as large in Band 11 as Band 10, and Band 10 is about twice as large as Landsat 7 ETM+ thermal band uncertainty. Due to the larger calibration uncertainty associated with Band 11, it is recommended that users refrain from relying on Band 11 data in quantitative analysis of the TIRS data, such as the use of split window techniques for atmospheric correction and retrieval of surface temperature values. Users should note the errors from this stray light effect are dependent on the surrounding area temperatures (including clouds), so 1-sigma variances may be misleading.

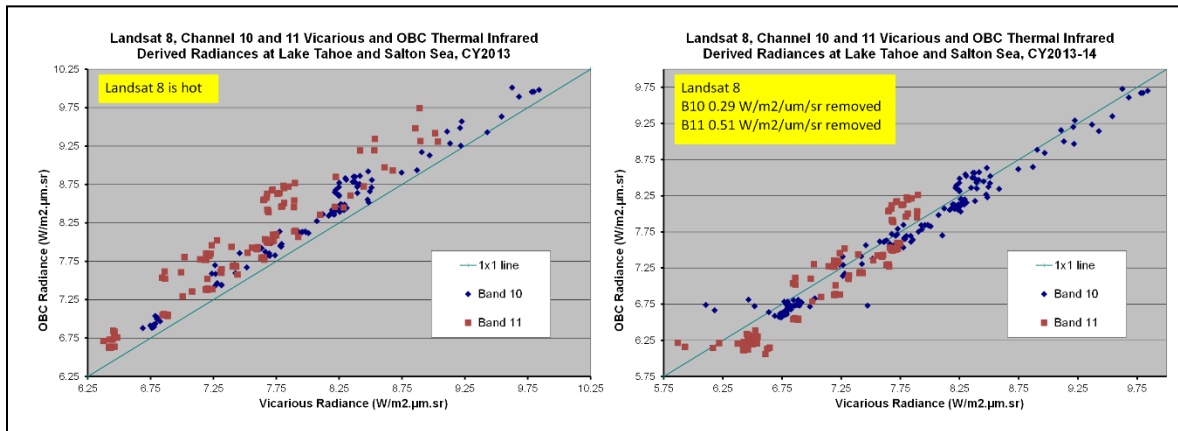


Figure A-3. Thermal Band Errors (left group) Prior to Calibration Adjustment and (right group) After Calibration Adjustment

TIRS Bands	Radiance Offset [W/m ² /sr/um]	Temperature Offset [K @ 300K]
10	-0.29 +/- 0.12	-2.1 +/- 0.8
11	-0.51 +/- 0.2	-4.4 +/- 1.75

Table A-1. TIRS Band Variability

Correction for the TIRS stray light requires knowledge of the temperature of the areas surrounding TIRS scenes. Several methods are being pursued to obtain this information: (1) using GOES or another coincident data set to estimate the out of FOV sigma; and (2) estimating the out view signal based on in-scene statistics. Each of these approaches has pros and cons, and none has been proven effective in every case. However, all of these approaches are in early exploratory stages and improvements are expected.

Once the stray light issue is fully understood and a correction method chosen, all TIRS products will be reprocessed to include a stray light correction.

A.2 Striping and Banding

Striping is a phenomenon that appears as columns of consistently lighter or darker pixels in a single band of radiometrically corrected data. Banding is a similar phenomenon, but occurs across multiple contiguous columns. Both are often caused by

incorrect calibration of detectors with respect to one another. These effects in OLI imagery are less than 4 DN in its 12-bit dynamic range, or less than 0.5 percent of the radiance of a typical Earth image, and are generally seen in OLI Bands 1 (CA), 2 (Blue), and 9 (Cirrus). This low level of non-uniformity is typically not visible to most users of L8 data. Figure A-4 and Figure A-5 are examples of striping and banding.

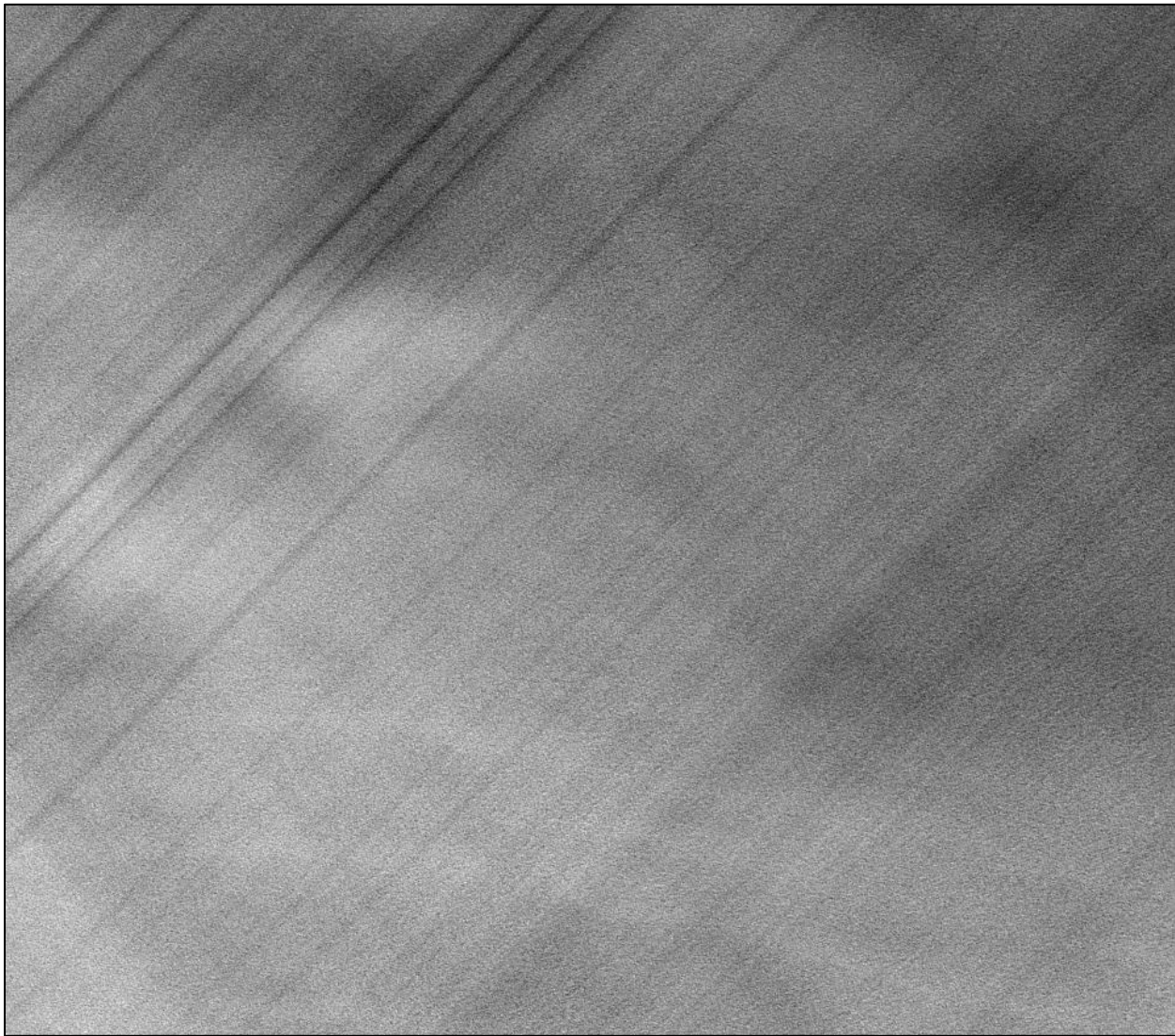


Figure A-4. Striping and Banding Observed in Band 1 (CA Band)

Figure A-4 displays the striping and banding observed in Band 1 (Coastal Aerosol band) in image LC80160042013118LGN00, which is over a very homogenous region of the Greenland ice sheet. Single-pixel wide columns are considered striping; the thicker columns are banding.

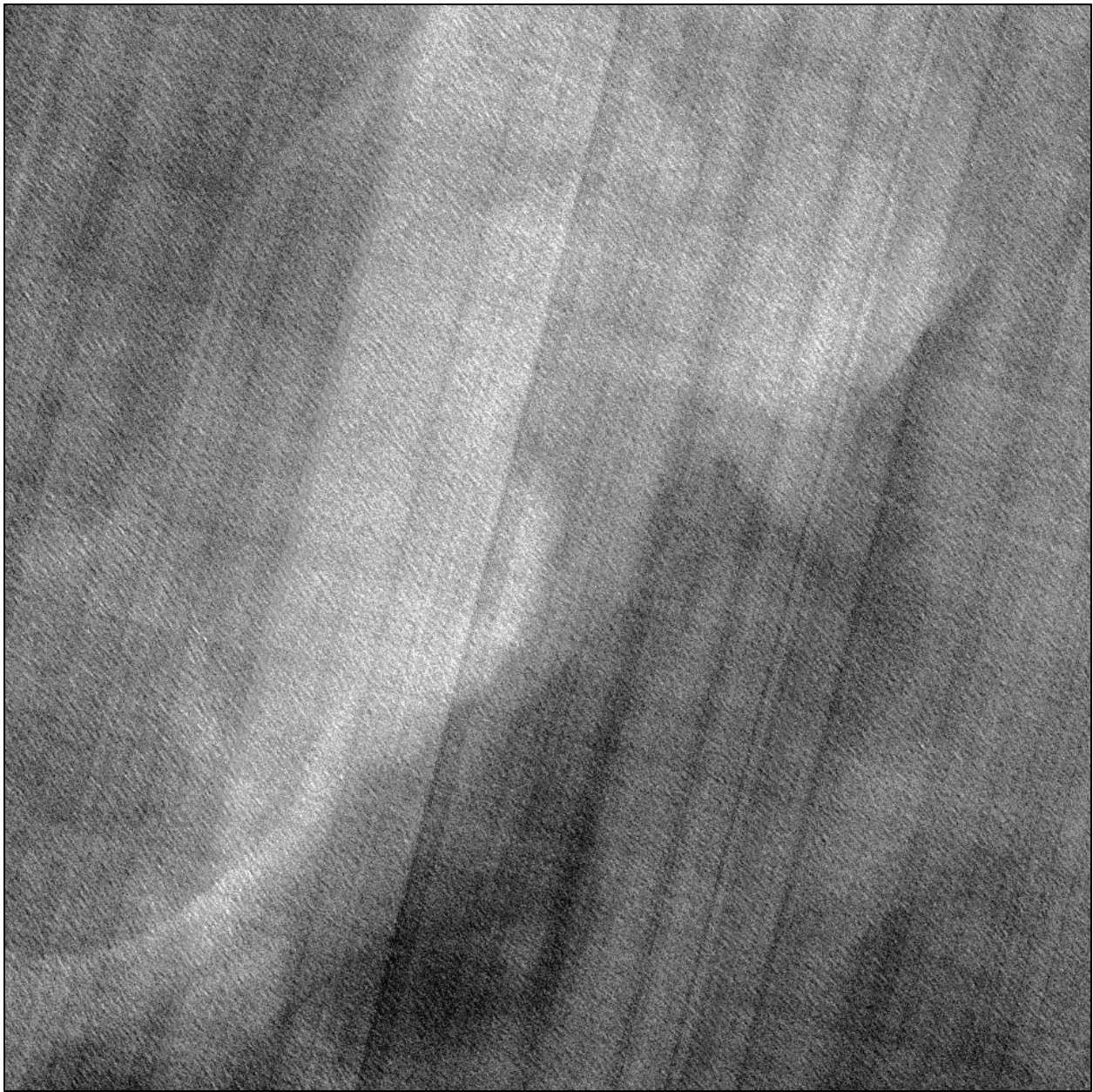


Figure A-5. Striping and Banding observed in Band 2 (Blue)

Figure A-5 displays the striping and banding observed in Band 2 (Blue band) in image LC80750882013131LGN01, which is over clear, calm ocean water.

Striping and Banding also affect TIRS imagery, as seen in Figure A-6.

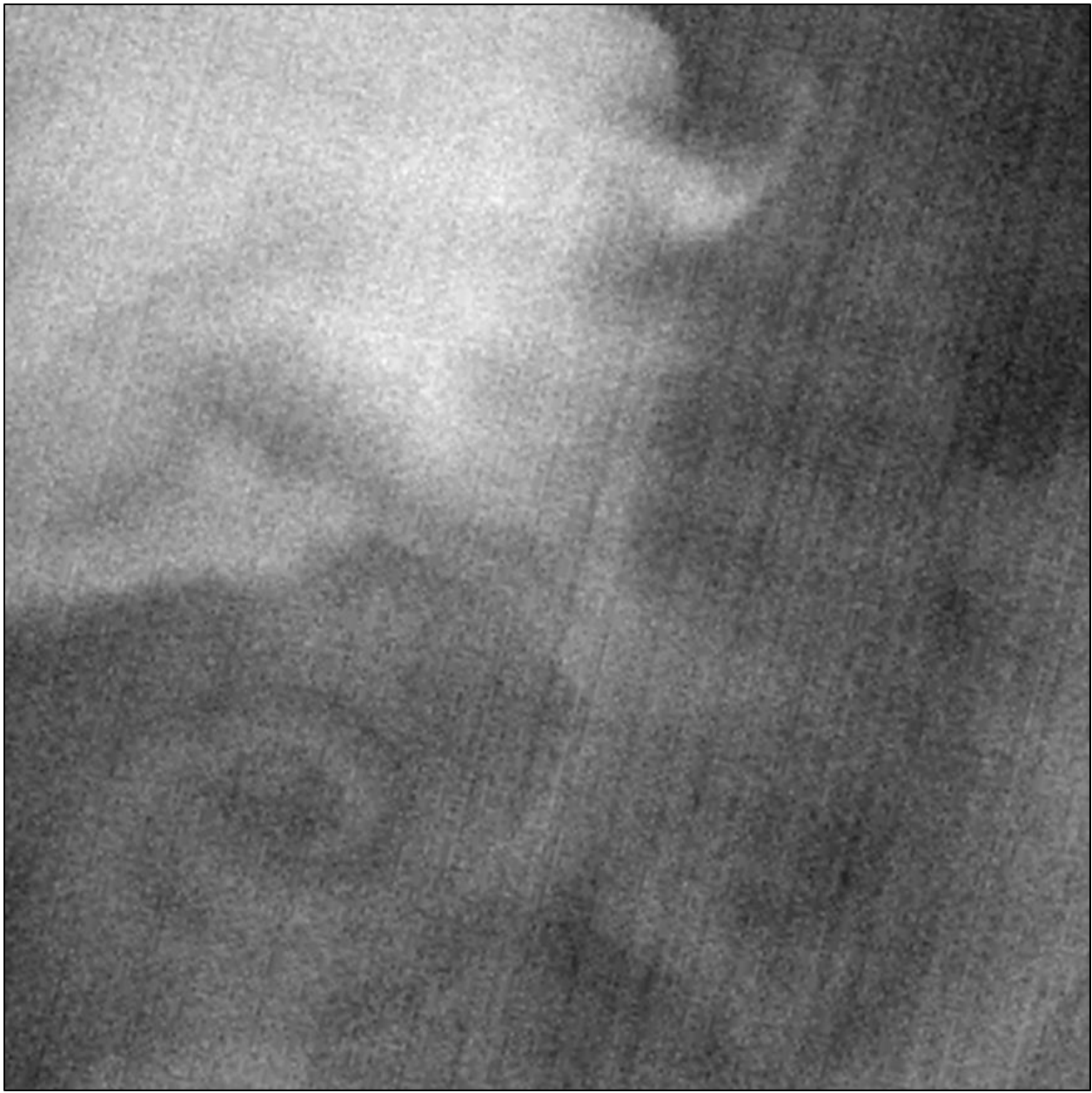


Figure A-6. Striping and Banding observed in TIRS Band 10

Figure A-6 displays the striping and banding observed in TIRS Band 10 in image LC80750882013131LGN01, which is over clear, calm ocean water. This low level of non-uniformity is typically not visible to most users of L8 data.

Normal radiometric processing removes the majority of banding and striping in OLI and TIRS imagery. The CPF used during Level 1 processing provide the parameters for corrections. However, minor responsivity changes in individual detectors cannot be accounted for, so some non-uniformity will remain in the data. Some of this striping may be corrected with future calibrations.

A.3 SCA Overlaps

Both OLI and TIRS are designed with discrete SCAs, which have some detectors overlapping the adjacent SCAs. This causes a small region between each SCA to be viewed by multiple detectors. The imagery for this region is created by averaging over the detectors viewing each pixel. In some situations, this can cause an artifact that resembles banding, but it is in fixed locations and often transient, depending on the underlying terrain.

SCA overlap artifacts are most visible over high clouds, as the detectors on each SCA view a slightly different area of each cloud. Figure A-7 shows an example of this.

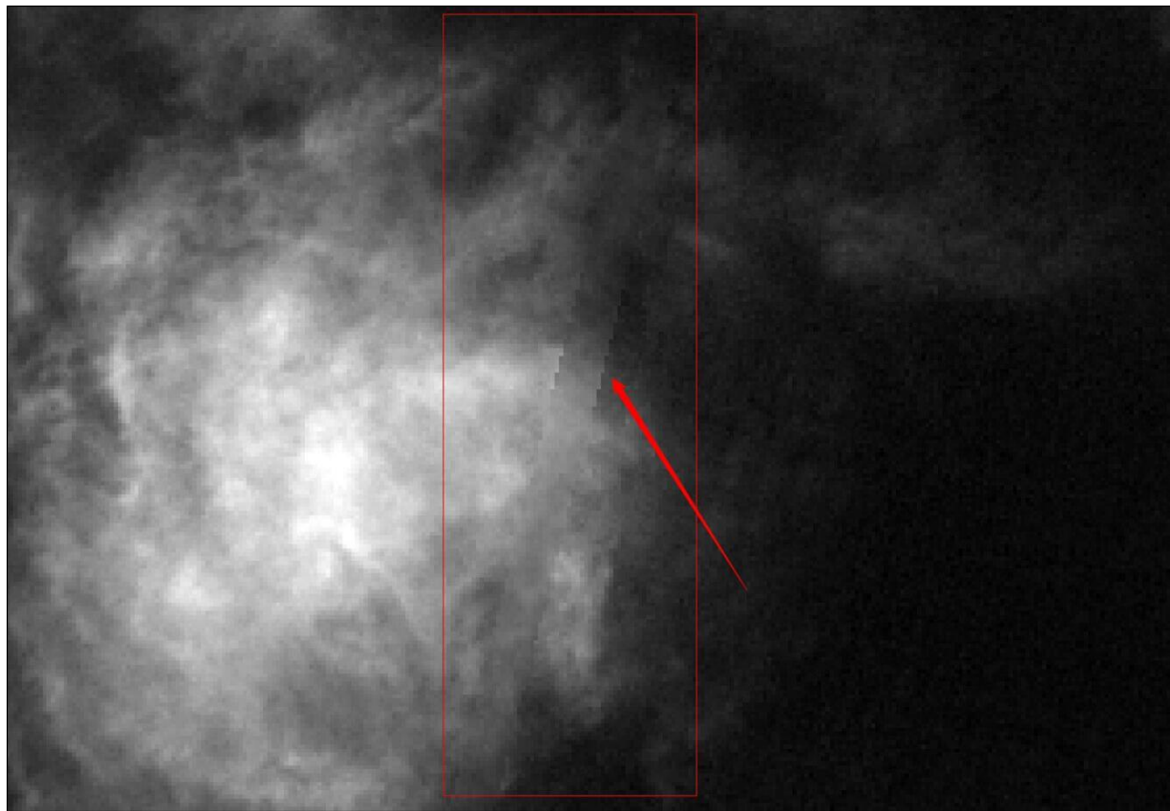


Figure A-7. SCA Overlap Visible in Band 9 (Cirrus Band)

Figure A-7 displays the SCA overlap artifact observed in Band 9 (cirrus band) in image LC80140362014091LGN00, where high clouds were visible at the boundary between two SCAs.

SCA overlaps are commonly seen in TIRS imagery because of contributions from the stray light artifact.

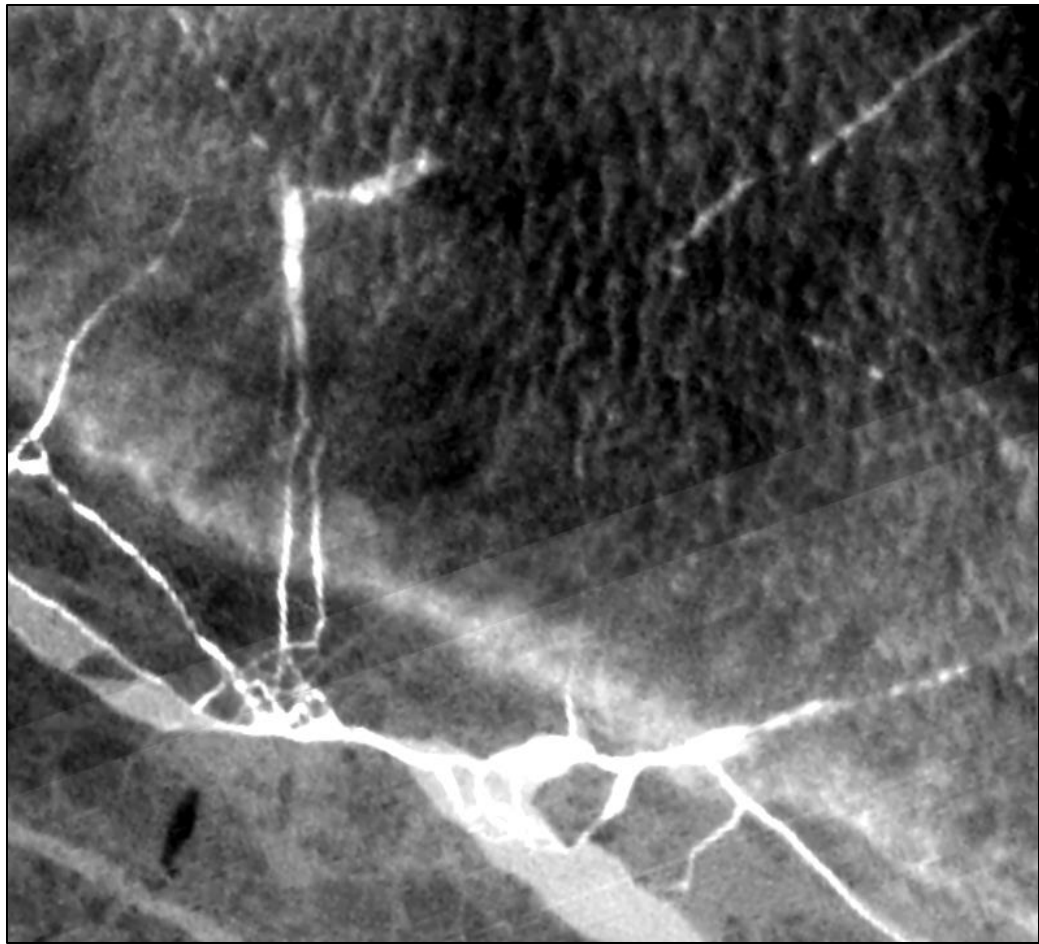


Figure A-8. SCA Overlap Visible in TIRS Band 10

Figure A-8 displays the SCA overlap artifact observed in TIRS Band 10 in image LC80372482013137LGN01 at the boundary between two SCAs. In this image, stray light has shifted the calibration of two adjacent SCAs, making the overlap region visible.

A.4 Oversaturation

Oversaturation occurs when a detector views an object that is much brighter than the maximum radiance the instrument was designed to handle. This causes the detector to deliver a voltage that is larger than expected by the 12-bit electronics, so the detector's value rolls over the 12-bit limit and records as a very small integer. Therefore, this artifact appears as dark spots in the middle of very bright objects. Figure A-9 represents an oversaturation example in OLI SWIR Bands 6 and 7.

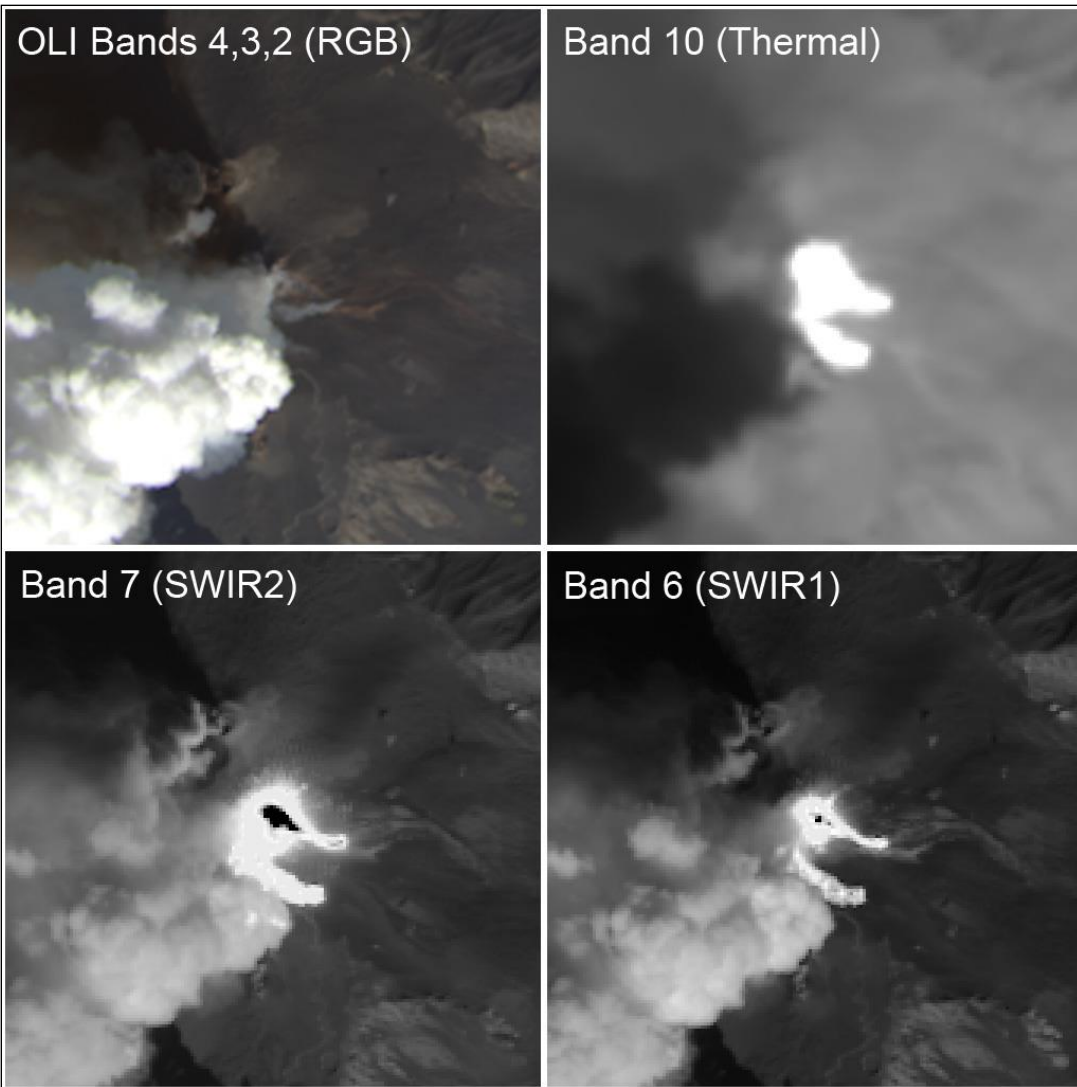


Figure A-9. Oversaturation Example in OLI SWIR Bands 6 & 7

Oversaturation artifacts are typically rare, but are repeatable artifacts that normally occur in OLI Bands 7 and 6 over large fires or volcanic events. Additionally, oversaturation may occur in other OLI bands over land surface objects that are very bright or exhibit strong specular reflectance. Oversaturation does not cause permanent harm to the instrument, and the detectors recover immediately with no visible memory effect.

A.5 Single Event Upsets

An SEU is a “catch-all” term used for any electronic fault that causes brief, instantaneous artifacts in the imagery. Usually, SEUs are caused by charged particles from the Earth’s radiation belts striking the detectors or instrument electronics. These particle hits are relatively rare, but are seen more commonly over the poles and over the South Atlantic Anomaly – a region where the Earth’s magnetic field is weakest and the

radiation belt is at its lowest altitude. Transmission errors can also cause SEUs, but due to the design of L8, these errors are not possible with OLI or TIRS imagery.

SEUs appear in OLI as single-frame bright spots that may affect several detectors in a line. The electronics design is such that SEUs often affect only odd or even detectors, but as seen in the lower portion of Figure A-10, can affect both odd and even detectors, with a two-pixel gap between the odd and even detectors. Users may never notice an SEU because they are rare, typically only a single pixel, and geometric resampling distorts or erases these small artifacts in L1 products. They are most visible in Level-1R (radiometrically corrected) or L0 imagery. Figure A-10 is an example of a couple SEU events measured by OLI. As noted above, the SEU clearly manifests as a line of single-frame bright spots.

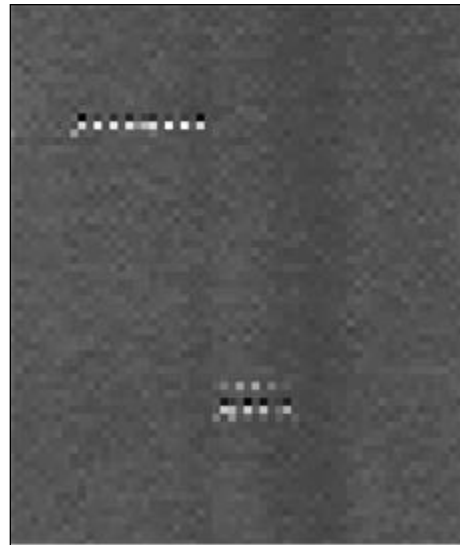


Figure A-10. Example of SEU Event Measured by OLI – SEU Manifests as a Line of Single-Frame Bright Spots

SEUs occur at random. They cannot be corrected, but their effect on the imagery is minor. They do not cause permanent harm to the instrument detectors.

A.5.1 Observatory Component Reference Systems

The L8 IAS geometry algorithms use ten coordinate systems. These coordinate systems are referred to frequently in the remainder of this document and are briefly defined here to provide context for the subsequent discussion. They are presented in the order in which they would be used to transform a detector and sample time into a ground position.

A.6 OLI Instrument Line-of-Sight (LOS) Coordinate System

The OLI LOS coordinate system is used to define the band and detector pointing directions relative to the instrument axes. These pointing directions are used to construct LOS vectors for individual detector samples. This coordinate system is

defined so that the Z-axis is parallel to the telescope boresight axis and is positive toward the OLI aperture. The origin is where this axis intersects the OLI focal plane. The X-axis is parallel to the along-track direction, with the positive direction toward the leading, odd numbered, SCAs (see Figure A-11). The Y-axis is in the across-track direction with the positive direction toward SCA01. This definition makes the OLI coordinate system nominally parallel to the spacecraft coordinate system, with the difference being due to residual misalignment between the OLI and the spacecraft body.

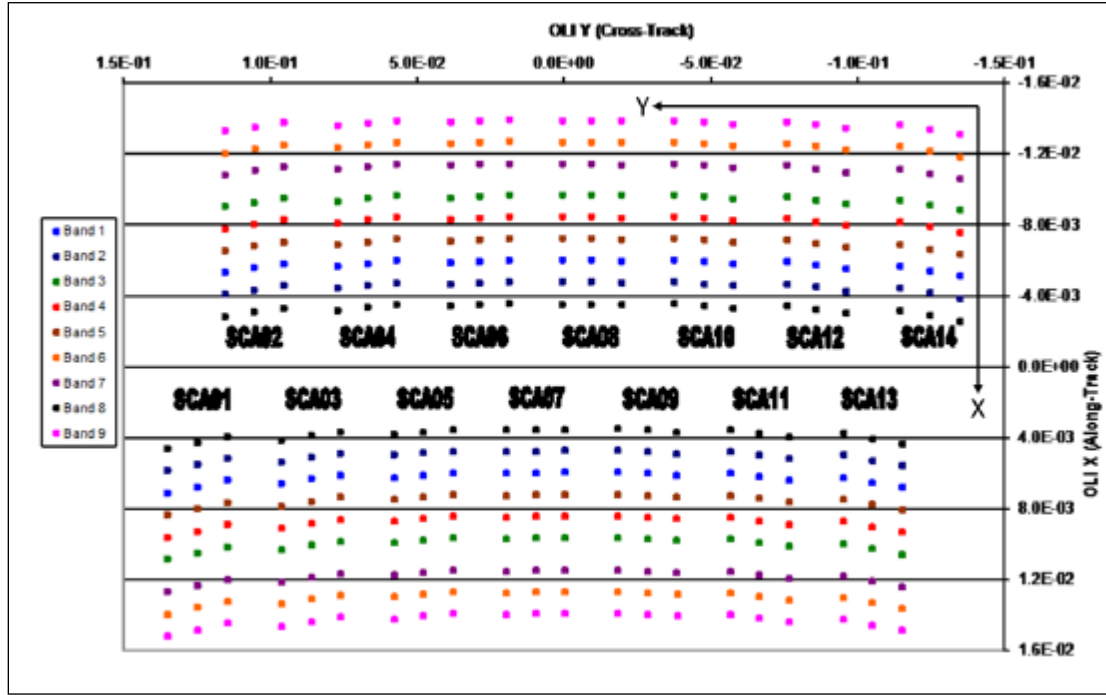


Figure A-11. OLI Line-of-Sight (LOS) Coordinate System

A.7 TIRS Instrument Coordinate System

The orientations of the TIRS detector LOS directions and of the TIRS Scene Select Mirror (SSM) are both defined within the TIRS instrument coordinate system. TIRS LOS coordinates define the band and detector-pointing directions relative to the instrument axes. These pointing directions are used to construct LOS vectors for individual detector samples. These vectors are reflected off the SSM to direct them out of the TIRS aperture for Earth viewing. The TIRS LOS model is formulated so that the effect of a nominally pointed SSM is included in the definition of the detector lines-of-sight, with departures from nominal SSM pointing causing perturbations to these lines-of-sight. This formulation allows TIRS LOS construction to be very similar to OLI. This is described in detail below, in the TIRS LOS Model Creation algorithm.

The TIRS coordinate system is defined so that the Z-axis is parallel to the TIRS boresight axis and is positive toward the TIRS aperture. The origin is where this axis intersects the TIRS focal plane. The X-axis is parallel to the along-track direction, with the positive direction toward the leading SCA (SCA02 in Figure A-12). The Y-axis is in

the across-track direction with the positive direction toward SCA03. This definition makes the TIRS coordinate system nominally parallel to the spacecraft coordinate system, with the difference being due to residual misalignment between the TIRS and the spacecraft body.

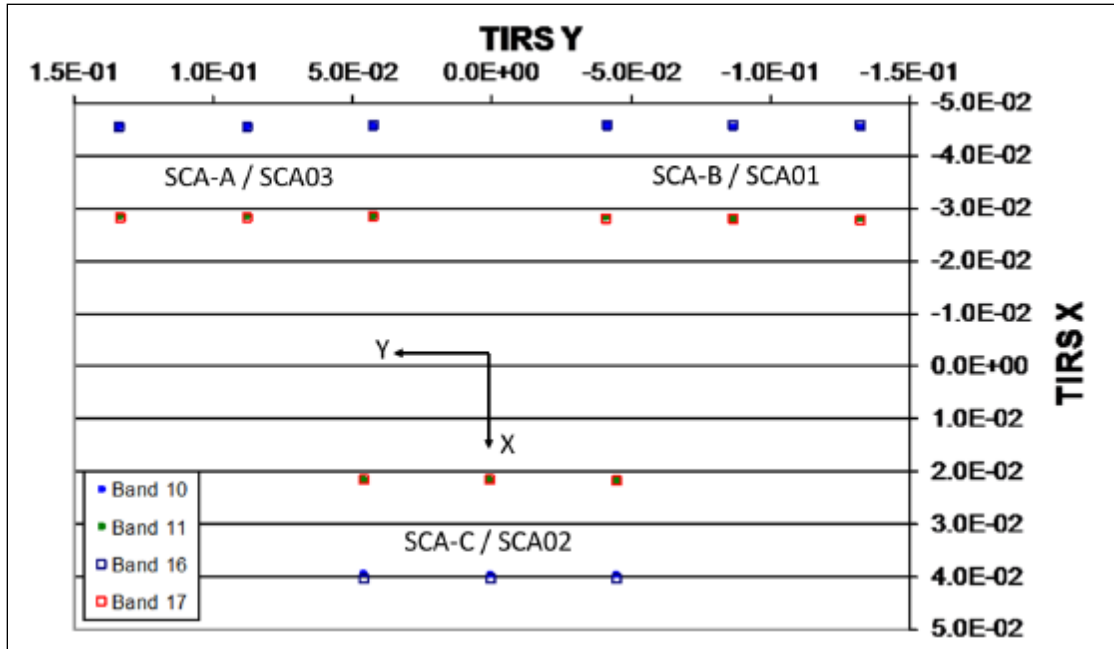


Figure A-12. TIRS Line-of-Sight (LOS) Coordinates

A.8 Spacecraft Coordinate System

The spacecraft coordinate system is the spacecraft-body-fixed coordinate system used to relate the locations and orientations of the various spacecraft components to one another and to the OLI and TIRS instruments. It is defined with the +Z axis in the Earth-facing direction, the +X axis in the nominal direction of flight, and the +Y axis toward the cold side of the spacecraft (opposite the solar array). This coordinate system is used during Observatory integration and prelaunch testing to determine the prelaunch positions and alignments of the attitude control sensors (star trackers and SIRU) and instrument payloads (OLI and TIRS). The spacecraft coordinate system is nominally the same as the navigation reference system (see below) used for spacecraft attitude determination and control. However, for reasons explained below, these two coordinate systems are treated separately.

A.9 Navigation Reference Coordinate System

The navigation reference frame (a.k.a., the attitude control system reference) is the spacecraft-body-fixed coordinate system used for spacecraft attitude determination and control. The coordinate axes are defined by the spacecraft ACS, which attempts to keep the navigation reference frame aligned with the (yaw-steered) orbital coordinate system (for nominal nadir pointing) so that the OLI and TIRS boresight axes are always pointing

toward the center of the Earth. The orientation of this coordinate system relative to the inertial coordinate system is captured in spacecraft attitude data.

Ideally, the navigation reference frame is the same as the spacecraft coordinate system. In practice, the navigation frame is based on the orientation of the absolute attitude sensor (i.e., star tracker) being used for attitude determination. Any errors in the orientation knowledge for this tracker with respect to the spacecraft body frame will lead to differences between the spacecraft and navigation coordinate systems. This becomes important if the absolute attitude sensor is changed, for example by switching from the primary to the redundant star tracker during on-orbit operations. Such an event would effectively redefine the navigation frame to be based on the redundant tracker, with the difference between the spacecraft and navigation frames now resulting from redundant tracker alignment knowledge errors, rather than from primary tracker alignment knowledge errors. This redefinition would require updates to the on-orbit instrument-to-ACS alignment calibrations. Therefore, the spacecraft and navigation reference coordinate systems are different because the spacecraft coordinate system is fixed but the navigation reference can change.

A.10 SIRU Coordinate System

The spacecraft orientation rate data provided by the spacecraft attitude control system's inertial measurement unit are referenced to the SIRU coordinate system. The SIRU consists of four rotation-sensitive axes. This configuration provides redundancy to protect against the failure of any one axis. The four SIRU axis directions are determined relative to the SIRU coordinate system, the orientation of which is itself measured relative to the spacecraft coordinate system both prelaunch and on-orbit, as part of the ACS calibration procedure. The IAS uses this alignment transformation to convert the SIRU data contained in the L8 spacecraft ancillary data to the navigation reference coordinate system for blending with the ACS quaternions.

A.11 Orbital Coordinate System

The orbital coordinate system is centered at the spacecraft, and its orientation is based on the spacecraft position in inertial space (see Figure A-13). The origin is the spacecraft's center of mass, with the Z-axis pointing from the spacecraft's center of mass to the Earth's center of mass. The Y-axis is the normalized cross product of the Z-axis and the instantaneous (inertial) velocity vector, and corresponds to the negative of the instantaneous angular momentum vector direction. The X-axis is the cross product of the Y- and Z-axes. The orbital coordinate system is used to convert spacecraft attitude, expressed as Earth-Centered Inertial (ECI) quaternions, to roll-pitch-yaw Euler angles.

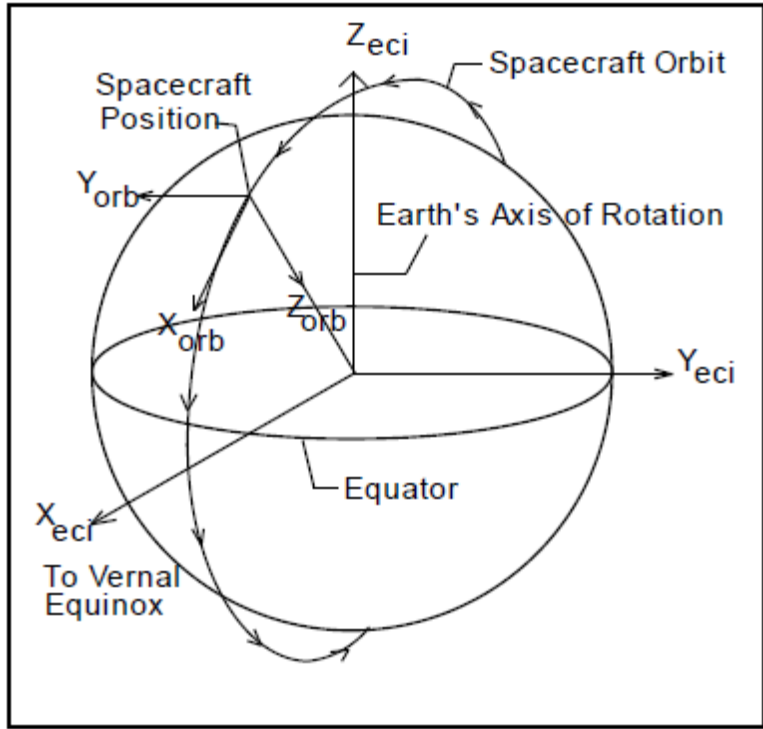


Figure A-13. Orbital Coordinate System

A.12 ECI J2000 Coordinate System

The ECI coordinate system of epoch J2000 is space-fixed with its origin at the Earth's center of mass (see Figure A-14). The Z-axis corresponds to the mean north celestial pole of epoch J2000.0. The X-axis is based on the mean vernal equinox of epoch J2000.0. The Y-axis is the cross product of the Z and X axes. This coordinate system is described in detail in the Explanatory Supplement to the Astronomical Almanac published by the U.S. Naval Observatory. Data in the ECI coordinate system are present in the L8 spacecraft ancillary data form of attitude quaternions that relate the navigation frame to the ECI J2000 coordinate system.

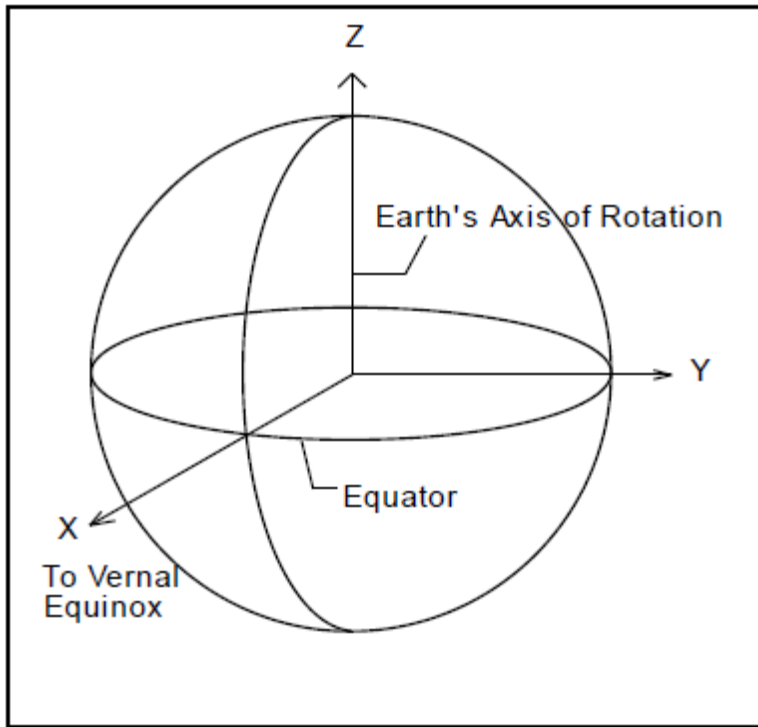


Figure A-14. Earth-Centered Inertial (ECI) Coordinate System

A.13 ECEF Coordinate System

The Earth-Centered Earth Fixed (ECEF) coordinate system is Earth-fixed with its origin at the Earth's center of mass (see Figure A-15). It corresponds to the Conventional Terrestrial System defined by the Bureau International de l'Heure (BIH), which is the same as the U.S. Department of Defense World Geodetic System 1984 (WGS84) geocentric reference system. This coordinate system is described in the Supplement to Department of Defense World Geodetic System 1984 Technical Report, Part 1: Methods, Techniques, and Data Used in WGS84 Development, TR 8350.2-A, published by NGA.

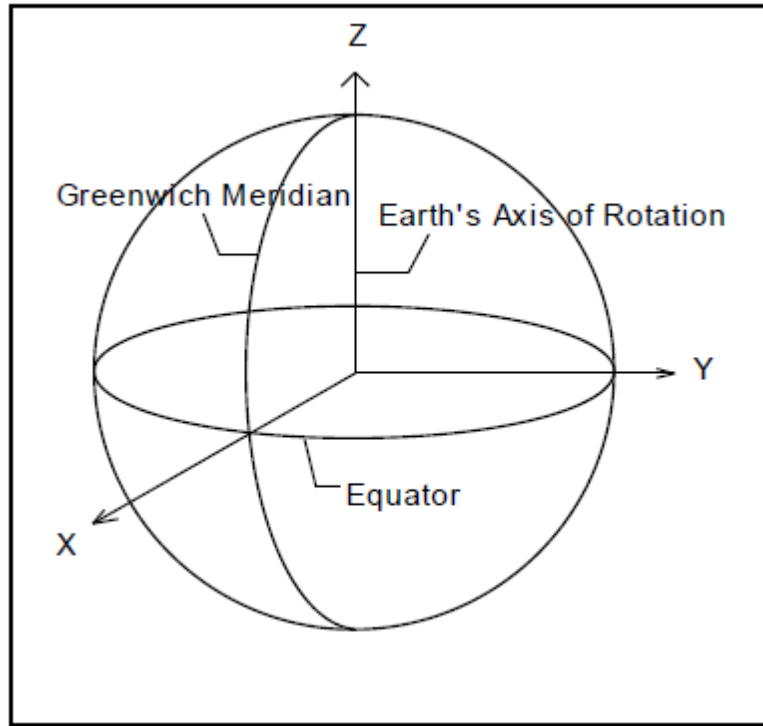


Figure A-15. Earth-Centered Earth Fixed (ECEF) Coordinate Systems

A.14 Geodetic Coordinate System

The geodetic coordinate system is based on the WGS84 reference frame, with coordinates expressed in latitude, longitude, and height above the reference Earth ellipsoid (see Figure A-16). No ellipsoid is required by the definition of the ECEF coordinate system, but the geodetic coordinate system depends on the selection of an Earth ellipsoid. Latitude and longitude are defined as the angle between the ellipsoid normal and its projection onto the Equator and the angle between the local meridian and the Greenwich meridian, respectively. The scene center and scene corner coordinates in the Level 0R product metadata are expressed in the geodetic coordinate system.

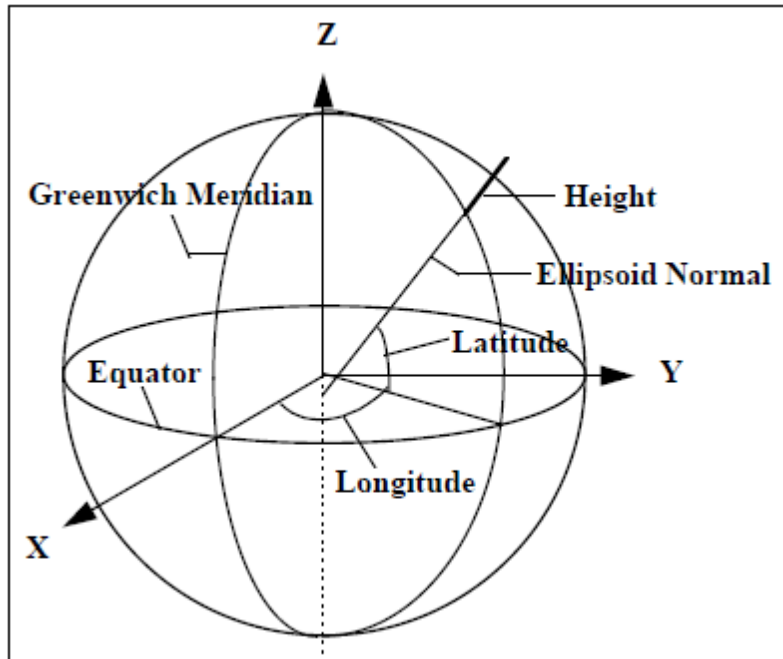


Figure A-16. Geodetic Coordinate System

A.15 Map Projection Coordinate System

Level 1 products are generated with respect to a map projection coordinate system, such as the UTM, which provides mapping from latitude and longitude to a plane coordinate system that is an approximation of a Cartesian coordinate system for a portion of the Earth's surface. It is used for convenience as a method of providing digital image data in an Earth-referenced grid that is compatible with other ground-referenced data sets. Although the map projection coordinate system is only an approximation of a true local Cartesian coordinate system at the Earth's surface, the mathematical relationship between the map projection and geodetic coordinate systems is defined precisely and unambiguously.

Appendix B Metadata File (MTL.txt)

The MTL.txt file is included with all L8 Level 1 Data Products. Landsat MTL files contain beneficial information for the systematic searching and archiving practices of data. Information about data processing and values important for enhancing Landsat data (such as conversion to reflectance and radiance) are also included in this file.

Data Format Control Books (DFCBs) define and describe Landsat metadata. DFCBs for all sensors are located at http://landsat.usgs.gov/tools_project_documents.php.

Sample L8 MTL.txt file:

```
GROUP = L1_METADATA_FILE
GROUP = METADATA_FILE_INFO
ORIGIN = "Image courtesy of the U.S. Geological Survey"
REQUEST_ID = "0501408100509 00025"
LANDSAT_SCENE_ID = "LC81880352014222LGN00"
FILE_DATE = 2014-08-10T14:53:31Z
STATION_ID = "LGN"
PROCESSING_SOFTWARE_VERSION = "LPGS_2.3.0"
END_GROUP = METADATA_FILE_INFO
GROUP = PRODUCT_METADATA
DATA_TYPE = "L1T"
ELEVATION_SOURCE = "GLS2000"
OUTPUT_FORMAT = "GEOTIFF"
SPACECRAFT_ID = "LANDSAT_8"
SENSOR_ID = "OLI_TIRS"
WRS_PATH = 188
WRS_ROW = 35
NADIR_OFFNADIR = "NADIR"
TARGET_WRS_PATH = 188
TARGET_WRS_ROW = 35
DATE_ACQUIRED = 2014-08-10
SCENE_CENTER_TIME = 09:36:28.4482251Z
CORNER_UL_LAT_PRODUCT = 37.09391
CORNER_UL_LON_PRODUCT = 13.68458
CORNER_UR_LAT_PRODUCT = 37.09426
CORNER_UR_LON_PRODUCT = 16.28392
CORNER_LL_LAT_PRODUCT = 34.97122
CORNER_LL_LON_PRODUCT = 13.71941
CORNER_LR_LAT_PRODUCT = 34.97154
CORNER_LR_LON_PRODUCT = 16.24992
CORNER_UL_PROJECTION_X_PRODUCT = 383100.000
CORNER_UL_PROJECTION_Y_PRODUCT = 4106100.000
CORNER_UR_PROJECTION_X_PRODUCT = 614100.000
CORNER_UR_PROJECTION_Y_PRODUCT = 4106100.000
CORNER_LL_PROJECTION_X_PRODUCT = 383100.000
```

```

CORNER_LL_PROJECTION_Y_PRODUCT = 3870600.000
CORNER_LR_PROJECTION_X_PRODUCT = 614100.000
CORNER_LR_PROJECTION_Y_PRODUCT = 3870600.000
PANCHROMATIC_LINES = 15701
PANCHROMATIC_SAMPLES = 15401
REFLECTIVE_LINES = 7851
REFLECTIVE_SAMPLES = 7701
THERMAL_LINES = 7851
THERMAL_SAMPLES = 7701
FILE_NAME_BAND_1 = "LC81880352014222LGN00_B1.TIF"
FILE_NAME_BAND_2 = "LC81880352014222LGN00_B2.TIF"
FILE_NAME_BAND_3 = "LC81880352014222LGN00_B3.TIF"
FILE_NAME_BAND_4 = "LC81880352014222LGN00_B4.TIF"
FILE_NAME_BAND_5 = "LC81880352014222LGN00_B5.TIF"
FILE_NAME_BAND_6 = "LC81880352014222LGN00_B6.TIF"
FILE_NAME_BAND_7 = "LC81880352014222LGN00_B7.TIF"
FILE_NAME_BAND_8 = "LC81880352014222LGN00_B8.TIF"
FILE_NAME_BAND_9 = "LC81880352014222LGN00_B9.TIF"
FILE_NAME_BAND_10 = "LC81880352014222LGN00_B10.TIF"
FILE_NAME_BAND_11 = "LC81880352014222LGN00_B11.TIF"
FILE_NAME_BAND_QUALITY = "LC81880352014222LGN00_BQA.TIF"
METADATA_FILE_NAME = "LC81880352014222LGN00_MTL.txt"
BPF_NAME_OLI = "LO8BPF20140810091759_20140810094745.01"
BPF_NAME_TIRS = "LT8BPF20140810091405_20140810094838.01"
CPF_NAME = "L8CPF20140701_20140930.01"
RLUT_FILE_NAME = "L8RLUT20130211_20431231v09.h5"
END_GROUP = PRODUCT_METADATA
GROUP = IMAGE_ATTRIBUTES
CLOUD_COVER = 0.07
IMAGE_QUALITY_OLI = 9
IMAGE_QUALITY_TIRS = 9
ROLL_ANGLE = -0.001
SUN_AZIMUTH = 129.94408789
SUN_ELEVATION = 61.58869412
EARTH_SUN_DISTANCE = 1.0136271
GROUND_CONTROL_POINTS_MODEL = 233
GEOMETRIC_RMSE_MODEL = 9.460
GEOMETRIC_RMSE_MODEL_Y = 5.281
GEOMETRIC_RMSE_MODEL_X = 7.849
GROUND_CONTROL_POINTS_VERIFY = 39
GEOMETRIC_RMSE_VERIFY = 13.179
END_GROUP = IMAGE_ATTRIBUTES
GROUP = MIN_MAX_RADIANCE
RADIANCE_MAXIMUM_BAND_1 = 739.76367
RADIANCE_MINIMUM_BAND_1 = -61.08992
RADIANCE_MAXIMUM_BAND_2 = 757.52698
RADIANCE_MINIMUM_BAND_2 = -62.55682

```

```

RADIANCE_MAXIMUM_BAND_3 = 698.05463
RADIANCE_MINIMUM_BAND_3 = -57.64558
RADIANCE_MAXIMUM_BAND_4 = 588.63898
RADIANCE_MINIMUM_BAND_4 = -48.61000
RADIANCE_MAXIMUM_BAND_5 = 360.21771
RADIANCE_MINIMUM_BAND_5 = -29.74690
RADIANCE_MAXIMUM_BAND_6 = 89.58287
RADIANCE_MINIMUM_BAND_6 = -7.39778
RADIANCE_MAXIMUM_BAND_7 = 30.19422
RADIANCE_MINIMUM_BAND_7 = -2.49345
RADIANCE_MAXIMUM_BAND_8 = 666.17737
RADIANCE_MINIMUM_BAND_8 = -55.01314
RADIANCE_MAXIMUM_BAND_9 = 140.78125
RADIANCE_MINIMUM_BAND_9 = -11.62576
RADIANCE_MAXIMUM_BAND_10 = 22.00180
RADIANCE_MINIMUM_BAND_10 = 0.10033
RADIANCE_MAXIMUM_BAND_11 = 22.00180
RADIANCE_MINIMUM_BAND_11 = 0.10033
END_GROUP = MIN_MAX_RADIANCE
GROUP = MIN_MAX_REFLECTANCE
    REFLECTANCE_MAXIMUM_BAND_1 = 1.210700
    REFLECTANCE_MINIMUM_BAND_1 = -0.099980
    REFLECTANCE_MAXIMUM_BAND_2 = 1.210700
    REFLECTANCE_MINIMUM_BAND_2 = -0.099980
    REFLECTANCE_MAXIMUM_BAND_3 = 1.210700
    REFLECTANCE_MINIMUM_BAND_3 = -0.099980
    REFLECTANCE_MAXIMUM_BAND_4 = 1.210700
    REFLECTANCE_MINIMUM_BAND_4 = -0.099980
    REFLECTANCE_MAXIMUM_BAND_5 = 1.210700
    REFLECTANCE_MINIMUM_BAND_5 = -0.099980
    REFLECTANCE_MAXIMUM_BAND_6 = 1.210700
    REFLECTANCE_MINIMUM_BAND_6 = -0.099980
    REFLECTANCE_MAXIMUM_BAND_7 = 1.210700
    REFLECTANCE_MINIMUM_BAND_7 = -0.099980
    REFLECTANCE_MAXIMUM_BAND_8 = 1.210700
    REFLECTANCE_MINIMUM_BAND_8 = -0.099980
    REFLECTANCE_MAXIMUM_BAND_9 = 1.210700
    REFLECTANCE_MINIMUM_BAND_9 = -0.099980
END_GROUP = MIN_MAX_REFLECTANCE
GROUP = MIN_MAX_PIXEL_VALUE
    QUANTIZE_CAL_MAX_BAND_1 = 65535
    QUANTIZE_CAL_MIN_BAND_1 = 1
    QUANTIZE_CAL_MAX_BAND_2 = 65535
    QUANTIZE_CAL_MIN_BAND_2 = 1
    QUANTIZE_CAL_MAX_BAND_3 = 65535
    QUANTIZE_CAL_MIN_BAND_3 = 1
    QUANTIZE_CAL_MAX_BAND_4 = 65535

```

```

QUANTIZE_CAL_MIN_BAND_4 = 1
QUANTIZE_CAL_MAX_BAND_5 = 65535
QUANTIZE_CAL_MIN_BAND_5 = 1
QUANTIZE_CAL_MAX_BAND_6 = 65535
QUANTIZE_CAL_MIN_BAND_6 = 1
QUANTIZE_CAL_MAX_BAND_7 = 65535
QUANTIZE_CAL_MIN_BAND_7 = 1
QUANTIZE_CAL_MAX_BAND_8 = 65535
QUANTIZE_CAL_MIN_BAND_8 = 1
QUANTIZE_CAL_MAX_BAND_9 = 65535
QUANTIZE_CAL_MIN_BAND_9 = 1
QUANTIZE_CAL_MAX_BAND_10 = 65535
QUANTIZE_CAL_MIN_BAND_10 = 1
QUANTIZE_CAL_MAX_BAND_11 = 65535
QUANTIZE_CAL_MIN_BAND_11 = 1
END_GROUP = MIN_MAX_PIXEL_VALUE
GROUP = RADIOMETRIC_RESCALING
    RADIANCE_MULT_BAND_1 = 1.2220E-02
    RADIANCE_MULT_BAND_2 = 1.2514E-02
    RADIANCE_MULT_BAND_3 = 1.1531E-02
    RADIANCE_MULT_BAND_4 = 9.7239E-03
    RADIANCE_MULT_BAND_5 = 5.9506E-03
    RADIANCE_MULT_BAND_6 = 1.4799E-03
    RADIANCE_MULT_BAND_7 = 4.9879E-04
    RADIANCE_MULT_BAND_8 = 1.1005E-02
    RADIANCE_MULT_BAND_9 = 2.3256E-03
    RADIANCE_MULT_BAND_10 = 3.3420E-04
    RADIANCE_MULT_BAND_11 = 3.3420E-04
    RADIANCE_ADD_BAND_1 = -61.10214
    RADIANCE_ADD_BAND_2 = -62.56934
    RADIANCE_ADD_BAND_3 = -57.65711
    RADIANCE_ADD_BAND_4 = -48.61972
    RADIANCE_ADD_BAND_5 = -29.75285
    RADIANCE_ADD_BAND_6 = -7.39926
    RADIANCE_ADD_BAND_7 = -2.49395
    RADIANCE_ADD_BAND_8 = -55.02415
    RADIANCE_ADD_BAND_9 = -11.62809
    RADIANCE_ADD_BAND_10 = 0.10000
    RADIANCE_ADD_BAND_11 = 0.10000
    REFLECTANCE_MULT_BAND_1 = 2.0000E-05
    REFLECTANCE_MULT_BAND_2 = 2.0000E-05
    REFLECTANCE_MULT_BAND_3 = 2.0000E-05
    REFLECTANCE_MULT_BAND_4 = 2.0000E-05
    REFLECTANCE_MULT_BAND_5 = 2.0000E-05
    REFLECTANCE_MULT_BAND_6 = 2.0000E-05
    REFLECTANCE_MULT_BAND_7 = 2.0000E-05
    REFLECTANCE_MULT_BAND_8 = 2.0000E-05

```

```

REFLECTANCE_MULT_BAND_9 = 2.0000E-05
REFLECTANCE_ADD_BAND_1 = -0.100000
REFLECTANCE_ADD_BAND_2 = -0.100000
REFLECTANCE_ADD_BAND_3 = -0.100000
REFLECTANCE_ADD_BAND_4 = -0.100000
REFLECTANCE_ADD_BAND_5 = -0.100000
REFLECTANCE_ADD_BAND_6 = -0.100000
REFLECTANCE_ADD_BAND_7 = -0.100000
REFLECTANCE_ADD_BAND_8 = -0.100000
REFLECTANCE_ADD_BAND_9 = -0.100000
END_GROUP = RADIOMETRIC_RESCALING
GROUP = TIRS_THERMAL_CONSTANTS
K1_CONSTANT_BAND_10 = 774.89
K1_CONSTANT_BAND_11 = 480.89
K2_CONSTANT_BAND_10 = 1321.08
K2_CONSTANT_BAND_11 = 1201.14
END_GROUP = TIRS_THERMAL_CONSTANTS
GROUP = PROJECTION_PARAMETERS
MAP_PROJECTION = "UTM"
DATUM = "WGS84"
ELLIPSOID = "WGS84"
UTM_ZONE = 33
GRID_CELL_SIZE_PANCHROMATIC = 15.00
GRID_CELL_SIZE_REFLECTIVE = 30.00
GRID_CELL_SIZE_THERMAL = 30.00
ORIENTATION = "NORTH_UP"
RESAMPLING_OPTION = "CUBIC_CONVOLUTION"
END_GROUP = PROJECTION_PARAMETERS
END_GROUP = L1_METADATA_FILE
END

```

References

Please see http://landsat.usgs.gov/tools_acronyms_ALL.php for a list of acronyms.

Storey, James, Michael Choate, and Kenton Lee. "Landsat 8 Operational Land Imager On-Orbit Geometric Calibration and Performance." *Remote Sensing* 6, no. 11 (2014): 11127-11152.

Storey, James, Michael Choate, and Donald Moe. "Landsat 8 thermal infrared sensor geometric characterization and calibration." *Remote Sensing* 6, no. 11 (2014): 11153-11181.

Markham, Brian, Julia Barsi, Geir Kvaran, Lawrence Ong, Edward Kaita, Stuart Biggar, Jeffrey Czapla-Myers, Nischal Mishra, and Dennis Helder. "Landsat-8 Operational Land Imager radiometric calibration and stability." *Remote Sensing* 6, no. 12 (2014): 12275-12308.

Montanaro, Matthew, Raviv Levy, and Brian Markham. "On-orbit radiometric performance of the Landsat 8 Thermal Infrared Sensor." *Remote Sensing* 6, no. 12 (2014): 11753-11769.

Barsi, Julia A., John R. Schott, Simon J. Hook, Nina G. Raqueno, Brian L. Markham, and Robert G. Radocinski. "Landsat-8 Thermal Infrared Sensor (TIRS) Vicarious Radiometric Calibration." *Remote Sensing* 6, no. 11 (2014): 11607-11626.

Cook, Monica, John R. Schott, John Mandel, and Nina Raqueno. "Development of an Operational Calibration Methodology for the Landsat Thermal Data Archive and Initial Testing of the Atmospheric Compensation Component of a Land Surface Temperature (LST) Product from the Archive." *Remote Sensing* 6, no. 11 (2014): 11244-11266.

Gerace, Aaron, John Schott, Michael Gartley, and Matthew Montanaro. "An Analysis of the Side Slither On-Orbit Calibration Technique Using the DIRSIG Model." *Remote Sensing* 6, no. 11 (2014): 10523-10545.

Montanaro, Matthew, Aaron Gerace, Allen Lunsford, and Dennis Reuter. "Stray light artifacts in imagery from the Landsat 8 Thermal Infrared Sensor." *Remote Sensing* 6, no. 11 (2014): 10435-10456.

Knight, Edward J., and Geir Kvaran. "Landsat-8 operational land imager design, characterization and performance." *Remote Sensing* 6, no. 11 (2014): 10286-10305.

Barsi, Julia A., Kenton Lee, Geir Kvaran, Brian L. Markham, and Jeffrey A. Pedelty. "The spectral response of the Landsat-8 operational land imager." *Remote Sensing* 6, no. 10 (2014): 10232-10251.

Montanaro, Matthew, Allen Lunsford, Zelalem Tesfaye, Brian Wenny, and Dennis Reuter. "Radiometric calibration methodology of the Landsat 8 Thermal Infrared Sensor." *Remote Sensing* 6, no. 9 (2014): 8803-8821.

Morfitt, Ron, Julia Barsi, Raviv Levy, Brian Markham, Esad Micijevic, Lawrence Ong, Pat Scaramuzza, and Kelly Vanderwerff. "Landsat-8 Operational Land Imager (OLI) radiometric performance on-orbit." *Remote Sensing* 7, no. 2 (2015): 2208-2237.

Mishra, Nischal, Md Obaidul Haque, Larry Leigh, David Aaron, Dennis Helder, and Brian Markham. "Radiometric Cross Calibration of Landsat 8 Operational Land Imager (OLI) and L7 Enhanced Thematic Mapper Plus (ETM+)." *Remote Sensing* 6, no. 12 (2014): 12619-12638.

Wenny, Brian N., Dennis Helder, Jungseok Hong, Larry Leigh, Kurtis J. Thome, and Dennis Reuter. "Pre-and post-launch spatial quality of the Landsat 8 Thermal Infrared Sensor." *Remote Sensing* 7, no. 2 (2015): 1962-1980.

Irons, James R., John L. Dwyer, and Julia A. Barsi. "The next Landsat satellite: The Landsat data continuity mission." *Remote Sensing of Environment* 122 (2012): 11-21.

Irons, James R., and John L. Dwyer. "An overview of the Landsat Data Continuity Mission." In *SPIE Defense, Security, and Sensing*, pp. 769508-769508. International Society for Optics and Photonics, 2010.

Arvidson, Terry, Samuel Goward, John Gasch, and Darrel Williams. "Landsat-7 Long-Term Acquisition Plan." *Photogrammetric Engineering & Remote Sensing* 72, no. 10 (2006): 1137-1146.

Rice, Robert F., Pen-Shu Yeh, and Warner H. Miller. "Algorithms for high speed universal noiseless coding." In *Proceedings of the AIAA Computing in Aerospace 9 Conference*, pp. 19-21. 1993.

EarthExplorer Tutorial. <https://lta.cr.usgs.gov/ee_help>

EarthExplorer Registration. <<https://ers.cr.usgs.gov/register/>>

GloVis Quick Start Guide. <<http://glovis.usgs.gov/QuickStart.shtml>>

LandsatLook Viewer User Documentation.
<http://landsat.usgs.gov/LandsatLook_Viewer.php>

Landsat Data Products. <<http://landsat.usgs.gov>>

LSDS-749. Landsat 8 (L8) Mission Data Format Control Book (DFCB).
<<http://landsat.usgs.gov/documents/LDCM-DFCB-001.pdf>>

LSDS-750. Landsat 8 (L8) Level 0 Reformatted (L0R) Data Format Control Book (DFCB).

<<http://landsat.usgs.gov/documents/LDCM-DFCB-002.pdf>>

LSDS-809. Landsat 8 (L8) Level 1 (L1) Data Format Control Book (DFCB).

<<http://landsat.usgs.gov/documents/LSDS-809.pdf>>

LSDS-649, Landsat 8 (L8) Calibration and Validation (Cal / Val) Algorithm Description Document (ADD).

<http://landsat.usgs.gov/documents/LDCM_CVT_ADD.pdf>

Note: The above listed files are located

at http://landsat.usgs.gov/tools_project_documents.php

Landsat 8 Fact Sheet.

<<http://pubs.usgs.gov/fs/2013/3060/pdf/fs2013-3060.pdf>>

(linked from http://landsat.usgs.gov/about_project_descriptions.php)

Landsat 8 (L8) Operational Land Imager (OLI) and Thermal Infrared Sensor (TIRS) Calibration Notices. <http://landsat.usgs.gov/calibration_notices.php>

Landsat 8 Overview. <<http://landsat.usgs.gov/landsat8.php>>

LandsatLook Images. <<http://landsat.usgs.gov/LandsatLookImages.php>>

USGS Landsat User Services

Contact USGS Landsat User Services with any questions regarding these interfaces or Landsat data products, M-F 8:00 a.m. to 4:00 p.m. CT:

landsat@usgs.gov

1-605-594-6151

1-800-252-4547